EXPERIMENTAL AND COMPUTATIONAL INVESTIGATION OF SNOW MELTING ON A HYDRONICALLY HEATED CONCRETE SLAB

By

DIEGO PATRICIO ESPIN TOBAR

Bachelor of Science

Army Polytechnic School

Quito, Ecuador

1998

Submitted to the Faculty of the
Graduate College of the
Oklahoma State University
in partial fulfillment of
the requirements for
the Degree of
MASTER OF SCIENCE
December, 2003

EXPERIMENTAL AND COMPUTATIONAL INVESTIGATION OF SNOW MELTING ON A HYDRONICALLY HEATED CONCRETE SLAB

Thesis Approved:

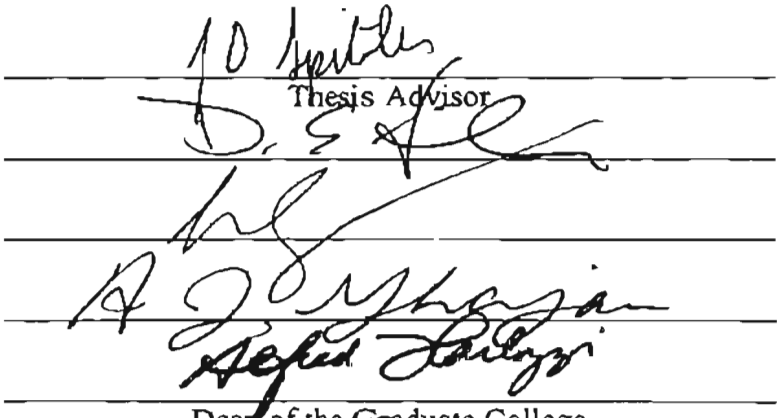

Thesis Advisor

Dean of the Graduate College

ACKNOWLEDGEMENTS

This thesis could not been completed without the participation of several persons. I wish to express my gratitude to all those who directly and indirectly participated in this process.

In addition, I would like to thank my advisor Dr. Spitler for his practical and theoretical guidance and support. Dr. Spitler has used his expertise in the field of thermal systems to guide me in the development of this thesis.

The love and support from my family have been of major importance. I would like to thank my wife, Siri, for all her support and understanding. She has always been there for me. Further I would like to thank my "adopted" American grandparents for all their support and love during my stay in Stillwater. Last but not least, to my parents (Lupita and Ruben Espín) for their great support throughout my life. This has enabled me to be where I am today.

My gratitude to Dr. Mark Rockley who has been very supportive with his critical questioning and for the long hours spent helping with the revision of this thesis.

I would further like to thank to my fellow research assistants and friends. Xiaobing Liu and Dongyi Xiao for their advice and help during the development of my research.

TABLE OF CONTENTS

TABLE OF FIGURES

CHAPTER 1

INTRODUCTION

1.1 Overview

Freezing rain, frost, and snow formed by water or ice crystals falling and collecting on the ground can create dangerous travel situations. Snow, freezing rain or frost on airport runways, on highways and roads, or on bridges can be a serious threat to human travel safety. Bridges are especially critical to travel safety - not being in contact with the ground, they freeze quicker than the adjacent roadway.

To increase travel safety, snow can be removed or melted from paved surfaces. The use of chemicals (e.g. salt) or mechanical devices (e.g. snow plows) is a frequent practice. The most commonly used chemical on roads is salt (Sodium Chloride). Salt interacts with water and ice and decreases the freezing point. Salt is an inexpensive deicing agent and it is efficient in melting snow and ice except when the surface temperature is lower than –9°C (15°F).

The primary disadvantage of using salt is its corrosive interaction with the bridge deck reinforcing steel and bridge structural steel over the long term. The resulting repair costs of bridges are often very high. The salt will further interact with the vehicles and over time corrode them also. Other disadvantages of chemical use are: environmental

damage on vegetation and adjacent water streams (Löfgren 2001) and the difficulty of application before a snowstorm arrives. Salt is not applied before storms because it will not react without moisture and can be swept away before the snow arrives.

Another method of ice/snow removal is the use of mechanical devices (e.g. snow plows), but these can damage the pavement and can be associated with high maintenance costs. Machinery vibration and improper use of the mechanical device lead to surface and structural damage (Nixon 1993). Again, it is a purely reactive method is used once the freezing condition is present and therefore the safety concern is present. Moreover, severe environmental conditions may preclude use of the equipment. For these reasons, alternative ice melting methods that permit cost savings, lower maintenance, and reduce road and bridge damage should be considered.

One alternative method is to embed hydronic tubing in critical points of roads, highways and bridges to melt the snow. A fluid can be heated using a ground source heat pump that transfers heat from the ground to the fluid. The warm fluid is circulated through the embedded pipes in order to prevent freezing conditions on the pavement. In this way, the pavement surface can be kept free from ice or snow. This system is being investigated by researchers at Oklahoma State University and is referred to as the "Smart Bridge Project". The name comes from the use of local and remote weather data to forecast icing conditions and automatically control the heating system. The objective is to maintain a surface free of ice or snow during the whole storm period.

The key problem for the Smart Bridge System is the high initial cost. An important emphasis of the research at OSU is the optimal design and control of the Smart

Bridge system. Reliable mathematical models of all the system components are required in order to accomplish this task. The OSU research group has developed new component models of heat pumps, ground loop heat exchangers, and bridge decks for use in the modular simulation environments, TRNSYS and HVACSIM+. Testing and validation of the component models are essential to ensure their accuracy and the validity of the system simulation. This thesis is concerned with validation of the bridge deck model.

1.2 Steady state and transient models

Snow melting models can be classified as either steady state or transient. Earlier analyses of snow-melting systems performance and guidelines for the design of such systems have been based upon steady-state conditions. In a steady state analysis, the response of the dynamically heated slab and rapidly changing moisture conditions are not considered (i.e. no considerations are taken from the storm history). Since storms are dynamic in nature, steady state models can only give a very rough idea of the actual system behavior. Moreover, the system capacity can be over (or under) estimated and therefore make the system inadequate for the application, or unnecessarily expensive.

By contrast, transient models take into account the dynamic response of the slab to changing weather conditions. Two transient models have been developed to analyze snow melting. Chiasson, et al. (1999) developed the first model used as part of the "Smart Bridge" project at Oklahoma State University. Subsequently, Liu, et al. (2002) improved upon this early model by refining the correlations and grid corresponding to the pipe approximation used by the previous model. Rees, et al. (2002) developed an alternative model that accounted for the mixed geometries on the grid model used. This model uses a

different mathematical approach to solve the heat balance due to the transient conditions. However, the researchers have also established the need of further refinement and experimental validation for these models.

1.3 Problem statement

An important requirement in the design of a snow melting system is the determination of the optimum design parameters for a heated slab. These design parameters which must be optimized are: the depth and spacing of the heating elements within the slab, the operating temperature of the working fluid, and the proper layout of the embedded piping in order to obtain the desired surface condition (i.e. ice free). These parameters can only be optimized with a reliable model capable of predicting the response of the system to highly transient storm conditions.

Both of the models actually used for simulation require experimental validation in a controlled environment. Experimental (field) validation has been performed as part of the "Smart Bridge" project. However, the environmental conditions could not be controlled, and it is desirable to perform experiments under well-controlled conditions, where long and short wave radiation losses can be quantified more accurately. The results of the experimental validation used in the "Smart Bridge" project showed a difference of up to 2 °C (3.6 °F) from the measured temperature on bridge deck surface during the testing period (Liu, et al. 2002). The model presented in ASHRAE 1090-RP was partially validated by Hockersmith (2002). He only tested the snow-melting portion of the algorithm. Moreover in his validation he used an electric heated plate that instantly transferred the power to the surface. The actual transient response of the main component

(the slab) on a bridge deck was not considered. A real concrete slab needs to be tested under controlled conditions.

1.4 Objective

The objectives of this study are to experimentally validate the two transient, two-dimensional models of a hydronically-heated concrete slab with snow melting boundary conditions, under an environmentally controlled condition.

CHAPTER 2

LITERATURE REVIEW

2.1 Introduction

In this section, an overview of hydronic snow melting system technology is presented first. This overview is followed by a review of previous published research related to modeling of snow-melting systems. The reviewed models are presented in two groups. The first group of models uses steady state calculations. In the second group, models based on transient analysis tools are reviewed. Finally, experimental investigations are discussed.

2.2 Hydronic snow melting systems overview

Practical snow melting systems use embedded piping or electric heating elements. Both types of systems maybe used to reduce safety concerns over bridges and roads and to keep these surfaces maintenance free in the winter. The maintenance usually associated with winter periods includes plowing and applying de-icing chemicals. The use of snow melting systems can eliminate all this work and prevent potential damage to the concrete and structures by snow removal equipment and chemicals. Furthermore, it can prevent snow accumulation.

In the case of an electric heating system, an embedded electrical cable is used as heating element. In the case of hydronic systems, an embedded pipe circulating a mixture of antifreeze (e.g. propylene glycol or ethylene glycol) and water is used as the heating element. In both cases "the system time constant is in the order of hours" (Rees, et al., 2002). This is caused by the large thermal mass of the system and is important because of the highly transient nature of weather.

There are two configurations of hydronically-heated pavement systems that have been reported. The first one consists of pipes embedded in the pavement material evenly spaced and connected with U-Shaped tubes as shown in Figure 2.2-1. This system is commonly used for snow melting applications.

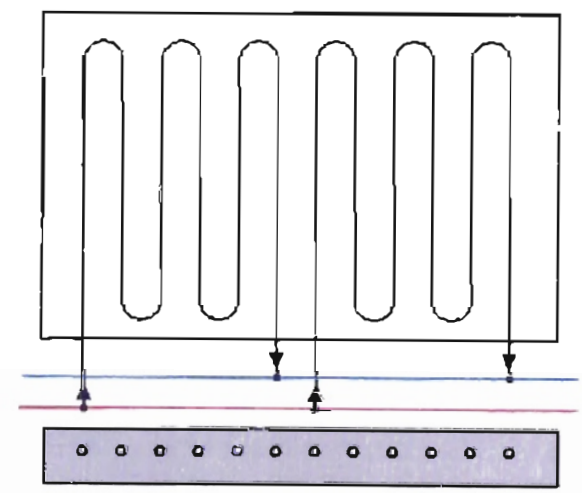

Figure 2.2-1: ***Serpentine pipe configuration in a hydronically- heated slab in plane and cross sectional view***

Another configuration consists in pipe coiled in circular fashion such that each loop overlaps the adjacent loop as shown in Figure 2.2-2 (Chiasson, et al. 1999). This

configuration has been used as heat rejection system for hybrid ground source heat pump systems.

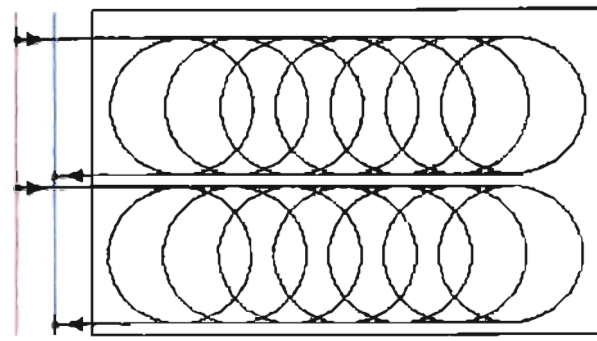

Figure 2.2-2: ***Slinky pipe configuration in a hydronically-heated slab***

A proper design of a heated slab requires the determination of the needed heat flux on the surface based on design weather conditions. To achieve this, it is necessary to specify the proper spacing of the heating elements and the depth at which they are embedded into the slab. Other parameters such as flow rate, insulation, and operating temperature also need to be specified to achieve the proper heat flux.

2.3 Steady State models

In this section, an analysis of the most accepted steady state models is presented. The steady state snow melting models are either 1-D or 2-D models. The development of snow melting models started with a classification of service done by Chapman (1956). Several authors have follow Chapman's work. Some of them based their analysis on 1-D models like Kilkis (1994a, 1994b) and Ramsey et al. (1999). Other authors developed the concept further to 2-D models like Schnurr and Rogers (1970). However, even with the increased use of 2-D models (steady state and transient), ASHRAE still presents 1-D

steady state model (Ramsey, et al. 1999) for snow melting systems design in the ASHRAE handbook series.

2.3.1 1-D Steady State Models

These types of models are surface-only models. They are based on the energy balance at the surface of the slab and do not concern themselves with conduction heat transfer in the slab. The main difference between the different models is the way the heat losses are evaluated. Chapman (1952, 1956), Kilkis (1994a, 1994b) and Ramsey et al. (1999) have followed this concept. These models were designed as a guideline for snow-melting applications with enough accuracy for system design.

Chapman Model

In this model the author originally classifies a heated slab according to the ability of the system to melt snow. This classification is used to prescribe the operating conditions of the slab. These classifications are based on the ratio of snow-free area to total area (A_r) of the slab during the snowfall. The classes are described as follows:

- **Class 1.** (Residential): The entire surface maybe fully covered with snow during the snowfall (A_r=0). The system is expected to melt the accumulated snow some time after the snowfall. Examples of this type are: residential walks or driveways.
- **Class 2.** (Commercial): up to 50% of the surface maybe covered with snow. Examples of this type are: sidewalks, driveways and steps in hospitals.

- **Class 3.** (Industrial): The entire surface is kept free from snow accumulation. Examples of this type are: toll plazas in highways, bridges, loading areas in airports, etc.

For $A_r = 1$, the system should melt snow fast enough to prevent any accumulation over the entire surface. For $A_r = 0$, the entire surface of the slab it is assumed to be covered with snow thick enough to prevent any heat and evaporative loss. For this reason, the snow-free area ratio is considered as the main design parameter for snow melting system designs. This parameter is defined as:

$$A_r = \frac{A_f}{A_s + A_f} \tag{2.1}$$

Where:

A_r = Snow-free area ratio, (dimensionless).

A_f = Snow free area, (m^2 or ft^2).

A_s = Snow-covered area, (m^2 or ft^2).

$A_t = A_f + A_s$ = Total slab area, (m^2 or ft^2).

In this model, the correlation used to describe the heat requirement for the snow-melting process is the steady state energy balance for the required total heat flux at the upper surface of a snow-melting slab during snowfall. The correlation used for this purpose is shown below:

$$q_o = q_s + q_m + A_r(q_h + q_e) \tag{2.2}$$

Where:

q_o = total required heat flux per unit area of the surface, (BTU/hr.ft^2 or W/m^2).

q_s = Total sensible heat flux, (BTU/hr.ft^2 or W/m^2).

q_m = Heat of fusion of snow, (BTU/hr.ft^2 or W/m^2).

A_r = Snow free area ratio, (non-dimensional).

q_h = Sum of convection and radiation losses, (BTU/hr.ft^2 or W/m^2).

q_e = evaporative losses, (BTU/hr.ft^2 or W/m^2).

The total sensible heat flux required to raise the snow (ice) temperature up to melting and is calculated as follows:

$$q_s = C_1 \left(T_f - T_a \right) s \tag{2.3}$$

Where:

T_f = Water film temperature, (°F or °C).

T_a = Ambient temperature, (°F or °C).

s = rate of snowfall in water equivalent, (in/hr or mm/hr).

C_1 = 2.6 [BTU/(°F ft^2 in)] or 194.4 [J/(°C m^2 mm)].

The total heat required for a change from solid (snow or ice) to liquid (water) state can be calculated as:

$$q_m = C_2 s \tag{2.4}$$

Where:

C_2 = 746 [BTU/(ft^2 in)] or 92.65 [W hr /(m^2 mm)].

The combined heat flux due to convection and radiation heat transfer over the slab surface was calculates as:

$$q_h = (f_c + f_r)(t_f - t_a) \tag{2.5}$$

Where:

f_c = film coefficient of heat transfer due to convection, [BTU/(h ft^2 °F) or W/(m^2 °C)].

f_r = film coefficient of heat transfer for radiation, [BTU/(h ft^2 °F) or W/(m^2 °C)].

The values for f_c and f_r are obtained from empirical correlations developed by the Chapman (1952). These equations were obtained with a wet test slab of 4ft^2. Then the values obtained under different environmental conditions for wind speed and temperature. Then the data was tabulated and plotted. Finally, the least square method was used to develop the equations. Under these circumstances, the evaporation load could be overestimated for bigger applications because the small thermal mass of the concrete slab which was never considered. The equations obtained were:

$$f_c = C_3 v + C_4 \tag{2.6}$$

$$f_r = C_5 \frac{\left[\left(T_p / 100 \right)^4 - \left(T_a / 100 \right)^4 \right]}{\left(t_p - t_a \right)} \tag{2.7}$$

Where:

C_3 = 0.27 [BTU/(ft^2 mi °F)] or 3.43 [J/(m^3 °C)].

C_4 = 2.5 [BTU/(hr ft^2 °F)] or 14.20 (W/(m^2 °C)].

T_p = Surface temperature of the panel, (°R or K).

T_a = Ambient temperature, (°R or K).

t_p = Surface temperature of the panel, (°F or °C).

t_a = Ambient temperature, (°F or °C).

v = wind speed velocity, (mph or m/s).

C_5 = 0.173 [BTU/(hr ft^2 °R^4)] or 5.73 [W/(m^2 K^4)].

The heat flux required to evaporate the water accumulated over the slab surface can be calculated from an empirical correlation. The derivation of this formula followed the same procedure as in the case for convection or radiation heat transfer. After the test the correlation obtained was:

$$q_e = \left(C_6 v + C_7 \right) \left(P_{wv} - P_{av} \right) \tag{2.8}$$

Where:

P_{wv} = vapor pressure of water, (inHg or Pa)

P_{av} = Vapor pressure of moist air, (inHg or Pa)

$C_6 = 0.0201$ [BTU/(ft^2 mi inHg)] or 4.188×10^{-5} [J/(m^3 Pa)].

$C_7 = 0.055$ [BTU/(hr ft^2 inHg)] or 5.134×10^{-5} [W/(m^2 Pa)].

Chapman (1956) recognized the transient nature of storms. He based all his calculations on four parameters: velocity of wind, air temperature, relative humidity of air, and amount of snowfall. In his study, Chapman (1956) stated, "the true analysis of heat output depends on an analysis of the weather". Moreover, in the determination of convection and radiation he used a mixed correlation to describe two losses that are sensitive to two different factors (temperature and wind speed) during different weather conditions. However, these were the only parameters tested under changing weather conditions.

The author of this model used collected data from specific cities to develop his correlations. This is a big limitation even in 1-D steady state calculations due to the impossibility to cover all the regions in a single country and all the possible weather conditions for each analyzed region. Furthermore, some important parameters such as sky temperature, sky cover, and relative humidity have not been considered. Finally, there is no discussion about the heating elements distribution.

Kilkis Model

Kilkis (1994a) notes, the minimum temperature of the system is located halfway between the heating elements. If the surface temperature is below 0°C (32°F) the snow will not melt or eventually become ice. Therefore, a good design will focus on raising the effective surface temperature in order to maintain the minimum temperature above 0°C (32°F). As described below, Kilkis uses an analogy to a fin in order to estimate the minimum temperature.

The energy balance equation for the surface of the slab is exactly the same as used by Chapman (1956) in his model (equation 2-2.). However, the correlations used to describe radiation, convection and evaporative heat losses are different. Kilkis (1994a) uses an updated correlation to describe radiation heat loss based on the net long wave radiation under cloudy skies (equation 2-9) and clear skies (equation 2-10). The mentioned correlations are:

$$q_r = C_1 + C_2\left[\left(T_f + T_a\right)\right]^3\left(T_f - T_a\right) - C_3 T_a^4 \tag{2.9}$$

$$q_r = C_4 + C_5\left(T_f - T_a\right) \tag{2.10}$$

Where:

C_1 = 10.3 [BTU/(hr ft^2)] or 32.49 (W/m^2).

C_2 = 8.14×10^{-10} [BTU/(hr ft^2 °R^4)] or 2.695×10^{-8} [W/(m^2 K^4)].

C_3 = 7.316 [BTU/(hr ft^2 °R^4)] or 2.423×10-9 [W/(m^2 K^4)].

C_4 = 30.15 [BTU/(hr ft^2)] or 95.11 (W/m^2).

C_5 = 0.74 [BTU/(hr ft^2 °R)] or 4.20 [W/(m^2 K)].

T_f = Water film temperature, (°R or K)

T_a = Ambient temperature, (°R or K)

In the case of the convection heat losses, the correlation used is based on experimental data. However, in his study Kilkis (1994a) used a more conservative approach and the developed empirical correlation was obtained using a bigger surface area for the testing slab (16ft^2). The correlation used is as follows:

$$q_c = (C_6 U + C_7)(T_f - T_a) \tag{2.11}$$

Where:

C_6 = 0.14 [BTU/(mi ft^2 °F)] or 1.78 [W/(m^3 °C)].

C_7 = 0.39 [BTU/(ft^2 °F)] or 2.22 [W/(m^2 °C)].

U = corrected wind velocity, (mph or m/s).

T_f = Water film temperature, (°F or °C).

T_a = Ambient temperature, (°F or °C).

Kilkis (1994a) used a corrected wind speed correlation based on previous assumptions that the wind speed data is recorded at a different altitude than the altitude of

the actual application. Therefore, his correlation includes the altitude adjustment factors as described in ASHRAE Handbook (1989):

$$U = (A_o)\left(\frac{H}{H_{ref}}\right)^{a}(U_{met}) \tag{2.12}$$

Where:

a = Wind speed adjustment factor with respect to height from the ground, (dimensionless).

A_o = Wind speed adjustment factor with respect to terrain, (dimensionless).

H = Height of snow melting surface from ground level, (ft or m).

H_{ref} = Wind speed recording height from ground level, (ft or m).

U_{met} = Wind speed from local meteorological data, (mph or m/s).

The heat flux required to evaporate the water is calculated based on required convective heat flux and the Bowen's ratio:

$$q_e = \frac{q_c(P_s - P_{av})}{R(T_f - T_a)} \tag{2.13}$$

Where:

P_{av} = Vapor pressure of moist air, (inHg or Pa).

P_s = Vapor pressure of saturated air at film temperature, (inHg or Pa).

R = Bowen's ratio, (inHg/°F or Pa/°C).

T_f = Water film temperature, (°F or °C).

T_a = Ambient temperature, (°F or °C).

The Bowen's ratio is the relation between latent and sensible heat flux and can be calculated as: The values for Bowen's ratio (R) and P_{av}, can be obtained from:

$$R = C_8 P_a \tag{2.14}$$

Where:

C_8 = 9.669×10-3 (1/°F) or 1.746×10-2 (1/°C).

Pa = atmospheric pressure, (inHg or Pa).

The values for the vapor pressure of moist in the rage between –28.8 °C (-20°F) to 1.6 °C (35 °F) air were obtained from the following correlation:

$$Pav = \theta\left(C_9 + C_{10}T_a + C_{11}T_a^2 + C_{12}T_a^3\right) \tag{2.15}$$

Where:

θ = Relative humidity, (dimensionless).

C_9= 0.0371 (inHg) or 125.64 (Pa).

$C_{10} = 1.64\times10^{-3}$ (inHg/°F) or 1.197×10^{1} (Pa/°C).

$C_{11} = 5.235\times10^{-5}$ (inHg/°F) or 3.202×10^{-1} (Pa/°C).

C_{12} =7.723×10^{-7} (inHg/°F) or 4.708×10^{-3} (Pa/°C).

T_o = Ambient temperature, (°F or °C).

The work presented by Chapman (1956) includes weather data from only 10 cities. But, one of the main design parameters is the rate of snowfall on the design location. For this reason, Kilkis (1994a) developed a statistical correlation to provide a design tool for the rate of snowfall based on available weather data for any location:

$$s' = \left[\frac{SF}{24} C\right] \frac{\Omega_s}{\Omega_w} \tag{2.16}$$

Where:

SF = Maximum amount of snowfall recorded at a given location in 24 hours, (in or mm).

C = Class, (dimensionless).

Ω_s = density of snow, (lb/ft^3 or kg/m^3).

Ω_w = density of water, (lb/ft^3 or kg/m^3).

In this study the author recognizes that the peak snowfall rate can be as much as three times bigger than a recorded average. Therefore, the data used is the peak snowfall rate. According to Kilkis's (1994a) study, the peak snowfall rate is the most common data in many countries. However, the density of snow is not common data in most meteorological surveys. For this reason, a correlation developed by Adlam (1950) is used to calculate this parameter:

$$\Omega_s = C_{13} + C_{14}T_a + C_{15}T_a^2 \tag{2.17}$$

Where:

C_{13} = 2.6 (lb/ft^3) or 41.65 (kg/m^3).

C_{14} = 0.06 [lb/(ft^3 °F)] or 1.73[kg/(m3 °C)].

C_{15} = 0.0027 [lb/(ft^3 °F^2)] or 0.1401[kg/(m^3 °C^2)].

Ω_s = density of snow, (lb/ft^3 or kg/m^3).

T_a = Ambient temperature, (°F or °C).

The analysis of the geometry of the slab and the piping distribution was a concern for Kilkis (1994b). The design temperature is based on the minimum temperature. However, the calculation of this temperature required a deeper analysis of the system geometry. His approach was the use of a composite fin surrounding the heating element. In this way Kilkis (1994b), was able to establish the minimum and maximum temperatures based on geometric information for the slab. A detailed analysis can be found in Kilkis (1994b) paper. The correlation used is:

$$T_{max} = T_a + \frac{\frac{q_f}{h_f} M}{\left(2W \cap + D_o\right)} \tag{2.18}$$

$$T_{min} = \frac{\left(T_{max} - T_a\right)}{Cos(mW)} + T_a \tag{2.19}$$

Where:

$\cap$ = Composite fin efficiency, (dimensionless).

M = Heating element spacing on centers, (ft or m).

m = Fin coefficient, (ft^{-1} or m^{-1}).

T_a = Ambient temperature, (°F or °C).

W = Half of the net spacing between adjacent heating elements, (ft or m).

In Kilkis (1994b), there is no consideration of side or bottom heat losses. To account for this type of energy loss, an approximation of 40% is used to reduce the heat transferred to the upper surface. Since this approximation is just an estimate on cases with ground contact and 1 ft dept, a new approach was performed for exposed lower surface and a new experimental correlation was obtained for this case. The heat lost in the back of the slab and the required heat flux to the surface was added to obtain the heat input required on the source for a certain application. The equation for back loss on exposed lower surface is:

$$q_b = (C_{16} + C_{17}U)(T_s - T_a) \tag{2.20}$$

Where:

C_{16} = 1.14 [BTU/(hr ft^2 °F)] or 7.496 [W/(m^2 °C)].

C_{17} = 0.13 [BTU/(ft^2 mi °F)] or 1.6512 [J/(m^3 °C)].

T_a = Ambient temperature, (°F or °C).

T_s = Surface temperature on the back of the slab if exposed, (°F or °C).

U = corrected wind velocity, (mph or m/s).

The experimental validation of this model was never done. The model was validated against finite-element solutions. The results showed an error of 10% compared with the numerical solution under steady state condition.

Ramsey et al. Model

Ramsey et al. (1999) presented this model; the concept used is that a good snow melting procedure should be developed as a simple design tool. His work is based on previous models presented by Chapman (1952) and Kilkis (1994a, 1994b). Ramsey used the same concept in developing the correlations in this model as Kilkis (1994a). "This tool must show enough accuracy for engineering calculations" (Ramsey, et al. 1999). As in the Kilkis (1994a) model, the only difference is the way in which the heat losses are calculated.

In Ramsey, et al (1999) model, the heat losses are assumed to happen only where no snow accumulation exists over the slab. Any snow-build up over the surface of the slab acts like insulation for the surface.

The suggested calculation procedure is based on the desired snow-free area ratio for a certain condition as input. By doing this, the heat losses are treated accordingly with the value selected (i.e. if A_r=0.6 is selected, the heat loss will be calculated only over this area and the heating system adjusted accordingly to this condition). The heating system

does not control the condition of the slab. This characteristics and the fact that this model is a steady state model makes it not useful for simulation purposes.

Heat losses due to convection and radiation are calculated using standard correlations. Then the heat losses are evaluated together as shown in equation (2.22). In the convective case, the correlation used corresponds to turbulent convective heat transfer from an exposed surface under a certain wind speed. This is not necessarily the case in every operating condition. However, it is a good approximation for exposed surfaces. The convection heat transfer is calculated as follows:

$$h_c = 0.037\left(\frac{k_{air}}{L}\right)\mathrm{Re}_L^{0.8}\,\mathrm{Pr}^{\frac{1}{3}} \tag{2.21}$$

Where:

k_{air} = Thermal conductivity of air at air temperature, [BTU/(h °F) or W/(m °C)].

L = Characteristic length of the surface, (ft or m)

Re_L = Reynolds number based on characteristic length, (dimensionless).

Pr = Prandtl number of air, taken as Pr=0.7, (dimensionless).

According to Ramsey, et al. (1999), for radiation losses, "the mean radiant temperature calculations use the same general principles as those used in determining the mean radiant temperature for indoor comfort and heat losses calculations". The correlation used is shown on equation (2.23):

$$q_h = h_c\left(T_f - T_a\right) + \sigma\varepsilon\left(T_f^4 - T_{MR}^4\right) \tag{2.22}$$

$$T_{MR} = \left[T_{cloud}^4 F_{sc} + T_{skyclear}^4 \left(1 - F_{sc}\right)\right]^{\frac{1}{4}} \tag{2.23}$$

Where:

q_h = Sum of convection and radiation losses, (BTU/ft^2 or W/m^2).

h_c = Convective heat transfer coefficient, [BTU/(ft^2 °R) or W/(m^2 K)].

T_f = Liquid film temperature, (R or K).

T_a = Ambient temperature, (R or K).

σ = Stephan-Boltzmann constant = 5.6705×10^{-8} [W/(m^2 K^4)] or 1.7123×10^{-9} [BTU/(ft^2 R^4)]

ε_s = Emissivity of surface (snow or dry), (dimensionless).

T_{MR} = Mean radiant temperature, (°R or K).

T_{cloud} = Temperature of the portion of sky that is covered, (°R or K).

$T_{skyclear}$ = Temperature of portion of sky that is clear, (°R or K).

F_{sc} = Fraction of radiation exchange between surface and clouds, (dimensionless).

A curve fit is used to calculate the temperature of a clear sky. The data corresponding to the equation fit can be found in Ramsey, et al. (1982). In case of the temperature for the clouds the guidelines of U.S. Standard Atmospheres (1962) was used

and the clouds are assumed to be at 3,048 meters (10,000 ft.). According to these guidelines, the temperature decreases about 6.4 K per 1000m (3.5 °R / 1000ft.). Therefore, the cloud temperature can be found by subtracting the temperature decrease from the ambient temperature.

The product of the evaporation rate and the heat of vaporization is used for the calculation of the evaporative heat loss. The evaporation rate can be calculated by multiplying the mass transfer coefficient with the differential humidity ratio between a liquid surface film and air. The equations used for this purpose are:

$$q_e = \rho_a h_m (W_f - W_a) h_{fg} \tag{2.24}$$

$$h_m = \left(\frac{\mathrm{Pr}}{Sc}\right)^{\frac{2}{3}} \frac{h_c}{\rho_a C_{pa}} \tag{2.25}$$

Where:

q_e = Evaporative losses, (BTU/m^2 or W/m^2)

ρ_a = Density of dry air, (lb$_a$/ft^3 or kg$_a$/m^3)

h_m = Mass transfer coefficient, (ft/s or m/s)

W_f = Humidity ratio of saturated air at the film surface temperature, (lb$_w$/lb$_a$ or kg$_w$/kg$_a$)

W_a = Humidity ratio of ambient air, (lb$_w$/lb$_a$ or kg$_w$/kg$_a$)

h_{fg} = Heat of vaporization, (BTU/lb$_w$ or J/kg$_w$)

Pr = Prantl Number (non-dimensional).

Sc = Schmidt number (non-dimensional)

h_c = Convective heat transfer coefficient, [BTU/(h ft^2 °R) or W/(m^2 K)]

C_{pa} = Specific heat capacity of air, [BTU/(lb °R) or J/(kg K)]

All the parameters used by these correlations have to be measured using coincident values for the climate factors (i.e. wind speed, snowfall rate, ambient temperature, etc.). This model "only analyzes the upper surface of the snow melting surface" (Ramsey, et al. 1999). No considerations are taken for edge and back losses during the analysis. The only criterion shown is that the losses can be considered in the range between 4% and 50% depending on the construction design. Moreover, a wide range of parameters should be considered and no correlation with the potential heat loss is shown.

In the Ramsey, et al (1999) model, no experimental validation was performed. The only validation done is comparison with previous case analyses in six cities. The error with previous cases ranges from 5% to 15%. Although more cities where included on the meteorological survey (38 in total), there is still a great limitation regarding the information required to perform this calculations.

2.3.2 2-D steady state models

On one hand, there are several steady state models that use a one-dimensional approach. On the other hand, there are only a few models that take two-dimensional analysis into consideration (e.g. Schnurr and Rogers 1970, finite-element techniques,

etc.). These models require some computational effort to perform the calculations. Nevertheless, these techniques can still be used in snow melting design.

Schnurr and Rogers Model

Schnurr and Rogers's (1970) model was developed using steady state finite difference equations to describe temperature gradients thru the heated slab. Energy balance equations were used to calculate the temperature at each nodal point. Unfortunately, this model uses variable sized grids equal to ¼ of the pipe diameter. This fairly coarse grid needs to be matched only for cases where the distance between pipes is a multiple of the diameter of the pipe. Another related problem to the use of a coarse grid is the impossibility of matching the round geometry of the pipes to the square nodal distribution.

This model does not clearly layout the assumptions required to model the effects of the exposed surface. The convection and radiation heat transfer coefficients are combined in the same way as in the one dimensional steady state model presented by Chapman (1956). The radiant temperature that is considered in the combined coefficient is fairly simple and does not take the radiation effects of the surroundings into consideration. The only considerations made are related to the air temperature and wind speed.

The heat balance is made following the original model of Chapman (1956). In the Chapman model simplified correlations were used to evaluate the different heat flux components. The heat balance equation is shown below:

$$q_o = q_s + q_m + q_e + h_c(C_1 - t_a) \tag{2.26}$$

Where:

C_1 = 32 (°F) or 0 (°C).

q_o = minimum required heat flux, [BTU/(h.ft^2) or W/m^2].

q_s = heat flux required for sensible heating of snow, [BTU/(h.ft^2) or W/m^2].

q_m = heat flux required to melt the snow, [BTU/(h.ft^2) or W/m^2].

q_e = heat flux required to vaporize the water film, [Btu/(h.ft^2) or W/m^2].

h_c = combined coefficient for convection and radiation, [Btu/(h.ft^2) or W/m^2].

t_a = dry bulb air temperature, (°F or °C).

One problem in this model is that it does not consider the snow accumulation over the slab surface. Therefore, this cannot be considered as a snow-melting algorithm. All the analyzed conditions are on surface free of snow during steady state in a class-3 heated slab. Another problem is that this model only can handle a single homogeneous layer of material (i.e. concrete). There is no consideration of different properties for materials used in the slab. The slab is analyzed from the outer surface of the pipe. Finally, the optimization is valid only in cases where adiabatic conditions are present in the bottom and sides of the slab. Even so, this model could be adapted to receive a different boundary condition on the bottom of the slab.

Schnurr and Rogers's (1970) model was able to provide some optimization compared with previous models. Analysis using this model showed that the surface of the slab is not homogeneous. There is a maximum temperature over the heating element position and a minimum temperature in between the pipes, as expected. The model further showed a strong relationship between the geometry of the slab and the surface temperature distribution. Kilkis (1994b) used this characteristic while developing his steady state model.

2.4 Transient models

In a steady state model, the dynamic response of the slab is not considered. With a time constant in the order of hours and since the system works intermittently depending on the weather conditions, the assumption of a steady state model is too conservative. Furthermore, the heat to the surface cannot be delivered instantaneously and the transient effects such as the period between the starting of the system and the assumed steady state can be significant (Rees, et al., 2002).

The models presented by Chiasson, et al. (1999) and Rees, et al. (2002) give detailed explanations for how a two-dimensional transient model can accommodate the pipe geometry and the slab geometry. The first model used a finite difference rectangular grid. Liu, et al. (2002) presented a refined version of the Chiasson et al. (1999) model for the 82nd TRB annual meeting. This second model is based on a finite volume method with structured boundary fitted grids in order to handle the complex geometries involved. In any case, all transient models require extensive computational effort. The big advantage is that transient models can be used for simulation purposes and design optimization.

According to Rees, et al. (2002), a comparison of the calculated steady state heat flux required to maintain the pavement snow-free for a number of hours and the transient analysis for the same condition can show that the power required is up to five times greater than what is projected using a steady state calculation. Another observation shows that some steady state calculations require of more heat flux thru the surface than is possible to provide in practice. Moreover, accounting for the transient nature of a storm can show that storms that start with low loads and then increase in intensity will require more heat flux than those that start with high loads which and decrease with time.

2.4.1 1-D transient models

Transient surface models have been developed as part of the solution of more detailed models. The only one-dimensional model developed is the one used by Rees, et al. (2002) to solve during the snow accumulation in their model. This transient model will be detailed as part of the complete 2-D analysis of their model.

2.4.2 2-D transient models

Only few models have managed to account in part for transient conditions. With the advance of computer science, more models representing a transient behavior have been developed. Some of them are following previous steady state models like Schnurr and Falk (1973) that is a natural extension from the previous model (Schnurr and Rogers (1970)). Unfortunately, in Schnurr and Falk's (1973) model the same assumptions and boundary conditions from the steady state counterpart are still on use. Since this model does not allow snow accumulation, it is not considered as a snow-melting model. However, some models followed the same concept of finite difference analysis (i.e. Chiasson et al. (1999) and Liu, et al. (2002)), and they do account for snow accumulation

and different boundary conditions on the slab. Moreover, new solution techniques are being developed. Rees, et al. (2002) developed new algorithm using boundary fitted grids that allow a detailed analysis of the transient behavior of the slab and complex geometries can be bond together.

Leal and Miller Model

Leal and Miller's (1972) model is an extension of the Schnurr and Rogers (1970) steady state model and the first two-dimensional transient model. The authors of this model developed a transient model based on the same boundary conditions as in the Chapman model. To account for the 2-D grid this model uses a polar coordinate system to generate the equation set. A point matching technique is used to achieve the solution for these equations. Unfortunately, the authors do not show any information about the grid geometry or the solution technique. For example, information concerning to the grid used to accommodate the round tube geometry in a transversally shaped square slab is not presented.

One of the main problems with this model is that the solution is oversimplified. For example, this model does not consider snow accumulation. Therefore, the model is not considered a snow-melting model. Moreover, the heated slab should be wet according to the heat loss equations used (equations (2.3), (2.4), (2.5), (2.8)). These equations where developed experimentally by Chapman (1956) over a wetted slab and used under this condition. But, the solution presented by Leal and Miller (1972) implies that there is no snow precipitation over the slab and no previous assumptions are made related to a wet

surface. If this is the case, the slab should be dry and not wet, thus making the heat balance used in the model inappropriate.

Finite Difference Rectangular Grid Model (FD-RG)

Originally, Chiasson et al. (1999) presented the FD-RG model. However, it was lately refined by Liu, et al. (2002). This model uses a finite difference in a rectangular grid with a node-centered approach. This model was implemented in HVACSIM+ software as a component model. The model implementation is somewhat convenient to use because of an effective GUI for the end user.

The domain in this model is a section equivalent to one half of the pipe spacing. This is quite reasonable because of the symmetry and small temperature differences between the flow on adjacent pipes. The y direction corresponds to the thickness of the slab. The x direction corresponds to the distance between the centerline of a pipe to half the distance of the adjacent pipe. The average top surface temperature obtained in this domain is considered to be the average surface temperature for the entire slab. This approximation is made because the model neglects the edge loss of the slab. Figure 2.4-3 shows a representation of the model domain. All heat flow is assumed to be into the node.

The governing equation is the two dimensional form of the transient heat diffusion equation:

$$\frac{\partial^2 T}{\partial x^2} + \frac{\partial^2 T}{\partial y^2} = \frac{1}{\alpha}\frac{\partial T}{\partial t} \tag{2.27}$$

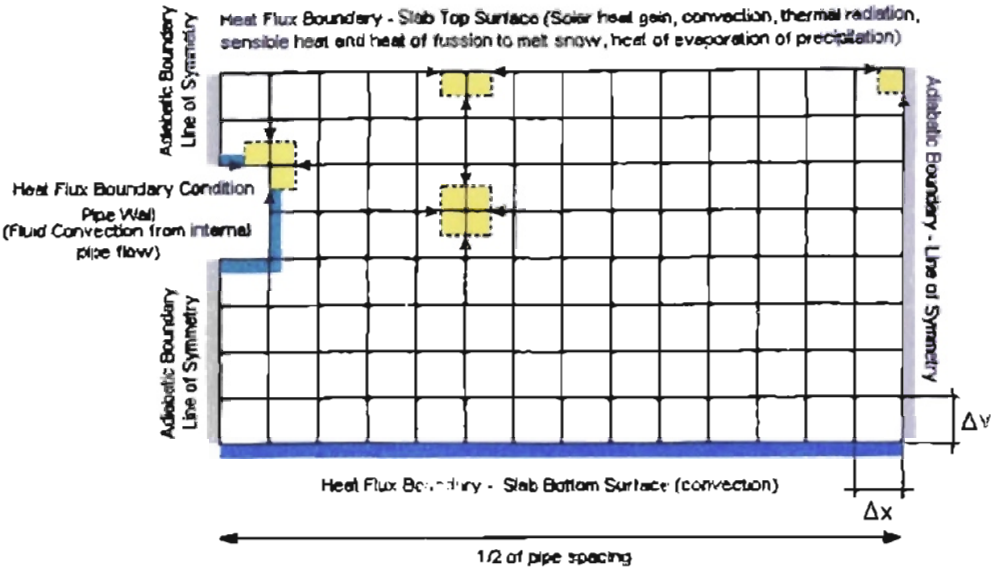

Figure 2.4-3: ***Model domain showing finite difference grid and boundary conditions***

When this equation is discretized in time, the finite difference form of the Fourier number appears in all nodal equations. The following equation shows the Fourier number with square nodal spacing, Δx equal to Δy.

$$Fo = \frac{\alpha \Delta t}{\left(\Delta x^2\right)} \tag{2.28}$$

Where:

Fo = Fourier number, (dimensionless).

α = Thermal diffusivity, (m^2/s or ft^2/s).

Δt = Time step, (s).

Δx = Grid size in x direction, (m or ft).

This model is not unconditionally stable. As a transient problem, the solutions must reach the steady-state condition with increasing time. However, according to Incropera and DeWitt (1996), the transient solution for the explicit finite difference approach is characterized by induced oscillations. These oscillations are physically impossible and may become mathematically unstable, causing the solution to diverge from the actual steady-state conditions. The stability criterion for a 2-D model is given by:

$$Fo \leq \frac{1}{4} \qquad (2.29)$$

Where:

Fo = Fourier Number, (dimensionless)

If Δx is equal to the radius times $\frac{\pi}{4}$, the grid domain in the x direction will be a multiple of the pipe radius and equivalent in length to quarter the perimeter of the pipe. In overall the sum of the y and x dimensions will be equivalent to the pipe perimeter. To calculate Δt, the prescribed value of α is evaluated in order to achieve mathematical stability.

The heat fluxes at the boundary nodes are caused by convection, radiation, evaporation of rain and melted snow, and melting of snow. On the upper surface the mentioned fluxes are considered according to the temperature and condition of the surface node. On the lower surface, it is possible to choose between exposed and perfectly insulated (adiabatic) surfaces. Only convection and radiation heat transfer is

calculated at the lower surface if it is exposed. The symmetry lines found at both sides of the model domain are by definition zero-flux boundary conditions. The heat flux at the pipe surface nodes and at the exposed slab surfaces are heat flux conditions. Inside the pipe, convection heat transfer causes the heat flux from the fluid. In the upper surface of the slab, convection, solar radiation, thermal radiation, sensible and latent heat conditions must all be accounted for. In the bottom surface of the slab only convection is used, although, if necessary, adiabatic conditions can be set.

The correlations used to calculate the convective heat flux over the surfaces are shown below:

$$q_c'' = h_c\left(T_{amb} - T_{(m,n)}\right) \tag{2.30}$$

Where:

q''_c = Convective heat flux, [BTU/(h.ft^2) or W/m^2].

h_c = Convection coefficient, [BTU/(hr ft^2 °F) or W/(m^2 °C)].

T_{amb} = Ambient temperature, (°F or °C).

$T_{(m,n)}$ = Temperature of node (m,n), (°F or °C).

To calculate the convection coefficient a Nusselt number is found. The appropriate number is calculated using the correlations for natural or forced convection according to the particular case. For the natural convection case, the correlations used are those for a heated upper surface. These correlations are shown below:

$$Nu = 0.54Ra^{\frac{1}{4}} \qquad (10^4<Ra<10^7 - \text{laminar flow}) \qquad (2.31)$$

$$Nu = 0.15Ra^{\frac{1}{3}} \qquad (10^7<Ra<10^{11} - \text{turbulent flow}) \qquad (2.32)$$

Where:

Nu = Nusselt Number, (dimensionless).

Ra = Rayleigh Number, (dimensionless).

For forced convection heat transfer, the correlations used are:

$$Nu = 0.664\,Re^{\frac{1}{2}}\,Pr^{\frac{1}{3}} \qquad \text{(Laminar flow regime)} \qquad (2.33)$$

$$Nu = 0.037\,Re^{\frac{4}{5}}\,Pr^{\frac{1}{3}} \qquad \text{(Mixed and turbulent flow regimes)} \qquad (2.34)$$

Where:

Nu = Nusselt Number, (dimensionless).

Re = Reynolds Number, (dimensionless).

Pr = Prandtl Number, (dimensionless).

The convection coefficient is then computed by:

$$h_c = \frac{Nu \cdot k}{L} \qquad (2.35)$$

Where:

h_c = Convection coefficient, [BTU/(hr ft^2 °F) or W/(m^2 °C)].

Nu = Nusselt Number, (dimensionless).

k = Thermal conductivity of air at pavement node, [BTU/(hr °F) or W/(m °C)].

L = Characteristic length, (ft or m).

The radiation heat flux is calculated over the upper and bottom surfaces. The long wave radiation is calculated using a linearized radiation coefficient shown in equation (2.36). Then the heat flux is calculated using equation (2.37). If the exposed surface is the upper one, the temperature used is the sky temperature. If the lower surface is exposed, an approximation to the ground temperature is made using the air temperature.

$$h_r = 4\varepsilon\sigma\left(\frac{T_{(m,n)} + T_2}{2}\right)^3 \tag{2.36}$$

$$q_r'' = h_r\left(T_2 - T_{(m,n)}\right) \tag{2.37}$$

Where:

h_r = Linearized radiation coefficient, [BTU/(hr ft^2 °R) or W/(m^2 K)].

ε = Emissivity coefficient, (dimensionless).

σ = Stephan-Boltzmann constant = 5.67x10^8, [BTU/(hr ft^2 °R^4) or W/(m^2 K^4)].

$T_{(m,n)}$ = Temperature of surface node, (°R or K).

T_2 = Temperature of sky or air (exposed lower surface), (°R or K).

q''_r = Radiation heat flux from pavement surface, [BTU/(hr ft^2) or W/m^2].

Solar radiation heat flux is considered directly for every time step on the FD-RG model. This information is directly applied as part of the environmental information. This information is used only over the upper surface of the slab.

Evaporative heat fluxes are considered only when the surface is wet or covered with a mixture of ice and water. This model presumes that there is no rain accumulation on the surface. Thus, all the rainfall is considered to leave the slab surface immediately after impact, while still forming a thin film over the slab surface. In the case of melted snow, the model uses the same approach as specified by Rees, et al. (2002) to approximate the effect of water being retained in the snow due to capillarity action.

The evaporative mass flux is calculated by equation (2.38) at each surface node:

$$\dot{m}''_{evap} = h_d \left(w_{air} - w_{(m,1)} \right) \tag{2.38}$$

Where:

w_{air} = Humidity ratio of the ambient air, (dimensionless).

$w_{(m,1)}$ = Humidity ratio of the saturated air at a top surface node, (dimensionless).

h_d = Mass transfer coefficient, [lb/(ft^2 s) or kg/(m^{2}s)].

The mass transfer coefficient is calculated with the Chilton-Colburn analogy by the following equation:

$$h_d = \frac{h_c}{C_p Le^{\frac{1}{4}}} \tag{2.39}$$

Where:

h_c = Convection heat transfer coefficient, [BTU/(h ft^2 °F) or W/(m^2 °C)].

C_p = Specific heat capacity of air at node temperature, [BTU/(lb °F) or J/(kg °C)].

Le = Lewis number, (dimensionless).

The Lewis number is the ratio between thermal diffusivity (α) and the Binary mass diffusion coefficient (D_{ab}). This last value is calculated using the correlations Marrero and Masson (1972):

$$D_{ab} = \frac{C_1 T^{2.072}}{P_{air}} \tag{2.40}$$

Where:

C_1 = 1.87×10^{-13} [(Pa m2)/(°K$^{2.072}$ s)] or 1.7585×10-16 [(Pa m^2)/(°K$^{2.072}$ s)]

T = Absolute temperature of air, (°R or K).

P_{air} = Pressure of air, (inHg or Pa).

The evaporative heat flux due to evaporation is calculated as follows:

$$q''_{evap} = h_{fg} \dot{m}''_{evap} \tag{2.41}$$

Where:

h_{fg} = heat of evaporation, (BTU/lb or J/kg).

$\dot{m}''_{evap}$ = Evaporative mass flux, [lb/(ft^2 hr) or kg/(m^2 s)].

The last heat flux value evaluated at the top surface corresponds to the combination of sensible and fusion heat required to melt the snow. The sensible heat flux corresponds to the energy required to elevate the temperature of the snow to 0°C (32°). This value is calculated as follows:

$$q''_{sen} = \dot{m}''_{pre} C_{pw} \left(T_{air} - T_{(m,1)} \right) \tag{2.42}$$

Where:

$\dot{m}''_{pre}$ = Mass flux of water equivalent of the snow or freezing rain, [lb/(ft^2 s) or kg/(m^2 s)].

C_{pw}= Specific heat of water, [BTU/(lb °F) or J/(kg °C)]

T_{air} = Temperature of ambient air, (°F or °C)

$T_{(m,1)}$ = Temperature of surface node, (°F or °C).

The fusion heat flux is the flux required to produce the change of state for the ice. It is determined with a heat and mass balance on a specified top surface node. The model evaluates the actual mass flow rate at each time step. This value is calculated as the

minimum between the potential snowmelt flow rate and the accumulated mass of ice on each time step. This equation is shown below:

$$\dot{m}''_{melt-actual} = \min\left(\dot{m}''_{melt-potential}, \frac{m''_{ice-accumulated-current}}{\Delta t}\right) \tag{2.43}$$

$$\dot{m}''_{melt-potential} = \max\left(\dot{m}''_{melt\_heatBalance}, 0\right) \tag{2.44}$$

$$\dot{m}''_{melt\_heatBalance} = \frac{q''_{solar} + q''_{rad} + q''_{conv} + q''_{sen} + q''_{evap} + q''_{cond\_surf}}{h_{if}} \tag{2.45}$$

Where:

q''_{solar} = Heat flux due to solar radiation, [BTU/(h ft^2) or W/m^2].

q''_{rad} = Heat flux due to long-wave radiation, [BTU/(h ft^2) or W/m^2].

q''_{conv} = Heat flux due to convection, [BTU/(h ft^2) or W/m^2].

q''_{sen} = Sensible heat flux on snow, [BTU/(h ft^2) or W/m^2].

q''_{evap} = Evaporative heat flux of slush or water, [BTU/(h ft^2) or W/m^2].

q''_{cond_surf} = Heat flux conducted to the surface of the slab, [BTU/(h ft^2) or W/m^2].

h_{if} = Latent heat of fusion of water, (BTU/lb or J/kg).

This model is designed for simulation only of hydronic systems. However, the model could be modified to account directly for the heat flux of a buried electric cable.

At present time, this boundary heat flux cannot be passed directly to the slab. This boundary condition is applied in the nodes where the internal piping is present.

In order to model heat flux due to heat exchange from the fluid the following correlation is applied:

$$q''_{fluid} = U\left(T_{fl\_avg} - T_{(x,y)}\right) \tag{2.46}$$

Where:

q''_{fluid} = Heat flux through the pipe wall, [BTU/(h ft^2) or W/m^2].

U = Overall heat transfer coefficient, [BTU/(h ft^2 °F) or W/(m^2 °C)].

$T_{(x,y)}$ = Non-surface node temperature, (°F or °C).

The overall heat transfer coefficient can be expressed as:

$$U = \frac{1}{\frac{1}{h_{fluid}} + \frac{l}{k_{pipe}}} \tag{2.47}$$

Where:

U = Overall heat transfer coefficient, [W/(m^2 °C)].

h_{fluid} = Convection heat transfer coefficient for fluid, [BTU/(h ft^2 °F) or W/(m^2 °C)].

k_{pipe} = Thermal conductivity of pipe material, [BTU/(h ft °F) or W/(m °C)].

l = Length, (ft or m).

The convection heat transfer coefficient is given by the following relationship:

$$h_c = \frac{Nu \cdot k_{fl}}{L} \tag{2.48}$$

Where:

h_c = Convection heat transfer coefficient for fluid, [BTU/(h ft^2 °F) or W/(m^2 °C)].

k_{fl}= Thermal conductivity of fluid, [BTU/(h ft^2 °F) or W/(m^2 °C)].

L = characteristic length (defined as the inner diameter of the pipe), (ft or m).

According to Liu, et al. (2002), the Nusselt Number (Nu) is computed with the Gnielinki equation as shown below:

$$Nu = \frac{\left(\frac{f}{2}\right)(\mathrm{Re}-1000)\mathrm{Pr}}{1+1.27\left(\frac{f}{2}\right)^{\frac{1}{2}}\left(\mathrm{Pr}^{\frac{2}{3}}-1\right)} \tag{2.49}$$

Where:

Nu = Nusselt Number, (dimensionless).

f = Friction factor, (dimensionless).

Re = Reynolds Number, (dimensionless).

Pr = Prandtl Number, (dimensionless).

The friction factor is given by:

$$f = [1.58\ln(\mathrm{Re}) - 3.28]^{-2} \tag{2.50}$$

Where:

Re = Reynolds Number, (dimensionless).

The fluids that can be used are water or antifreeze solutions. The thermal properties for the working fluid are calculated for each time step. The subroutine that performs this computation is based on the ASHRAE Handbook of fundamentals (SI) 1997. The thermal properties for water, Propylene Glycol and Ethylene Glycol can be calculated for a given average fluid temperature and antifreeze (% volume). The average fluid temperature is calculated iteratively using as initial value the previous time step converged value.

Finite Volume - Boundary Fitted Grid Model (FV-BFG)

In 1999 the ASHRAE project 926-RP entitled "Snow Melting Algorithms and Data for Locations Around the World" was presented. The objective of this project was to update the available data for the HVAC Applications Handbook (ASHRAE 1995). The ASHRAE 1090-RP is an extension of the 926-RP. The ASHRAE 926-RP presents a steady state load calculation procedure (Ramsey, et al. (1999) model) in order to find an instantaneous flux required to produce a given snow free area ratio. ASHRAE 1090-RP was developed by Rees, et al. (2002) and uses as many of the correlations previously developed as possible. However, one of the main objectives of this current project is to develop a two-dimensional transient analysis simulation tool. Under these conditions, the

free area ratio should be treated as an output for the model and not as an input, as is in the ASHRAE 926-RP.

Three parts form this model: the user interface, the finite volume solver, and the boundary condition model. The user interface is used to pass all the required information to the finite volume solver and the boundary condition model. The finite volume solver has two components, the grid generation module and the surface temperature calculator. The boundary condition model is used to evaluate the condition of the slab and provide information to the finite volume solver to calculate the surface temperature. This last component is considered as the 1-D transient model associated to the finite volume solver used to find iteratively a solution for the surface temperature.

The finite volume solver model is based on the integral form of the partial differential equation of the Fourier equation for heat conduction, as shown below:

$$\frac{\partial}{\partial t}\int_{v}\phi\, d\mathbf{V} = \int_{S}\Gamma\,\nabla\phi\,\mathbf{n}\, d\mathbf{S} \qquad (2.51)$$

Where:

ϕ = Temperature.

Γ = Thermal diffusivity.

$\mathbf{V}$ = Control volume.

$\mathbf{S}$ = Surface of the control volume.

$\mathbf{n}$ = vector normal to the surface of the control volume.

The right hand side of the equation represents the diffusion fluxes. In its discrete form the sum of the diffusion fluxes through each cell face can be represented as:

$$\int_S \Gamma \nabla \phi \, \mathbf{n} \, d\mathbf{S} \approx \sum_i F_i^D \tag{2.52}$$

Where:

$\nabla \phi$ = Temperature gradient

$\mathbf{S}$ = Surface of the control volume

$\mathbf{n}$ = vector normal to the surface of the control volume

i – north, south, west, east (for a 2-D cell)

D = Count for the diffusion term

On a particular cell the equation (2.52) is transformed into:

$$F_e^D = \left(\Gamma \nabla \phi \cdot \mathbf{n}\right)_e S_e \tag{2.53}$$

Where:

S_e = Area of the east face

The main challenge in using equation (2.53) is the calculation of the temperature gradient ($\nabla \phi$) at each cell face. To overcome this difficulty, Rees, et al. (2002) use the values of the variable at the cell centroid (ϕ_P and ϕ_E) and the distance between these

points ($L_{P'E'}$). This is a valid approximation if the cell is orthogonal. The equation (2.53) is reduced to:

$$F_e^D = \Gamma_e S_e \left(\frac{\partial \phi}{\partial \xi} \right)_{e'} \tag{2.54}$$

As expressed by Rees, et al. (2002), the main idea is to "preserve the second order accuracy by making the calculation of the gradient along the normal face". The use of the values of the variable at the P' and E' is essential. See Figure 2.4-4.

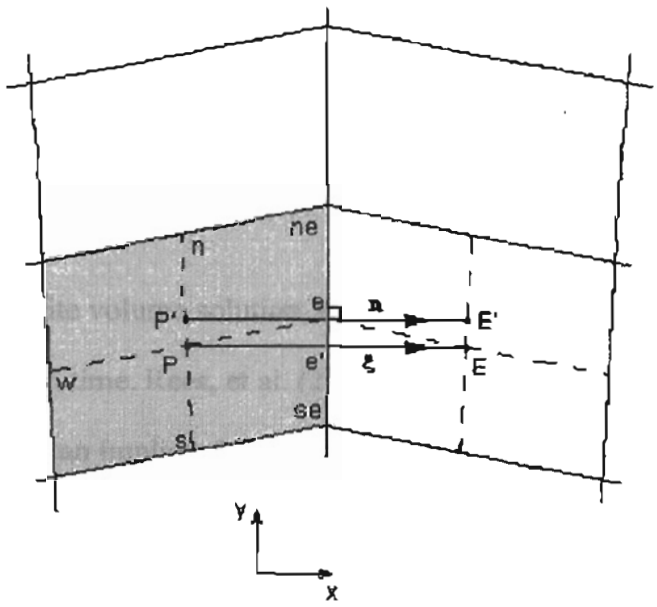

Figure 2.4-4: ***The local coordinate system at the east face of a typical finite volume cell***

The values at these points are calculated using a "deferred correction" approach, as follows:

$$F_e^D = \Gamma_e S_e \left(\frac{\partial \phi}{\partial \xi} \right)_{e'} + \Gamma_e S_e \left[\left(\frac{\partial \phi}{\partial n} \right)_s - \left(\frac{\partial \phi}{\partial \xi} \right)_{e'} \right]^{old} \tag{2.55}$$

In this equation, the values in the square brackets can be explicitly calculated. This is done using the previous values of the variable ϕ. When the solutions approach convergence, the gradient terms along ξ cancel and the gradient along the normal to the face is preserved as desired. The $(\partial\phi/\partial n)_n$ term can be explicitly calculated from the central difference as:

$$\left(\frac{\partial \phi}{\partial n}\right)_n = \left(\frac{\phi_{P'} - \phi_{E'}}{L_{P'E'}}\right) \tag{2.56}$$

Where:

$L_{P'E'}$ = Distance between P' and E'

$\phi_{P'}; \phi_{E'}$ = Variable evaluated at P'; E'

To obtain the finite volume solution, the partial differential equation needs to be integrated with respect to time. Rees, et al. (2002) used a first-order backward differencing approach in an implicit formulation. This procedure is fully described by Rees (2000). This approach results in an unconditionally stable equation. It is said to be first-order accurate on time and second-order accurate on space. This equation is shown below:

$$\rho \Delta V\left(\phi_P^{n+1} - \phi_P^n\right) = \left[F_N^D + F_S^D + F_W^D + F_E^D\right]^{n+1} \Delta t \tag{2.57}$$

Where:

n = Variables at previous time step

n+1 = Variables at current time step

Δt = time step

N,S,W,E = sub index used to denote the face of the cell.

The final equation for a control volume can be determined after the integration and discretization procedures have been applied. Each control volume will have the form:

$$a_p \phi_p = \sum_n a_{nb} \phi_{nb} + b \qquad (2.58)$$

Where:

a , b = coefficients of the algebraic equations

ϕ_{nb} = Variable at defined cell

n = North, south, west, east

The a_p value for one control volume becomes a_{nb} for the next cell. Therefore, in a two dimensional model, a penta-diagonal matrix is formed and can be solved with a convenient matrix solver technique. The method used by Ress, et al. (2002) is the Strongly Implicit Method (Stone, 1968).

The grid is generated using blocks of cells. The blocks are described as a regular rectangular array of cells. Each interconnected block has the same number of cells. Thus, the shape of the edge (i.e. lines, arcs) is not particularly important. In general, it is necessary to have at least 4 blocks to represent the pipe and pavement layer containing the pipe. More blocks can be used if more layers are necessary. See figure below:

n+1 = Variables at current time step

Δt = time step

N,S,W,E = sub index used to denote the face of the cell.

The final equation for a control volume can be determined after the integration and discretization procedures have been applied. Each control volume will have the form:

$$a_P \phi_P = \sum_{nb} a_{nb} \phi_{nb} + b \qquad (2.58)$$

Where:

a , b = coefficients of the algebraic equations

ϕ_{nb} = Variable at defined cell

n = North, south, west, east

The a_p value for one control volume becomes a_{nb} for the next cell. Therefore, in a two dimensional model, a penta-diagonal matrix is formed and can be solved with a convenient matrix solver technique. The method used by Ress, et al. (2002) is the Strongly Implicit Method (Stone, 1968).

The grid is generated using blocks of cells. The blocks are described as a regular rectangular array of cells. Each interconnected block has the same number of cells. Thus, the shape of the edge (i.e. lines, arcs) is not particularly important. In general, it is necessary to have at least 4 blocks to represent the pipe and pavement layer containing the pipe. More blocks can be used if more layers are necessary. See figure below:

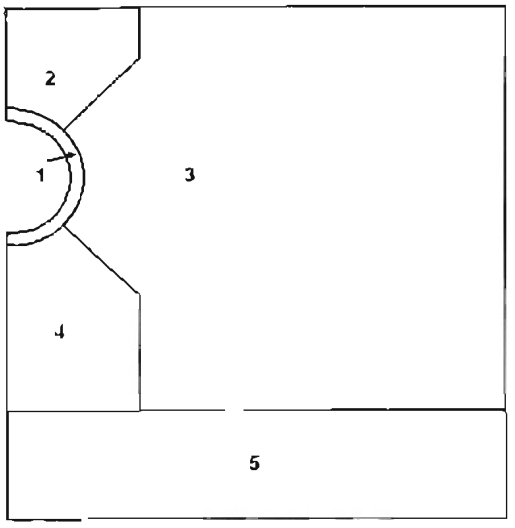

Figure 2.4-5: ***Block definitions on a typical grid layout***

The cell distribution on the grid must be optimized. To optimize the grid a higher cell density is applied where higher temperature gradients are expected. Other regions use large cell sizes. The density of the cells determines the accuracy of the solution. However, there is also a strong relation between the density of the cells and the computational time required. The higher the cell density, the more computational time required.

According to Spitler, et al. (2001), a higher density grid for this application is desirable close to the pipe. It is in this point where the higher temperature gradients are found. To follow this criterion, an exponential distribution of the grid is applied between the corresponding block edges. The equation used for the distribution is shown below:

$$exponential_i = \frac{e^{\frac{i \cdot exponent}{n}} - 1}{e^{exponent} - 1} \tag{2.59}$$

Where:

i = cell counter that varies from i to n-1 (number of cells in distribution line).

exponent = normalized distribution along the line or arc.

The grid generation rests on several prior determinations. In order to ensure there is enough space for a correct grid generation the value of pipe spacing and depth under the surface are checked. The minimum value can be shown to be 1.5 times the outer diameter of the pipe. An example of the grid generated for this model is shown in Figure 2.4-6.

The estimated number of cells is obtained from the geometric description of the slab. The model determines the number of cells required for slabs of different sizes. A full description of the cell generation procedure can be obtained form Spitler, et al. (2001).

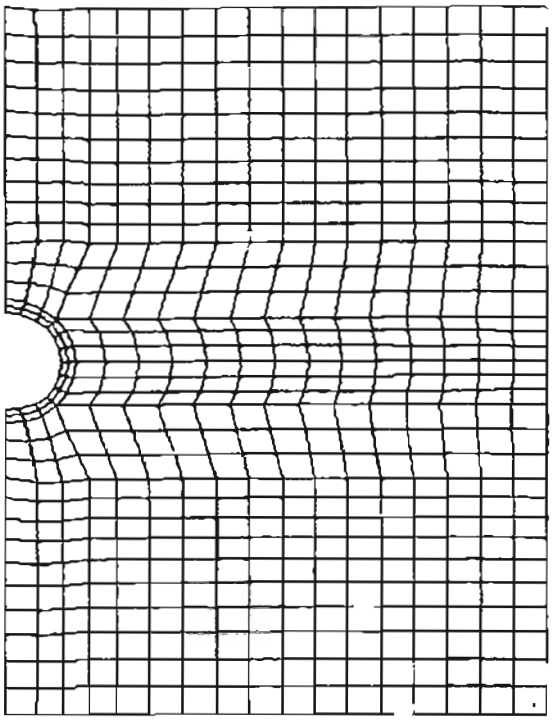

Figure 2.4-6: ***Grid generated for hydronic system***

The finite volume solver is coupled with the boundary condition models by exchanging information about the surface temperature. However, since the temperature is constant at the melting point it is necessary to use the heat flux calculated by the finite volume solver. The boundary condition solver is used for the surface temperature calculation. This process is iteratively repeated until the temperature converges. At convergence, the heat flux calculated by the finite volume solver is consistent with the temperature calculated by the boundary condition model.

The boundary conditions used in this model are similar to those used in the previously analyzed model (FD-RG). The boundary condition model is a collection of models. The heat balance is satisfied at the surface nodes according to the condition of the slab. The conditions on the surface of the slab can be: dry, wet, dry snow, slush, snow

and slush, solid ice, and solid ice and water. These conditions are summarized in Table 2.4-1. Probably the most complex and interesting model is the model describing snow melting.

Surface condition	Properties
Dry	Surface free of liquid.
Wet	Surface with liquid and above the freezing point.
Dry Snow	Fresh fallen snow with no liquid or previous precipitation. Surface below the freezing point so no snow melting occurs.
Slush	Surface contains ice with snow crystals that are fully saturated with water. Surface temperature at freezing point.
Snow and slush	Surface contains snow that is partially melted. The lower part of snow is saturated with water and the upper part is fresh snow. Surface temperature at freezing point.
Solid ice	Frozen water over the surface of the slab. Surface temperature under the freezing point.
Solid ice and water	This condition can occur when the ice is being melted or if there has been a rain even over the icy condition.

Table 2.4-1: ***Surface conditions over the heated slab***

Heat and mass transfer is calculated for each cell of the grid on each time step. According to Rees, et al. (2002) the calculation of the height of the saturated layer in the snow permits calculation of the mass of dry snow. So, in addition to heat balance, it is necessary to keep track of mass transfer for each time step. In order to keep track of the surface condition the slab is considered dry unless any of the conditions that would change this dry condition arise.

The 1-D snow-melting model

As described by Rees, et al. (2002), during the melting process the snow can be considered as a layer of "dry" snow (only crystals with no liquid) and a layer of saturated

snow (slush) close to the slab surface. Both are considered to be porous media, one with air and the other with water in the void space between crystals.

Mass transfer occurs as shown in Figure 2.4-7. The quantity of snow and rain is determined from weather data. Snowmelt rate is determined by energy balance. As a result, the slush line moves such that previously dry snow becomes slush. Some mass is exchanged with the snow layer, and some mass change results from evaporation of the liquid layer.

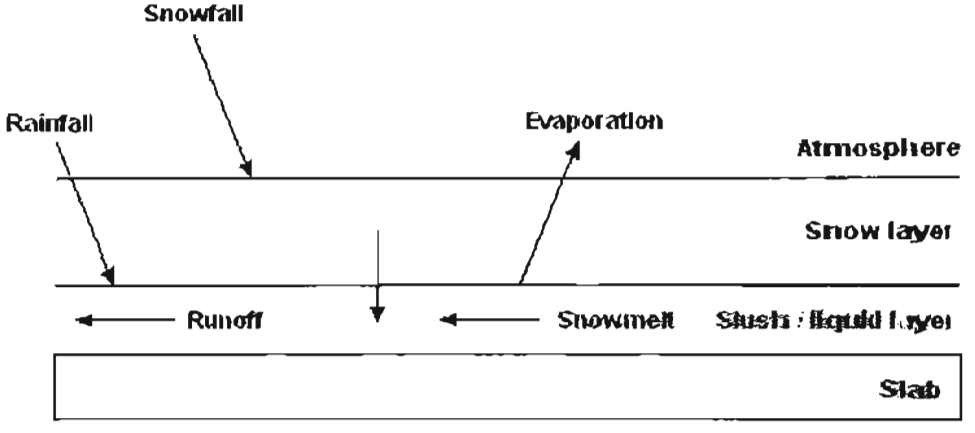

Figure 2.4-7: ***Mass transfer on snow melting model***

A three-node model is used to model the heat transfer for the snow-melting model. The first node is located at the upper surface of the snow layer. The second node is located at the center of the snow layer. The last one is located at the saturated slush layer. This model is represented in Figure 2.4-8.

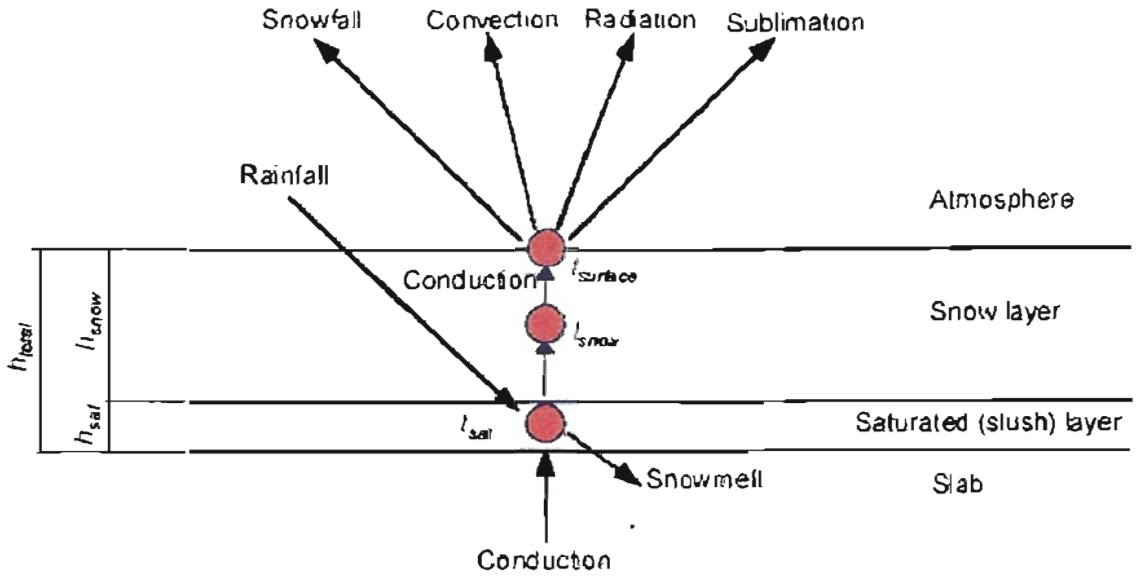

Figure 2.4-8: ***Schematic representation of heat transfer in the three-node snowmelt model***

The assumptions of this model are:

- Uniform temperature in the slush/liquid layer.
- Melting of snow occurs at the lower node only.
- Transfer of solid snow form the snow layer to the slush layer is explicitly accounted by the mass balance.
- While convection from the upper surface of the snow is accounted for, convection due to airflow through the porous snow layer is neglected. (The model can include this condition if necessary).
- Convection and evaporation from the slush layer are neglected when covered with a layer of dry snow.

- Rainfall occurring after a snow layer has formed is accounted for directly only at the saturated layer.

- The snow melting process is treated as a quasi-one dimensional process.

This model is formed by five primary equations: mass balance for the solid ice, a mass balance for liquid water, and a heat balance on each node.

Mass balance for ice:

$$\frac{dm_{ice}}{d\theta} = m''_{snowfall} - m''_{melt} \tag{2.60}$$

Where:

m_{ice} = Mass of snow per unit area in the snow layer, (kg/m^2 or lb/ft^2)

θ = Time, (s or hr)

$m''_{snowfall}$ = Snowfall rate in mass per unit area, [$kg/(m^2s)$ or $lb/(ft^2h)$]

m''_{melt} = Rate of the snow transferred to the slush in solid form, [$kg/(m^2s)$ or $lb/(ft^2h)$]

Mass balance on the liquid is given by:

$$\frac{dm_l}{d\theta} = m''_{rain} + m''_{melt} - m''_{runoff} \tag{2.61}$$

Where:

m_l = Mass of liquid water per unit area in the slush layer, (kg/m^2) or (lb/ft^2)

θ = Time, (s) or (h)

m''_{rain} = Rainfall rate in mass per unit area, [kg/(m^{2}s) or lb/(ft^{2}h)]

m''_{melt} = Snowmelt rate in mass per unit area, [kg/(m^{2}s) or lb/(ft^{2}h)]

m''_{runoff} = Rate of runoff in mass per unit area, [kg/(m^{2}s) or lb/(ft^{2}h)]

The amount of runoff is defined as the excess water on the slush layer due to melting. To take account for the capillarity action, the runoff is limited to 10% of the melt rate. This consideration is done until the saturated layer has 5.08 cm (2 in.). When this condition is reached the runoff is increased to the melt rate to prevent more water to be retained. This consideration is done due to the fact that capillary forces reach balance with gravitational forces. This assumptions where experimentally verified by Hockersmith (2002).

The total mass of snow and slush are required for the heat balance. This is done using a relative density of the snow and calculating the thickness of the layers. The total height is calculated by:

$$h_{total} = \frac{m_{ice}}{\rho_{ice}\left(1-\eta_{eff}\right)} \tag{2.62}$$

Where:

h_{total} = The total thickness of the snow and saturated layers, (m or ft).

m_{ice} = Mass of snow per unit area in the snow layer, (kg/m^2 or lb/ft^2)

η_{eff} = The effective porosity of the ice matrix (applies to both layers), (dimensionless).

ρ_{ice} = The density of ice, (kg/m^3 or lb/ft^3)

In the same way the thickness of the liquid layer is calculated from the mass of liquid:

$$h_{sat} = \frac{m_l}{\rho_l n_{eff}} \tag{2.63}$$

Where:

h_{total} = The total thickness of saturated layers, (m or ft)

m_l = Mass of liquid water per unit area in the slush layer, (kg/m^2 or lb/ft^2)

ρ_l = density of saturated layer, (kg/m^3 or lbm/ft^3)

n_{eff} = The effective porosity of the ice matrix , (dimensionless)

The height of snow is calculated by subtracting the height of saturated layer from the total height. Once this value is found the mass of snow can be calculated. Thus, it is used on the energy balance equations.

$$m_{snow} C_p \frac{dT_{snow}}{d\theta} = q''_{conduction\_snow} - q''_{snowfall} - q''_{convection} - q''_{radiation} \tag{2.64}$$

The conduction heat flux of the slush layer to the snow layer is calculated as:

$$q''_{conduction,snow} = \frac{k_{snow}}{0.5h_{snow}}\left(T_{slush} - T_{snow}\right) \tag{2.65}$$

The heat flux due to new snow over the surface is given by:

$$q''_{snowfall} = m''_{snowfall} C_{p\ ice}\left(T_{snow} - T_a\right) \tag{2.66}$$

The convective heat flux in the upper surface of the snow is given by:

$$q''_{convection} = h_c\left(T_{surface} - T_a\right) \tag{2.67}$$

The radiative heat flux is given by:

$$q''_{radiation} = \sigma\varepsilon_s\left(T^4_{surface} - T^4_{MR}\right) \tag{2.68}$$

Where:

k_{snow} = conductivity of snow, [W/(m K) or Btu/(h ft °F)]

h_{snow} = height of snow, (m or ft)

T_{sluh} = Temperature of slush, (°C or °F)

T_{snow}= Temperature of snow, (°C or °F)

T_a = Temperature of air, (°C or °F)

$T_{surface}$ = Temperature of surface, (°C or °F)

T_{MR} = Mean radiant temperature, (°C or °F)

σ = Stephan-Boltzmann constant = 5.67×10^{8}, [W/(m^2 K^4) or BTU/(hr ft^2 °R^4)]

ε_s = Emissivity of surface (snow or dry), (dimensionless)

h_c = heat convection coefficient, [W/(m^2 °C) or Btu/(h ft^2 °F)]. (Convective heat transfer coefficient is calculated as described in equations (2.31) to (2.35))

An iterative process is used to calculate the snow surface temperature. Since the surface temperature is used in the convection and radiation heat calculations the equations (2.67), (2.68), and (2.69) are used for this purpose. Then, the energy balance of the slush node is used since at this point the mixture of liquid ice is at equilibrium. The energy balance is shown in equation (2.70).

$$T_{surface} = T_{snow} - \frac{0.5 h_{snow}}{k_{snow}} \left(q''_{convection} + q''_{radiation} \right) \tag{2.69}$$

Energy balance at slush node:

$$m''_{melt} h_{if} = q''_{conduction\_slab} + q''_{rainfall} - q''_{conduction\_snow} \tag{2.70}$$

Where:

m''_{melt} = Snowmelt rate in mass per unit area, [kg/m^{2}s or lb/ft^{2}h]

h_{if} = Latent heat of fusion of water, [J/kg or Btu/(h.lb)]

Assuming that rainfall is at air temperature, the heat flux due to rain is given by:

$$q''_{rainfall} = m''_{rainfall} C_{p\,water} \left(T_a - T_{slush}\right) \tag{2.71}$$

Where:

$q''_{rainfall}$ = Heat flux due to rain, [W/m^2 or BTU/(hr ft^2)]

$m''_{rainfall}$ = Rainfall in mass per unit area, [kg/m^{2}s or lb/ft^{2}h]

$C_{p\ water}$ = Specific heat of water, [J/(kg °C) or BTU/(lb °F)]

T_a = Temperature of air, (°C or °F)

T_{sluh} = Temperature of slush, (°C or °F)

This model has been only partially tested. Hockersmith (2002) used the snow-melting correlation of this model for his experimental investigation. However, his experimental apparatus was a lab-scale flat electrical heater. Therefore, the numerical solver used to calculate the heat flux on the surface was not used. In Hockersmith's (2002) investigation, the power used by the heater was directly passed to the snow-melting correlations. Thus, only the snow-melting correlations where tested.

2.5 Experimental investigations

There are several experimental investigation performed. Mainly, experimental investigations of snow melting have been done in cases where industrial de-icing or snow melting is required over industrial equipment using direct steam or hot air blowers in experimental designs. In the case of snow melting applications on slabs limited experimental validation is performed. The authors of the snow melting models do most of

the experimental investigation while developing their models. However, two experimental analyses are considered in this study.

The first one is the experimental validation presented by Aoki, et al. (1987). The paper presented showed the investigation of snow melting process by heating a plate covered with snow. The second study is a thesis presented by Hockersmith (2002). In this report an experimental and computational analysis of the 1-D transient snow-melting algorithm used by Rees, et al. (2002) in their model is discussed.

2.5.1 Snow melting by heating from the bottom (Aoki, et al. 1987)

In this experimental investigation the researchers based their work on the concept of capillarity rise of a fluid on porous media. This rise is caused by the difference in pressure of the hydrostatic column of the liquid with the one produced by the surface tension of the liquid in contact with the porous media inside the void space. This is the same phenomenon that occurs while snow is melting. The capillarity pressure is balanced with the hydrostatic pressure of the melted water. When the water column reaches the equilibrium point, it will overspill outside the snow media. Aoki uses this concept to formulate his model based on parallel capillary tubes of different sizes packed together.

The researchers heat up a plate with snow on it and observe the different melting process occurring on the snow. By doing these experiments they classified the snow in 3 classes depending on the air temperature surrounding the experimental snow:

Class A

Occurs when the temperature of the surroundings is near 0°C (32°F). The melting process occurs after the plate has been heated up. While the snow melts, the water rises due to capillary action of the porous media. The water infiltration moves upward. If the snowmelt rate is bigger than the water permeation the water drainage occurs. There are two subtypes in this class. A1 occurs when the snowmelt is bigger than the water permeation. Conversely, A2 occurs when the waterfront reaches the upper surface of the snow.

Class B

This type of snow melting is produced when the temperature of the surroundings is less than the freezing point. In this case a re-freezing of the melted water occurs. After the plate is heated, the snow melts and the water permeates by capillary action. During the time when the water raises a portion of the snow layer freezes. The freezing does decrease the permeation of water. At this point, two subclasses are recognized. B1 occurs if the water permeation front has reached the upper surface of snow. In this case, an ice lens is formed over the snow surface. B2 occurs if the drainage happens before the water permeation front reaches the upper snow surface

Class C

This class is recognized in the case that the waterfront freezes inside the snow. The permeation rate is lower than the freezing rate. At this point the waterfront decreases and until a point where the freezing rate is lower than the permeation rate. When this

condition has arisen, the problem can become a class "B" or "C" again until all the snow is melted.

Aoki, et al. (1987) based its analysis on snowmelt Class "C". The equations used to describe this class are divided according to the different layers of the model. The first layer is the water permeation layer where the temperature is considered constant at 0°C (32°F). In this layer a transient mass balance is performed:

$$\varepsilon\rho_w \frac{dS_{wp}}{dt} = -\frac{dm}{dx} - u_x \varepsilon\rho_w \frac{dS_{wp}}{dx} \tag{2.72}$$

Where:

ε = Porosity, (dimensionless)

ρ_w = Density of water, (kg/m^3 or lb/ft^3)

x = Height, (m or ft)

m = Water permeation flux, [kg/(hr m^2) or lb/(hr m^2)]

u_x = Velocity due to the reduction in volume, (m/hr or ft/hr)

S_{wp} = Water content ratio, (dimensionless)

The second layer is the ice layer, where the temperature changes with time. Convection and conduction effects are considered.

$$\frac{dT_i}{dt} = a_i \frac{d^2T_i}{dx^2} - u_x \frac{dT_i}{dx} \tag{2.73}$$

Where:

T_i = Temperature of ice layer, (°C or °F)

t = time, (hr)

a_i = Thermal diffusivity of ice, (m^2/hr or ft^2/hr)

u_x = velocity due to the reduction in volume, (m/hr or ft/hr)

x = Height, (m or ft)

The third and last layer is the "virgin snow" layer. In this layer, the temperature changes on time. This layer also includes convective and conductive effects but in this case a porous matrix is used.

$$\frac{dT_p}{dt} = a_p \frac{d^2T_p}{dx^2} - u_p \frac{dT_p}{dx} \tag{2.74}$$

Where:

T_p = Temperature of porous layer, (°C or °F)

t = time, (hr)

a_p = Thermal diffusivity of the porous layer, (m^2/hr)

u_x = velocity due to the reduction in volume, (m/hr)

x = Height, (m or ft)

Finally, the boundary conditions used in the model are convection only for the upper surface of the snow and constant heat flux and 100% water saturation on the bottom surface in contact with the plate. The equations are solved with a finite difference method and variable space network to move the boundary layers with the layers.

This study shows that heat loss from the upper surface vary depending on the snow pattern. Therefore, the melting time required by the snow depends on the water permeation and the saturated layer refreezing. The model was also able to estimate the water drained from each layer with the experimental observation.

2.5.2 Hockersmith experimental investigation

The experimentation performed by Hockersmith (2002), is based on an extensive research of the snow melting theory. The properties of snow and its metamorphism are taking into consideration on this document. Metamorphism is a characteristic of snow due to the change in shape of the snow crystals during the melting process.

For his experiments, Hockersmith (2002) used an electrically heated plate to melt snow from the bottom in a controlled environmental chamber. Measurements on the crystal size, water runoff, capillarity height of snow (maximum saturation layer height), and plate temperature under different values of heat flux were evaluated. The results from these experiments were compared with the 1-D transient model used by Rees, et al. (2002).

The results of the experimentation showed that the model predict a linear snow melting rate. However, compared to the experimental data, the snow-melting rate decelerated during the last hour of the experiment. Hockersmith (2002) attribute this

effect mainly to "inhomogeneous melting" of the snow. The phenomenon is associated with the snow metamorphism when the water has saturated the snow (during the slush period). Nevertheless, the 15% difference observed during the experimentation was also associated with uncertainties due to the model itself. In the model, side and bottom heat loss were not considered.

Another important observation was the water runoff model. This parameter has a direct influence on the maximum saturation layer height. When compared with the experimentation, a time delay between the modeled runoff and the experimental runoff was confirmed with an error of up to 20%. To correct this problem, Hockersmith (2002), include a simple runoff model that drained water form the slab at a constant rate. The error then was reduced to 5% for the same case scenario.

CHAPTER 3

EXPERIMENTAL APPARATUS

3.1 Introduction

The experimental apparatus consists primarily of a hydronically heated concrete slab and a snow-making environmental chamber. The concrete slab was embedded with hydronic tubing and is connected to a circulating pump and a controllable electric heater. The slab is instrumented with a number of thermocouples. Power input to the heater and the pump is measured as function of flow rate and differential temperature of the fluid.

The environmental chamber is used to control the conditions surrounding the slab. In the environmental chamber, it is possible to maintain temperatures around the concrete slab and to simulate snowfall over its surface. Air and surface temperatures were measured at a number of locations in the chamber. A detailed description of each component is given in this section. A data logger is used to collect the information provided by the slab and from the environmental chamber.

Two auxiliary experimental apparati were required. The first one was used to measure the conductivity of the concrete used in the slab. The second one was used to measure the specific heat of the concrete. These two important parameters are basic data

required by the snow melting models. The experimental apparatus used in each case are described at the end of this section.

3.2 Concrete Slab

The concrete slab was constructed using a wooden frame (mold), which subsequently remains attached to the slab. The plywood is 0.0191 m. (0.75 in) thick. The void space is filled up with fast setting concrete (Quikrete). The dimensions of the concrete are: 0.914 m (36 in) length, 0.864 m (34 in) wide, and 0.152 m. (6 in) depth. The length dimension is said to be the same direction as the hydronic tubing.

Three parallel lines of hydronic tubing were located inside the frame in the direction of the length as shown in Figure 3.2-1. The distance between the pipes is 29 cm. (11.5 in) taking as reference the pipe located in the center of the frame. The pipe used has an outer diameter of 15.87mm (5/8 in) and wall thickness of 2.4 mm. (3/32 in). The specification for the pipe material is Polyethylene PEX, SDR-9.

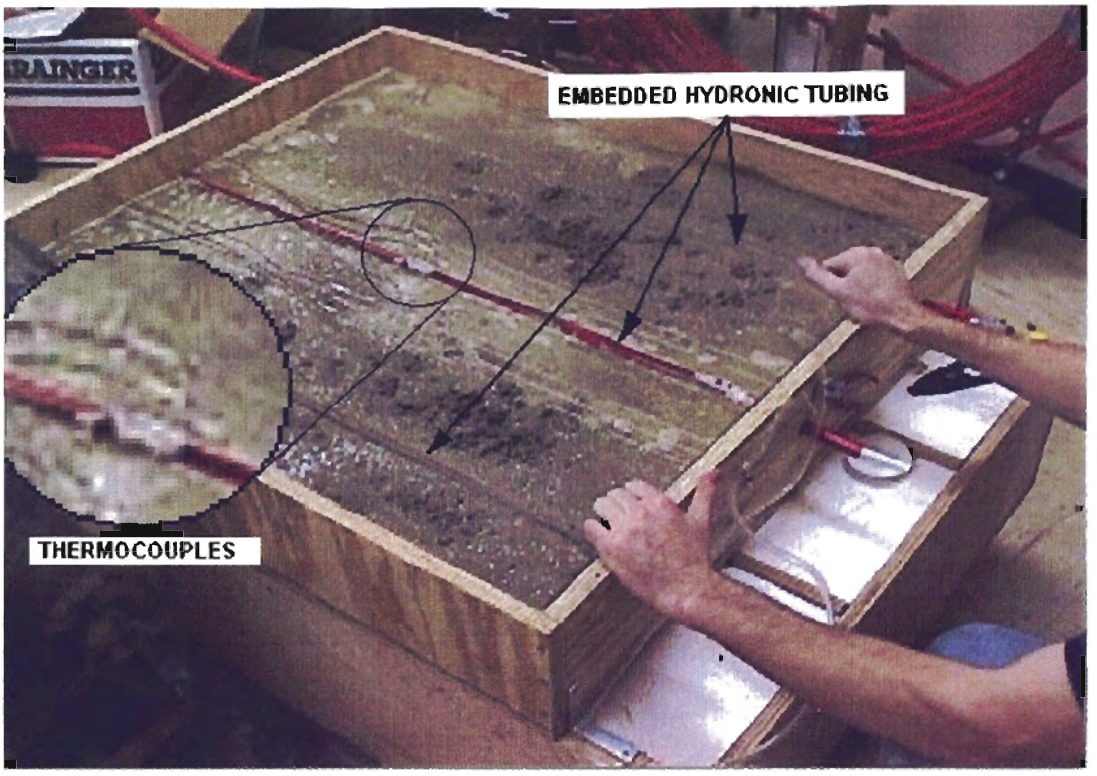

Figure 3.2-1: ***Thermocouple and tubing placement during concrete pouring process***

Thermocouples are placed in several positions across the central section of the concrete slab as shown in Figure 3.2-1. Thermocouple positions are given below in section 3.2.3.

Concrete was poured inside the wooden frame to create the concrete slab. The tubes were held in position during the construction process by rigid aluminum pipes inserted into the tubing. The thermocouples were hold in position using taut line. The freshly poured product is shown in Figure 3.2-2.

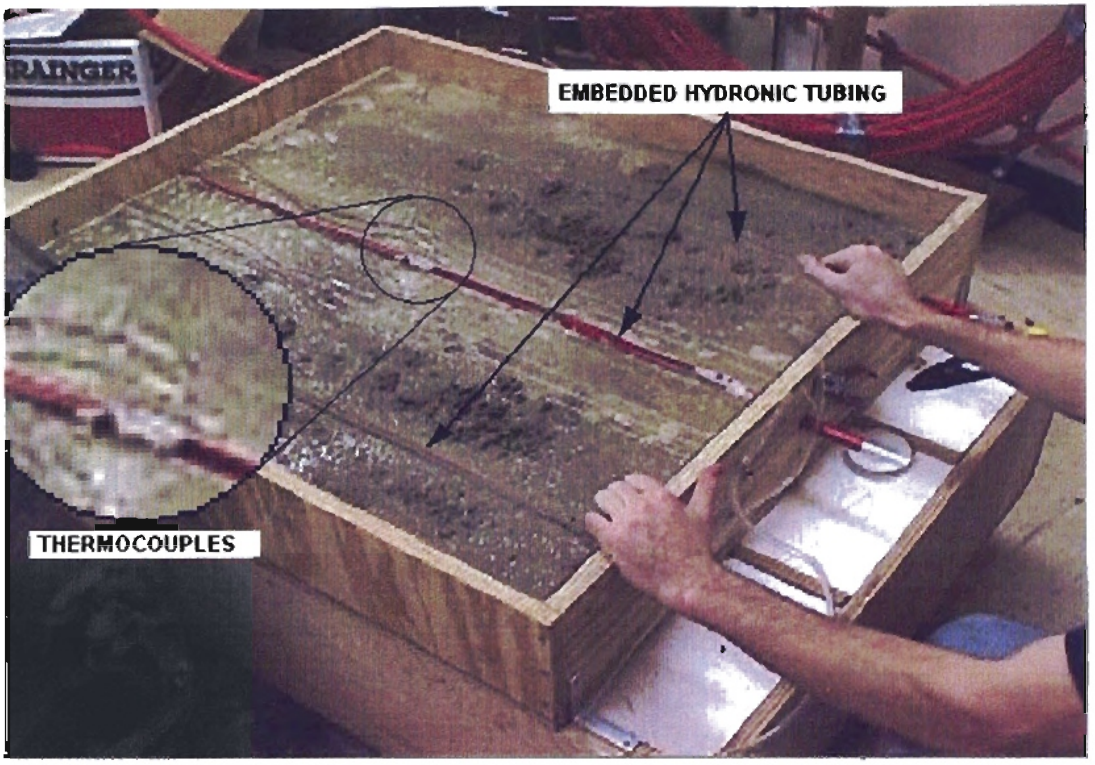

Figure 3.2-1: ***Thermocouple and tubing placement during concrete pouring process***

Thermocouples are placed in several positions across the central section of the concrete slab as shown in Figure 3.2-1. Thermocouple positions are given below in section 3.2.3.

Concrete was poured inside the wooden frame to create the concrete slab. The tubes were held in position during the construction process by rigid aluminum pipes inserted into the tubing. The thermocouples were hold in position using taut line. The freshly poured product is shown in Figure 3.2-2.

3.2.1 Base

An insulated base on casters supports the concrete slab. This section was constructed with 0.019 m (0.75 in) thick plywood. This section is filled with 0.254 m (10 in) of extruded polystyrene. Plexiglas was used under the central section where the slab is placed in order to prevent that concrete from flowing into the insulation during the construction process. The total dimensions of the base are 0.851 m (33.5 in) wide, 1.251 m (49.25 in) long, and 0.279 m (11 in) tall.

The base and slab are covered on the sides by 0.127m (5 in) of extruded polystyrene, which is covered with 0.019 m (0.75 in) thick plywood. A diagram of the slab and base is shown in Figure 3.2-4. The side covers are held on tightly by rubber grips and sealed with silicon in order to prevent circulation of air between the side cover and the slab.

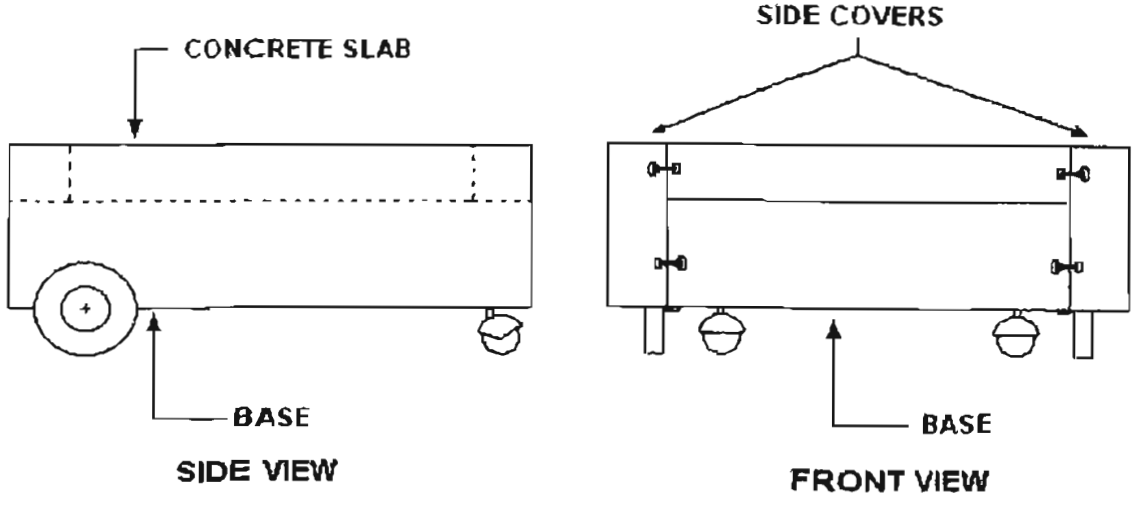

Figure 3.2-4: ***Concrete slab and base***

The whole system needs to be transportable in order to move it in and out of the controlled chamber. Therefore, two pairs of wheels are attached to the base. The first pair is located in the 0.152 m (6 in) from the front side of the base. This pair of wheels is 0.254 m (10 in) in diameter. They are attached to an axle, which is fixed to the bottom of the base. The second pair is located at 0.1016 m (4 in) from the backside of the base. A detailed central section for the base construction is shown in appendix C.

3.2.2 Heating System

The hydronic heater included in the slab uses Ethylene Glycol (50% volumetric concentration) as working fluid. It is circulated using a Grundfos pump, model 2P410. An AC electric heater was also integrated in the piping system and allows adjustment of the power input to the working fluid. The maximum capacity of the heater is 1500 W. In order to measure the flow rate in the system, an in-line liquid flow meter was used. Additionally, two calibrated thermocouples were used. One was placed in the inlet pipe of the system. The second is positioned on the outlet pipe of the system. A simplified piping diagram of the system is shown in Figure 3.2-5.

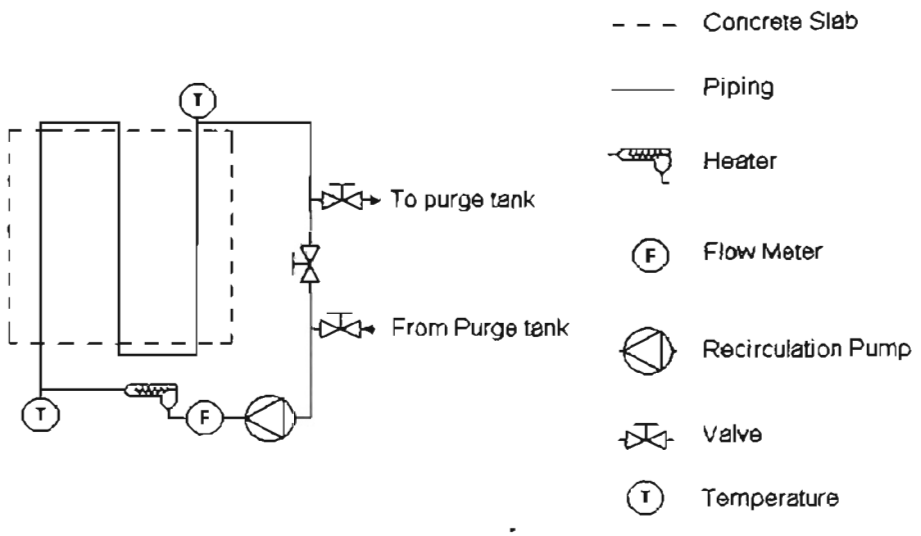

Figure 3.2-5: ***Concrete Slab simplified piping diagram***

Before the first run of the system it is necessary to remove tramped air from the system. For this reason, a set of ball valves was used before the inlet of the pump. The ball valves allow the user to connect a purge tank where the working fluid can be separated from the air and circulated. After the first run the purge tank is removed and the valves aligned for flow through the slab.

The free space in the front of the concrete slab is used to place all the auxiliary equipment. The auxiliary equipment includes the circulation pump, the in-line liquid flow meter, the heater, connection piping, and in-flow thermocouples. The auxiliary equipment was covered with insulation. However, it was necessary to reduce the insulation for the slab in this point in order to make room for the auxiliary equipment.

Since the main elements (i.e. heater, pump) require almost all the space available it is not possible to cover this side with a wooden cover. As a result, the insulation around these elements is only 38.1 mm (1.5in) thick and additional energy loss is expected from

the slab in this region. In Figure 3.2-6a, the auxiliary equipment can be seen before being covered with insulation. Figure 3.2-6b shows the auxiliary equipment after being covered with insulation.

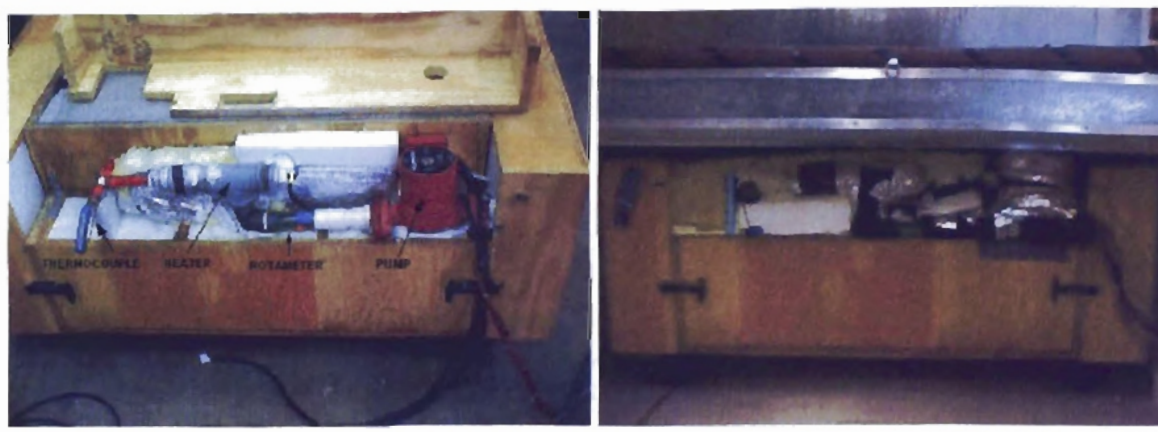

Figure 3.2-6: a) ***Auxiliary equipment, b) auxiliary equipment covered with insulation inside the snow chamber***

The pump and the heater produce the power input in the system. The power input produced by the pump is regulated with a VARIAC (Variable ratio transformer) device. The VARIAC can control the voltage from 0 to 130% of the nominal voltage (115 V) and has a maximum capacity of 7.5 A of current. Additional power input is available by using the electric heater. A second VARIAC controls the power input produced by the electric heater.

3.2.3 Instrumentation

The concrete slab and the hydronic heater are fully instrumented. The temperature measurement is done with 20 type T thermocouples. It is possible to observe the position of some thermocouple during the construction process in Figure 3.2-3. A 2-D schematic

drawing shows the thermocouple position in Figure 3.2-7. The coordinates where the thermocouples are placed in reference to the central pipe are shown on Appendix C.

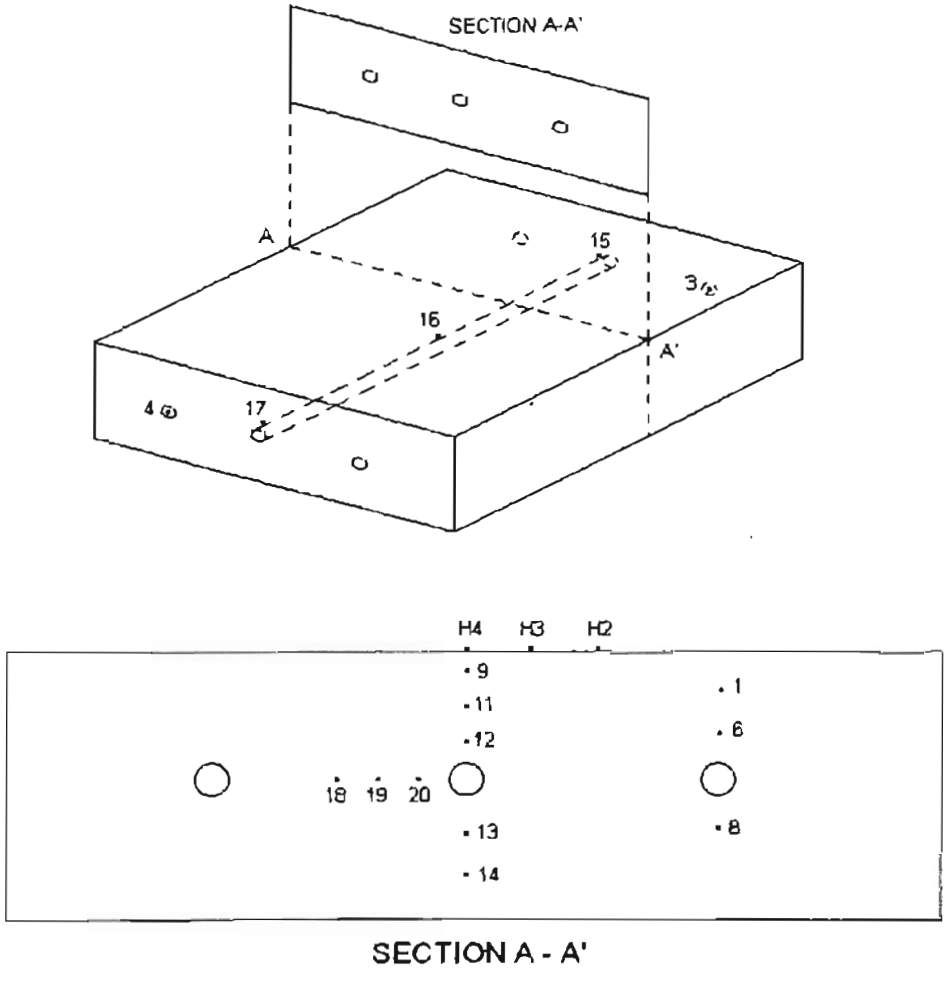

Figure 3.2-7: ***Position of thermocouple at the concrete slab***

Only thermocouples 4 and 3 (inlet and outlet of the embedded piping) are calibrated. The thermocouples were calibrated to ± 0.05°C. The calibration process can be found in appendix A. Unfortunately, there was no documentation about the calibration for the rest of the thermocouples used in the concrete slab. Therefore, the expected accuracy for them is ± 0.5°C.

The power used by the circulation pump and the heater is also measured with watt transducers installed in line with each component. Originally, the flow rate measurement was intended only as a control parameter only and was not important for the power calculation. But, due to uncontrolled heat losses from the piping outside the slab, it is not possible to use the measured value directly. Still, the power measured by the watt transducers is used as a check. The heat transfer to the slab is estimated using the flow rate reading available from the in-line rotameter and the inlet and outlet thermocouples.

The in-flow rotameter is a VTP-4020. This model provides a measurement with accuracy of ±8% full scale (±0.8 Lpm or ±0.20 GPM). This rotameter is viscous independent for fluids in the range of 1 to 100cSt. The variation for the viscosity for the Ethylene Glycol is between 1.85-4.55 cSt for these application. The rotameter cannot be accessed during the experimentation process, so the flow rate is measured at the beginning and end of the experiment.

One FLUKE Hydra II data logger is used to store the temperatures and reference power. The time interval used was 5-minutes. The information is downloaded and processed after the test.

3.3 Snow making / Environmental Chamber

The environmental chamber was designed to study the snow melting phenomena in interaction with the concrete slab. The system facilitates the study in the laboratory of similar process occurring on a bridge deck. Since it is not possible to get fresh snow all year round (it is even difficult to obtain during the winter season in Oklahoma), it is necessary to have equipment to produce artificial snow when required. Once the snow is

obtained, it is also necessary for the study purposes to maintain and control the environmental condition. This equipment can accomplish both tasks. Additionally, the environmental chamber has a specific compartment in which the concrete slab is placed.

The main criteria of design for the environmental chamber were the required dimensions. The first requirement was the ability to hold the concrete slab inside the chamber. For this reason the working area of the snow chamber top and central section is 0.91m x 0.91m (3ft x 3ft). The second requirement was that the size of the chamber should fit in the available room. This limits the height to 2.60m (8.53ft).

The environmental chamber was constructed in three separate sections in order to facilitate the movement to a different location if necessary. Each section has a specific objective. The bottom section holds the concrete slab. The central section has the equipment necessary to generate snow. The top section provides the necessary space for the snow to be formed. The top and central sections have the same working area in order to allow the formed snow to fall directly over the concrete slab. The bottom section has a working area of 1.52m (5ft) by 1.52m (5ft) in order to allow the whole concrete slab and the circulation equipment to fit into the chamber.

The front side of the environmental chamber has two access doors. The first is located in the bottom section and is used to allow the concrete slab to be rolled into the chamber. A door located in the central zone allows the operator to obtain digital pictures from the inside of the chamber during the melting process. Further discussion will be made in section 3.3.2. Both doors are insulated and closed during operation. The three sections are shown in Figure 3.3-8.

Figure 3.3-8: ***Environmental chamber sections***

3.3.1 Top section

The top section is a 1.00m (3.25ft) extension of the central section. The dimensions of the inside box are the same as in the middle section 0.91m x 0.91m (3ft x 3ft). In the roof of the top section is removable and contains a fluorescent light. The walls were built with 3.8cm x 14.0cm (1.5in x 5.5in) pine wood construction on 0.4m (16in) centers and filled with 13cm (5in) thick extruded polystyrene insulation. The inside walls were covered with 1.6 mm (0.0625 in) of hard plastic sheets that were sealed with silicone caulking to the surface of the insulation. This was done in order to provide an

internal waterproof insulation. The exterior wall uses 0.8mm (0.0313in) sheet metal jacket that prevent damage to the insulation.

The roof is made of extruded polystyrene since it has no associated load. The inside of the roof is covered with a hard plastic sheet to prevent water infiltration into the fluorescent light. The light was added to aid in photographic documentation of the experiments. The light is a standard 1.2m (4ft) fluorescent shop light. A sheet of Plexiglas was placed over the rectangular slot from the inside to reduce heat gain to the chamber and let the light shine inside. The light is controlled to automatically turn on during the picture acquisition only. This is discussed in section 3.6.

A 0.127m (5in) diameter hole was made on the backside of the top section. It holds a 0.61m (2ft) long piece of polyvinyl chloride (PVC) pipe used as the air return duct for the mechanical refrigeration system. If no mechanical refrigeration is needed this hole can be blocked with PVC end caps. The mechanical refrigeration system will be discussed later on in this section.

3.3.2 Central section

The central section has the same cross-sectional dimensions as the top section. The central section height is 1.60m (63in). Together the central and top section provides the room necessary for the snow to form. Longwill, et al. (1999) found that the snow making process require a height of 2.1m (7ft) for the snow to be produced. Further development and experimentation of Hockersmith (2001) shows that a better quality of snow can be achieved with longer residence time for the water droplets. Consequently, the total dimension of the tower is 2.60m (8.53ft).

The central section contains the snow making equipment. Two holes were made in the bottom of the sidewalls. On each side, a water nozzle uses the first hole and a liquid nitrogen nozzle uses the second. The holes were filled with hard plastic pipes and sealed with silicone. This prevents water from entering into the insulation or wood damaging it. The hard plastic pipes also allow an easy introduction of the nozzles into position. The snow making equipment will be discussed later on in this section.

The central section also contains the 0.61m by 1.22m (2 ft by 4 ft) access window, which has two purposes. The first one is to allow the operator access to the chamber. The window is hinged to allow access. The second purpose is to provide a clear view of the inside of the chamber while the system is running. A small opening of 12.7cm x 12.7cm (5in x 5in) was made in the clear cover. Thru this opening the digital camera's lens is placed. This device is used to acquire digital pictures of the surface of the slab during the snow-melting process.

During snow production the window is not in use, so a 12.7cm (5in) extruded polystyrene plug is used to cover it. On the other hand, during the melting process digital pictures are required. So, an alternate plug that holds the space for a Kodak digital camera replaces the standard plug. In order to prevent heat losses from the chamber the lens opening is sealed with Polyurethane foam. The lens opening is shown in Figure 3.3-9.

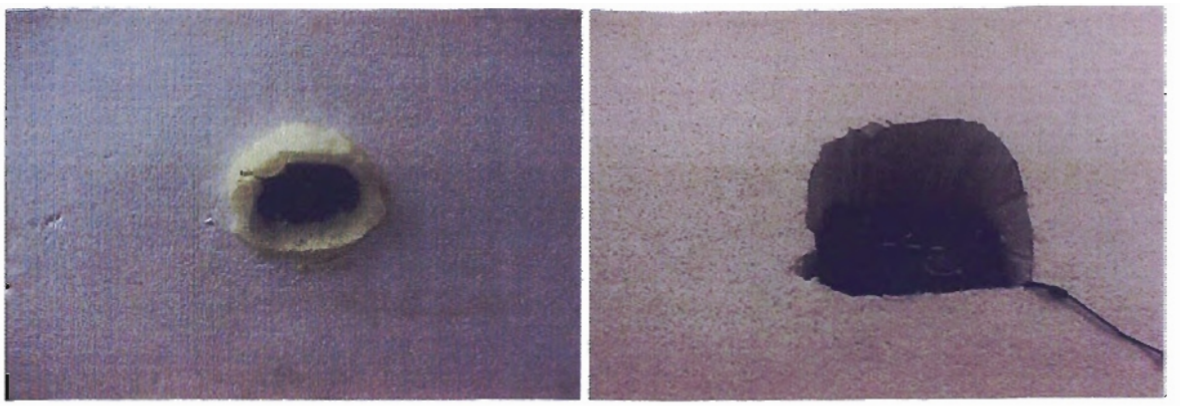

Figure 3.3-9: *a) Lens opening. b) Digital camera space in alternate plug*

3.3.3 Bottom section

The dimensions of the bottom section were established based on the requirements for the concrete slab and the diffuser for the mechanical cooling system. This section includes two doors of 0.91m (3ft) each in the front side to provide enough room for handling the concrete slab while loading. The material used for the doors are extruded polystyrene with a hard plastic cover for the inside, and sheet metal on the outside. The rest of the body construction is similar to the other sections using 3.8cm x 14.0cm (1.5in x 5.5in) pine wood construction on 0.30m (1ft) centers and 13cm (5in) of extruded polystyrene insulation. On the inside, the walls are covered with hard plastic and sealed with silicone caulking. The floor of the section is reinforced with 3.8cm x 14.0cm (1.5in x 5.5in) pine wood construction placed on 20.3cm (8in) centers in order to support the weight of the concrete slab.

A water collector and a drain hole were placed in the backside of the floor. The collector is used to drain the melt water. The drain channel, which runs from the side to side at the back of the chamber, is 2.54cm (1in) depth, 12.7cm (5in) wide. To remove the

liquid from the chamber, a hole was placed in the right side of the channel. The slope of the channel is produced by slightly tilting the structure.

The mechanical cooling diffuser is connected inside the bottom section by a 12.7cm (5in) hole. A 0.61cm (2ft) long piece of PVC pipe is inserted into the hole and sealed with silicon caulking. The diffuser has a U shape and is connected in the central section to the inlet pipe. The design of the diffuser is such that the velocity of the flow is kept to a minimum in order to prevent forced convection effects. The diameter of the diffuser is 12.7cm (5in) with 2.54cm (1in) holes. If the mechanical cooling is not used or the conditions don't allow the use of the diffuser, it can be removed and a PVC cap seals the inlet.

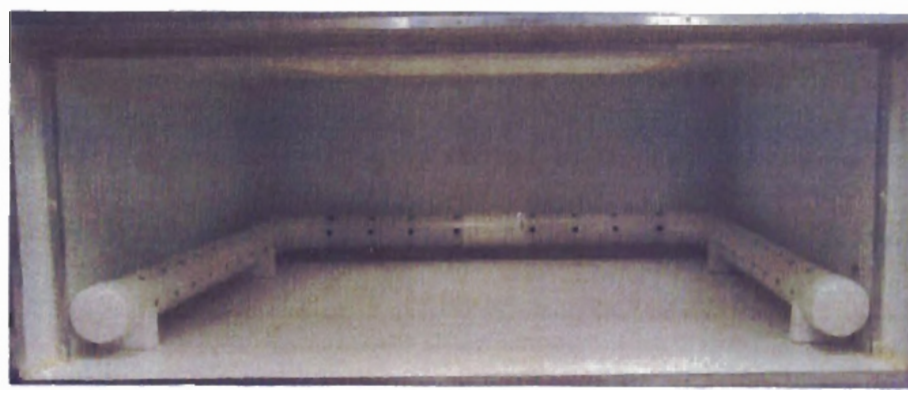

Figure 3.3-10: Mechanical cooling diffuser

3.4 Mechanical cooling

The environmental chamber is provided with a mechanical cooling system. This system is used to initially cool the environmental chamber to temperatures near freezing conditions. It also recreates the environmental conditions of the slab after the snow has been produced. The mechanical cooling apparatus is connected to the environmental

machine by the inlet pip

located in the top section. The elements used to produce the mechanical cooling are discussed next.

The system works with two recirculating chillers. The units consist of a Non-CFC air-cooled refrigeration system, circulation pump, work area bath (7L), and a microprocessor temperature controller. ThermoNeslab is the manufacturer of each unit (www.thermoneslab.com). The first unit has a cooling capacity of 750W (@ 0°C) (RTE-740) and the second unit has a cooling capacity of 500W (RTE-140) (@ 0°C). The pumping capacity of both chillers is 151 lpm @ 0 m head and 0 lpm @ 4.9 m head. The working fluid used is Ethylene Glycol with a volumetric concentration of 50%. Each of the chillers is connected in parallel arrangement to two fin-tube heat exchangers. The heat exchangers are located in an insulated box. It is made by 12.7cm (5 in) of extruded polystyrene insulation. The outside is covered with 6mm (0.25 in) plywood. Inside the box is covered with 1.6mm (0.0625 in) of hard plastic.

The heat exchanger box is connected to the inlet of the environmental chamber and to a fan box. The fan box is constructed in the same way as the heat exchanger box. It is covered with 0.8mm (0.0313in) sheet metal jacket. This fan box is used to supply air to the environmental chamber. Consequently, the fan inside the box can produce 0.08 m^3/s. The shaft of the fan was mounted thru the wall. So, the motor is installed outside the fan box in order to reduce as possible the heat gain by the system. The AC motor is a 120V/60Hz with power of 125 W.

The air-return duct connects the fan and the environmental chamber. The duct is connected to the top section of the environmental chamber. This duct was constructed with 10.16cm (4 in) PVC pipe and insulated in the outside with R-25 fiberglass bat insulation. The overall length of the duct is 4.6m (15 ft). A schematic drawing of the system is shown in Figure 3.4-11.

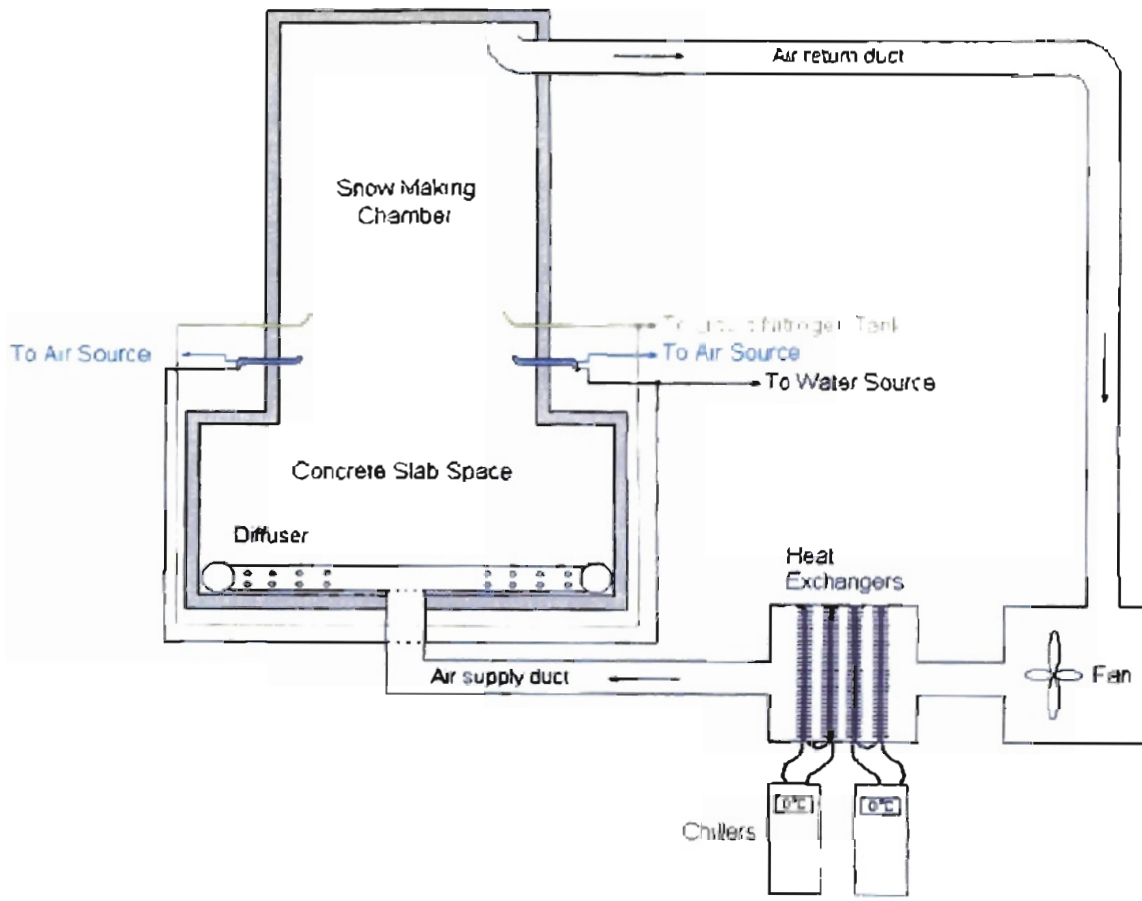

Figure 3.4-11: ***Snow making machine schematics***

3.5 Snow making equipment

The snow making equipment was designed in order to recreates the natural formation of snow. According to Hockersmith (2002), the natural snow is formed by

particles in the cloud that crystallize as they fall to the earth. Since the natural process has a fairly long residence time, the particles are able to grow in different shapes and sizes.

At lab scale, it is difficult to facilitate the formation of snow in a comparable short period of time. To maximize this effect the water droplets are jetted to the top of the chamber. This duplicates the traveled space for the particle. The traveled distance in the chamber is 5.2m (16ft). To form the jets several techniques have been suggested. Longwill, et al. (1999) proposed the use of a bottom nozzle array that mix air and water streams inside the piping system. In this way it boosts the water droplets using the 3 nozzles of the array. Hockersmith (2002) showed that the operation of the system is difficult and instead used two modified engine degreaser nozzles. In this approach water is pressurized to the nozzle and controlled with a trim valve on the degreaser. This system was very effective, but the trim valve was easily damaged. Longwill, et al. (1999) also showed that the temperature of water used for snow production has huge effect in the snow quality. For this reason, water near freezing is used in the system.

The system originally used was modified to avoid the use of the degreaser trim valve and to allow the use of pre-cooled water. The modification consists in connecting directly the air and water inlets to the nozzle. In this way the use of the trim valve was eliminated. Instead a globe valve was installed outside the nozzle body and directly on the water inlet pipe of each degreaser. The assembly is then connected directly to a pre-cooled water tank. The water inlet is controlled with the ball valves before each nozzle and the air is controlled using the regulating valve located in the control panel of the snow machine. See Figure 3.5-12a.

Two 0.64 cm (0.25 in) cooper-tubing lines are used to transport the liquid nitrogen into the chamber. The tubing is introduced by two 1.27cm (0.5 in) holes 12.7cm (5 in) above the water injection nozzles. The holes are fitted with 1.27cm (0.5in) PVC pipe and sealed with silicone caulking. The tubing is covered with 2.54 cm of foam wrap insulation. On the inside of the chamber the tubing is bend to direct the liquid nitrogen stream to water particles stream as shown in Figure 3.5-12. This rapid cooling helps on the snowmaking performance.

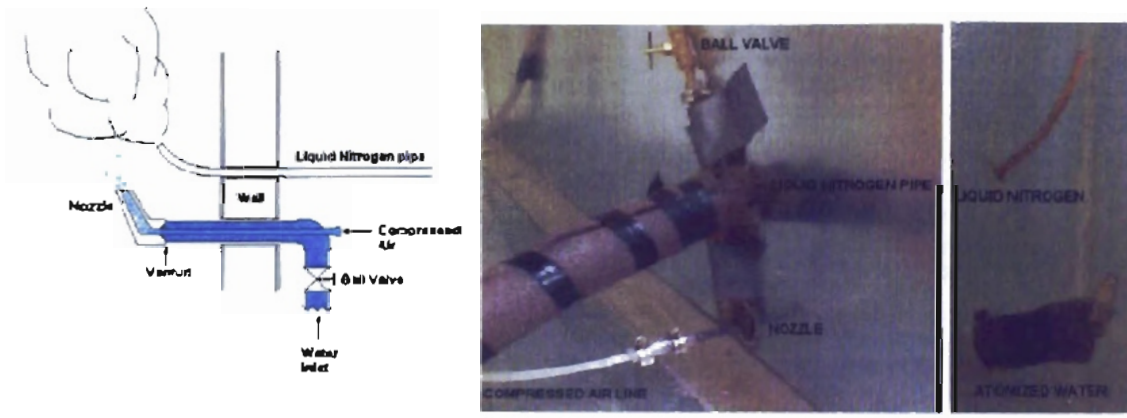

Figure 3.5-12: ***a) Modified nozzle schematics, b) Nozzles outside chamber, c) Nozzles inside the chamber***

3.6 Data acquisition controller

In order to acquire the digital images of the concrete slab surface a digital camera is used. A fluorescent light at the top of the chamber is switched on 2 seconds prior to the camera shutter opening and 2 seconds after the shutter is closed. Moreover, the digital picture has to be synchronized with the data logger data acquisition. All this effort is necessary to reduce the uncertainty produced by the introduction of unnecessary heat from the light inside the chamber.

The micro controller used is a Basic Stamp from Parallax Inc. The micro controller is timed to match the camera clock and reduce the total "on" time of the light to 7 seconds in each 10 minutes interval. Further discussion on the controller system can be found in Appendix B.

3.7 Concrete thermal conduction coefficient measurement apparatus

Two of the concrete samples made during the concrete slab construction were used to calculate the conductivity of the concrete used. The samples were cut to produce a 7.62 cm (3 in) diameter and 7.62 cm (3 in) tall cylinders. After polishing the top and bottom sides each sample was independently tested using a Single-Sided Hot-Plate apparatus similar to the one used in the ASTM C177-93 Standard.

This apparatus consists of a heavy insulated box, an electric heater plate, and a cooling plate. The insulation box is a 1.5 m x 1m x 1m box filled with extruded polystyrene and works as primary and secondary guard for the hot plate. A perfectly sized hole is made at the center of the insulation package were the sample, the heater plate, and the cooler plate are introduced as a single set. The testing pack can be seen in Figure 3.7-13.

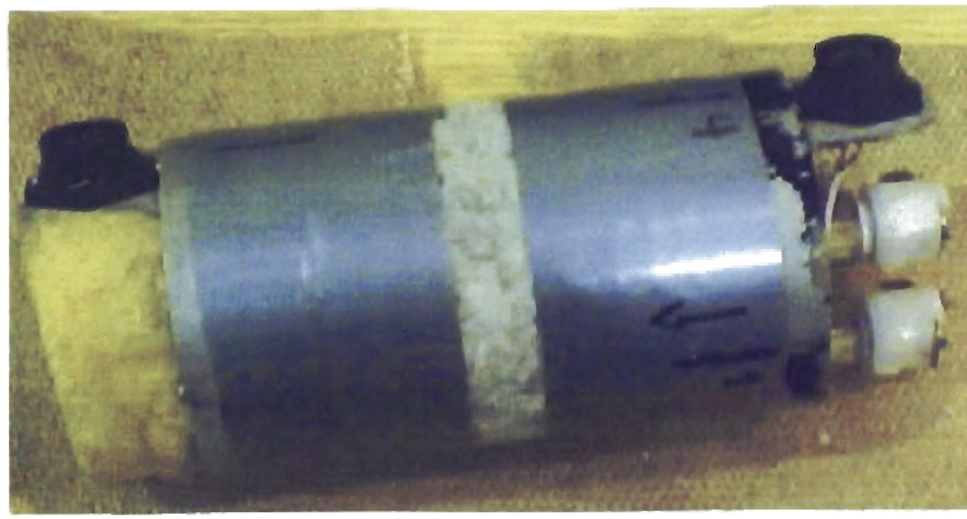

Figure 3.7-13: ***Concrete testing pack***

The heater plate is located in the left side of the pack. The heater uses an electrical resistance to produce the heat input. The sample and the plate are joined together by a thin film of a highly conductive paste (with known conductance) and held in place using duct tape. The heater plate is also provided with two temperature sensors (thermistors) to measure temperature symmetrically at the sample surface.

The cooling plate is located in the right side of the pack and it is used to keep the temperature of the sample from overheating. The circulation fluid is filtered water that runs in an internal channel of the plate. It is joint to the sample in the same way that the heat plate. The cooling plate has also two temperature sensors (thermistor) to measure the temperature symmetrically over the surface of the sample.

A 16-bit DAQ board connected to a PC computer does the data acquisition. The data samples are taken every minute. Consequently, it is possible to obtain a detailed temperature profile from each side of the sample and use it to calculate the conductivity

of the material. The analysis and results of the data acquired are shown in the next chapter.

3.8 Specific heat calculation apparatus

One concrete specimen was prepared for experimentation. The sample had the same characteristics as the one used for the conduction experiments. The only difference is that this sample has been supplied with a thermocouple placed in the center of the sample. The same thermocouple cable is used to place the sample in the correct position while inside the calorimeter. This is done to avoid the introduction of an alien object to support the sample into the calorimeter (i.e. wire basket to hold the sample). See Figure 3.8-14.

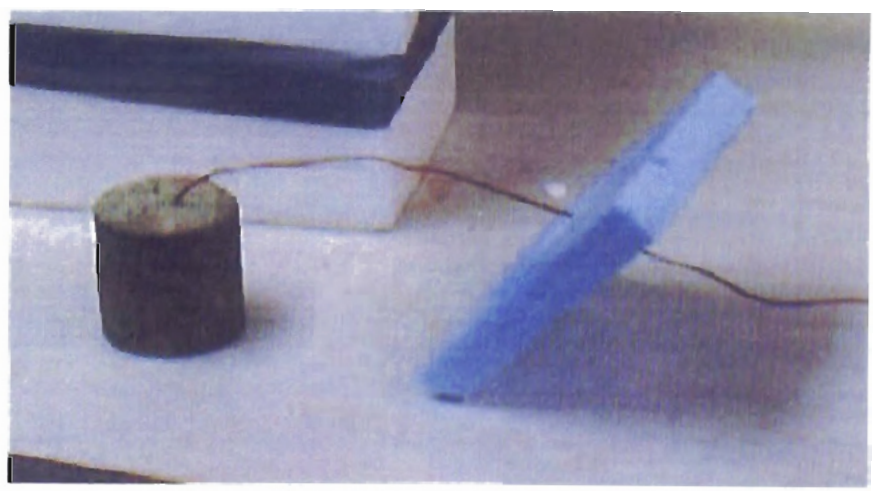

Figure 3.8-14: ***Concrete sample for Cp experimentation***

The calorimeter is a metallic Dewar flask with capacity of 2 liters. It is covered with a 101.6mm (4 in) extruded polystyrene insulation. This is done in order to prevent heat transfer from the environment. A blue foam cover is used at the top of the

calorimeter for the same reason. The hole created to pass the thermocouple cable was sealed with caulking. See Figure 3.8-15.

Figure 3.8-15: ***Calorimeter insulation***

An important part of the experiment is the drying of the sample. An electric oven was used to dry the sample. The sample needs to dry for 4 hours at a rated temperature of 150 °C (302 °F). After the oven-dried period, the sample must rest in a water bath for a period of 48 hours. Finally, the sample is weighted and introduced into a boiling water bath. The weighting process is done in order to make possible the measurement of the amount of water carried by the sample during the heating in the water bath. After the oven dry period, the wetting period, and the water bath period, the sample was weighted using a digital balance readable within ± 0.1g. The digital balance is shown in Figure 3.8-16.

Figure 3.8-16: ***Digital balance***

The temperature during the test period was measured at three different points. The first measurement point was the water bath used to heat up the sample. The second measurement point was the concrete sample. The third measurement point was placed inside the calorimeter to measure the temperature of the contained water. All the temperatures were acquired with cooper-constantan (Type T) calibrated thermocouples to ± 0.05°C (± 0.09 °F). The temperatures were recorded using a HP Hydra II data acquisition device.

CHAPTER 4

EXPERIMENTATION AND RESULTS

4.1 Introduction

This experimental investigation is oriented to validate the two snow melting models used to simulate and optimize snow-melting systems. These models are the Finite Difference Rectangular Grid (FD-RG) and the Finite Volume Boundary Fitted Grid (FV-BFG) models.

Several tasks were required in order to use these models. First, a model of the entire experimental apparatus (concrete slab and supporting frame) was developed. Since the specific thermal properties of the concrete used in the slab were not known, additional experimentation was necessary. The parameters investigated were conductivity and specific heat of the concrete. Third, modifications of the codes to accommodate the environmental conditions inside the snow chamber and the snow characteristics within the models were made. The final task involves the description of the initial conditions in each model. Therefore, the way in which each model is initialized is discussed in this chapter.

Two different scenarios were analyzed in order to validate the models: dry surface and snow covered conditions. Since a dry surface condition is the simplest case, it was

used to validate the conduction, convection and radiation portions of the mathematical model of the concrete slab. The second condition analyzed is the more complex scenario and used to validate the mathematical model of the snow-melting process. The experimental procedure used and the results obtained in each analyzed case are described in this chapter.

4.2 Thermal property measurements

Even with a correct implementation of the weather information the model will return wrong results without proper physical data for the materials used in the slab. Transient analysis requires the identification of specific heat for the material used. In this case the materials used are extruded polystyrene, plywood board, and concrete. The specific heat and thermal conductivity of extruded polystyrene and plywood have much lower volumetric specific heats than concrete and may be well characterized from the literature. However, according to Whiting, et al. (1978), concrete has a very wide range of variation (specific heat: 600-1500 J/(kg K) and thermal conductivity: 0.8 to 1.8 W/(m K)) depending on the composition (density) and water content of the concrete used. Therefore, it was necessary to measure the density, specific heat, and thermal conductivity of the concrete used.

4.2.1 Density measurement

The density of the concrete was established using the following correlation:

$$\rho = \frac{m}{V} \qquad (4.1)$$

Where:

ρ = Density, (kg/m^3 or lb/ft^3)

m = Mass, (kg or lb)

V = Volume, (m^3 or ft^3)

A concrete specimen was prepared using one of the concrete samples described shown in Figure 3.2-3. The dimensions of the sample were measured dividing the sample in quadrants. Therefore, two sets of diametric measurements on each side of the sample (top and bottom) and four length measurements were acquired. The instrument used to perform this task was a caliper readable within ±0.01mm. The values obtained after the measurements are shown in Table 4.2-1.

Quadrant	Core Length (mm)	Location	Diameter (mm)
1	76.32	U(1-3)	76.04
2	75.84	U(2-4)	76.04
3	76.30	L(1-3)	76.02
4	76.83	L(2-4)	76.02
AVG	**76.3**		**76.0**

Table 4.2-1: ***Geometric measurement values for concrete sample***

The volume of the sample is therefore determined with the following equation

$$V = \frac{\pi D^2}{4} L \tag{4.2}$$

Where:

V = Volume, [mm^3] or [ft^3]

π = Pi constant, [dimensionless]

D = Diameter, [mm] or [in]

L = Length, [mm] or [in]

The volume of the sample is 346572 ± 117 mm^3.

The concrete sample was oven dried during a period of 4 hours. After this period, the sample was weighed using a digital balance readable within ± 0.1g. The oven dried value obtained was: 725.4 ± 0.1g and the saturated value is 780.1 ± 0.1g.

Using equation (4.1), the density value obtained is: 2093.3 ± 0.6 (kg/m^3). The sample was retested under water saturation conditions and the obtained value is: 2250.8 ± 0.6 (kg/m^3).

4.2.2 Specific heat of concrete

The test procedure used to calculate the specific heat value for the concrete used in the slab followed the experimental procedure used by Whiting, et al. (1978). This is the same process used by the U.S. Army Corps of Engineers Specification CRD-C-124-73 (Method of Test for Specific Heat of Aggregates, Concrete, and Other Materials). The procedure consists of oven-drying the sample and then immersing it in a water bath at ambient temperature for at least 48 hours. After this period the sample has reached saturation and is weighed after drying the surface from remaining water. The sample is then placed in a boiling water temperature bath (99.1 ± 0.5 °C) at the local barometric pressure. The sample remains in the bath for at least 20 minutes. Then the sample and the

0 – Carry over water.

S – Sample.

e – Water equivalent of calorimeter.

Whiting, et al. (1978) used a standard material (sapphire) as calibration material. The next equation was used for this purpose:

$$M_e = \frac{C_{pS} M_S T_S + C_{p1} M_0 T_S + C_{pb} M_b T_S}{C_{p1} T_1} - M_1 \qquad (4.4)$$

Where:

M = Mass, (kg or lb).

C_p = Specific heat, [J/(kg K) or BTU/(lb °R)].

T = Temperature raise or fall, (K or °R).

Sub indexes:

e – Equivalent to water.

S – Sapphire

b – Basket.

0 – Carry over water.

1 – In calorimeter.

In the same way, the water equivalent of the calorimeter can be calculated by using pure water as calibration material instead of the recommended Sapphire. Thus, a simplified equation is required. This equation does not take into consideration the basket required for the sapphire or the water carried over. Consequently, the water equivalent of the calorimeter can be found using the next equation:

$$M_e = \frac{M_C T_C}{T_1} - M_1 \tag{4.5}$$

Where:

M_e = Mass equivalent of calorimeter, (kg or lb)

M_C = Mass of calibration water, (kg or lb)

M_1 = Mass of water in calorimeter, (kg or lb)

T_C = Temperature rise of fall of calibration water, (K or °R)

T_1 = Temperature rise or fall of water in calorimeter, (K or °R)

For this experiment, the mass of calibration water used was 0.25 ± 0.005 kg and the mass of water in the calorimeter was 1.75 kg (3.86 lb). The temperature fall of the calibration water was 38.32 ± 0.05 °C and the temperature rise of the water in the calorimeter were 5.17 ± 0.05 °C. Therefore, using equation (4.5), the mass equivalent of the calorimeter was found to be: 0.103 ± 0.060 kg (0.227. ± 0.1323 lb).

The mass of the carry-over water is calculated by measuring the sample before and after the boiling period. The carry-over water was measured to be: 0.04 ± 2.0E-4 kg.

Using equation 4.3, it is now possible to calculate the value of the specific heat for the concrete under SSD conditions. The obtained value is: 1036 ± 42 J/(kg K) [0.21 ± 0.01 BTU/(lb °F)].

According to Whiting, et al. (1978) it is possible to establish a relationship for specific heat of the concrete as function of specific heat under SSD conditions and the actual moisture content. The relationship takes the form:

$$C_p = \frac{C_{pSSD} + C_w \gamma (y-1)}{1 + \gamma (y-1)} \tag{4.6}$$

$$\gamma = \frac{W_{SSD} - W_{OD}}{W_{SSD}} \tag{4.7}$$

Where:

C_p = Specific heat of concrete at any moisture content, [J/(kg K) or BTU/(lb °R)]

C_{pSSD} = Specific heat of saturated-surface dry (SSD) concrete, [J/(kg K) or BTU/(lb °R)]

Cw = Specific heat of water, [J/(kg K) or BTU/(lb °R)]

γ = SSD moisture content, (dimensionless)

y = Moisture content expressed as a fraction of the saturation moisture content, (dimensionless)

W_{SSD} = SSD weight of concrete specimen, (kg or lb)

W_{OD} = Oven-dry weight of concrete specimen, (kg or lb)

Equation 4.6 can be used to estimate the new specific heat for the wet concrete during a snow test. The value of gamma (γ) corresponding to SSD moisture content was calculated as: 0.0706 (7.06%). Then the specific heat will range between: 799 J/(kg K) [0.191 BTU/(lb °R)] for oven-dry conditions to 1036 J/(kg K) [0.247 BTU/(lb °R)] for saturated (SSD) conditions.

4.2.3 Thermal conductivity

This parameter is measured using Hot-Plate Apparatus similar to that described in the ASTM C177-97 standard (ASTM, 2002). A detailed description of the apparatus used can be found in Section 3.7.

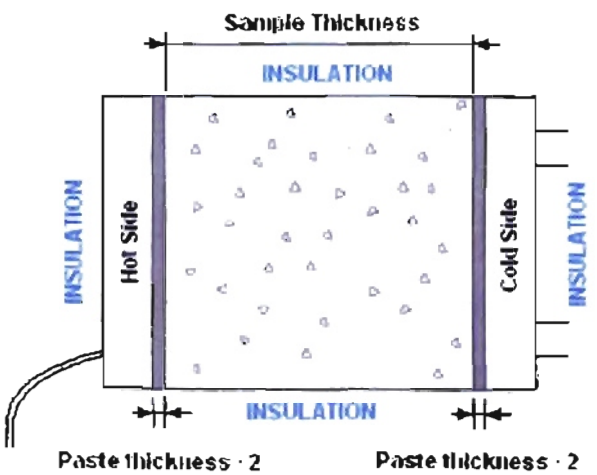

Figure 4.2-1: ***Schematic of heat conduction on concrete sample***

Based on the one-dimensional approximation, the heat conduction can be calculated from the steady state model as follows:

$$k_s = \frac{L_s}{\frac{\Delta T}{Q''} - \frac{L_p}{k_p}} \tag{4.8}$$

Where:

k_s = Concrete sample conductivity, [W/(m K) or BTU/(hr ft °F)].

K_p = Paste conductivity, [W/(m K) or BTU/(hr ft °F)].

ΔT = Differential temperature between cold and hot side, (°C or °F).

Q'' = Heat flux on hot side, [W/m^2 or BTU/(hr ft^2)].

L_s = Thickness of concrete sample, (m or ft).

L_p = Thickness of paste sample, (m or ft).

The thermal conductivity for the paste is given by the manufacturer (0.416 ± 0.0042 W/m-°C). By using this value and measuring the dimensions, all the parameters of the equation 4.8 are set. Two test samples were analyzed. The conductivity value found was: 1.15 ± 0.0063 W/(m °C) [0.664 ± 0.0036 BTU/(hr ft °F)] at oven-dry conditions and 1.61 ± 0.0063 W/(m °C) [0.664 ± 0.0036 BTU/(hr ft °F)] at saturation conditions following Rhodes (1978) criterion.

The charts and data used for the calculation of the conductivity value can be found in appendix D. A calibration done with a material (Stainless Steel 308) with known thermal conductivity gave errors of less than ±2% (Smith, 2003).

4.2.4 Water diffusion in concrete experiment

An experiment was performed in order to investigate the rate of water diffusion into the concrete slab. One of the cylindrical concrete slab samples (Figure 3.2-3) was used. The sample was inserted into a close-fitting Mylar tube. Then the top surface of the concrete was sealed around the outer edge, so that water could be ponded on the upper surface of the concrete without leaking around the edges. Then 160 ml. of water was placed on the upper surface of the concrete slab sample. A picture is taken every 5 minutes to observe the water diffusion process into the concrete sample.

After the water was placed on the sample, it was noticed that the porosity was higher near the top of the sample than at the bottom. Some water quickly passed through the upper surface to the space between the Mylar tube and the concrete sample as shown in Figure 4.2-2. The percentage of the outer surface of the sample that was saturated was estimated visually at 5-minute intervals. The estimates and an equation are plotted in Figure 4.2-2.

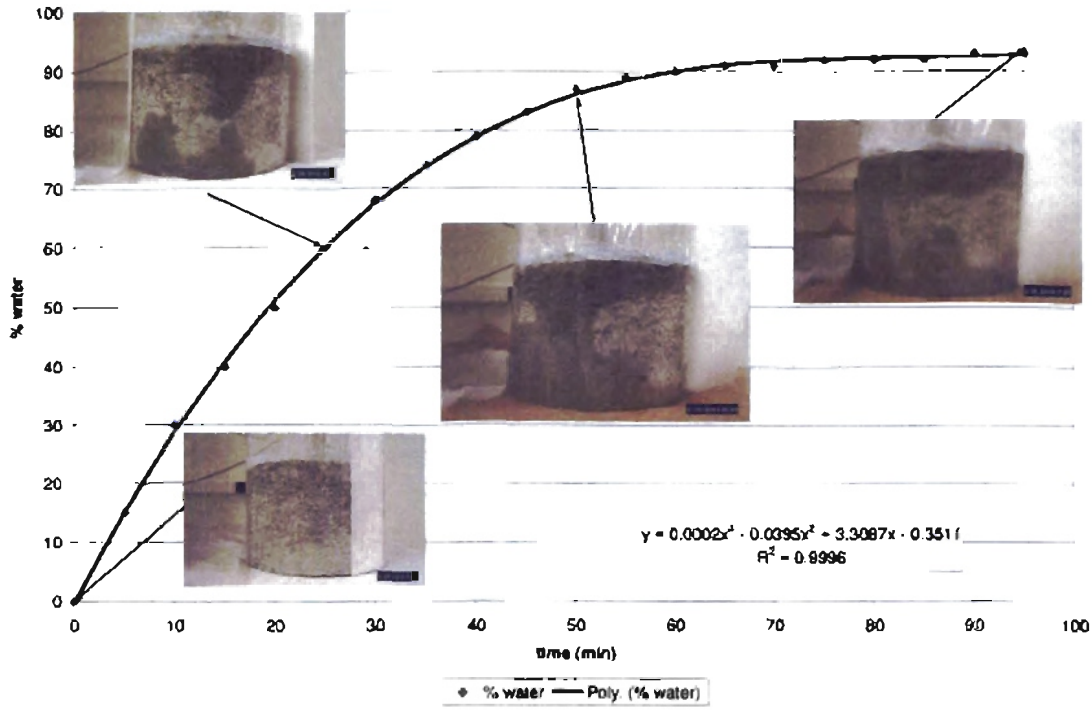

Figure 4.2-2: ***Water diffusion in concrete slab sample***

The following equation is used to correlate the water content with time:

$$wc = C_{11}t^3 + C_{12}t^2 + C_{13}t + C_{14} \tag{4-9}$$

Where:

wc = water content (%)

t = time, [min]

C_{11} = 2x10-4, [1/min^3]

C_{12} = -3.96x10-2, [1/min^2]

C_{13} =3.3087, [1/min]

C_{14} = -0.3511, [non dimensional]

Since the concrete sample and the concrete slab have the same thickness (150mm or 6 in) the penetration depth at any time may be approximated as:

$$PD = \frac{wc}{100} * Th_s \tag{4-10}$$

Where:

PD = Penetration depth

Th_s = Concrete slab thickness (0.152 m or 0.5 ft)

wc = water content (non-dimensional)

The penetration depth is used to change the specific heat and thermal conductivity values from dry to saturated conditions. This procedure is done on a cell-by-cell basis to approximate the water absorption of the concrete during the snow-melting phase of the experimentation.

Once the snow melting is finished the specific heat and thermal conduction of saturated cells are returned to dry conditions. The process is assumed to occur on a cell-by-cell basis starting from the deepest row to the surface. The application of this experiment is shown in section 4.5.3.

4.3 Mathematical model of the concrete slab

The mathematical model of the concrete slab is based on a center section as shown in Figure 4.3-3. Two planes of symmetry (through the tube and between the tubes)

are approximately adiabatic and assumed to be so for the model. Another assumption is that the fluid temperature remains approximately constant along the tube, and therefore a 2-D model is appropriate.

4.3.1 Heat conduction

During construction, the central section of the testing slab was reinforced with wood, and the void space filled with extruded polystyrene. Therefore, the central section became a very complex structure as shown in Figure 4.3-3a.

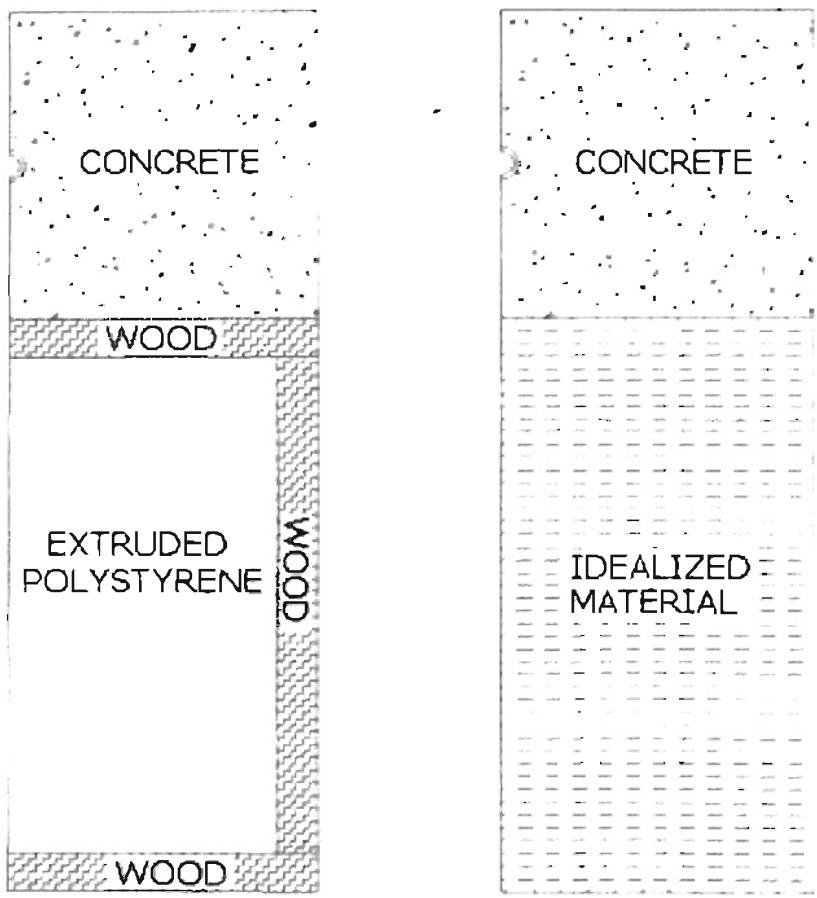

Figure 4.3-3: ***Central Section. a) Construction model, b) Mathematical representation***

A simplified model for the base was established. An ideal material that represents the combined properties of wood and extruded polystyrene was created. The combined heat conduction was calculated assuming an ideal 1-D heat transfer case. This is a reasonable assumption since the horizontal wood layers have relatively low conductivity and do not serve as effective fins.

The model can be represented as a resistance network as shown below:

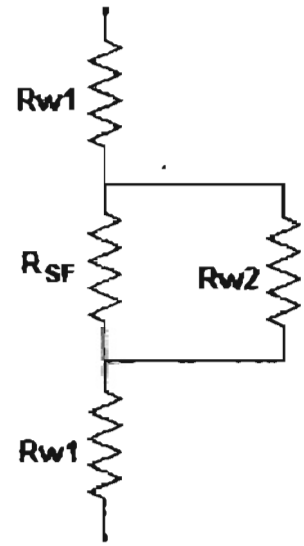

Figure 4.3-4: ***Resistance representation of slab's base***

Equation (4.11) represents the diagram in Figure 4.3-4:

$$R_{eq} = R_{W1} + \left(\frac{1}{R_{SF}} + \frac{1}{R_{W2}} \right)^{-1} + R_{W2} \tag{4.11}$$

Where:

R_{eq} = Equivalent resistance, [K/W or (°R hr)/BTU]

A simplified model for the base was established. An ideal material that represents the combined properties of wood and extruded polystyrene was created. The combined heat conduction was calculated assuming an ideal 1-D heat transfer case. This is a reasonable assumption since the horizontal wood layers have relatively low conductivity and do not serve as effective fins.

The model can be represented as a resistance network as shown below:

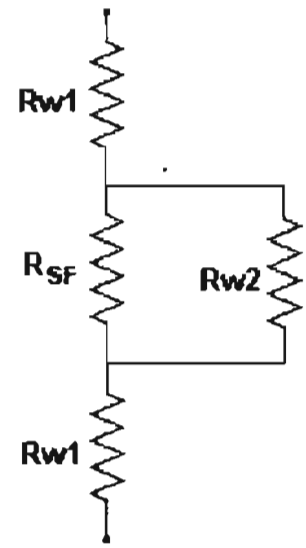

Figure 4.3-4: ***Resistance representation of slab's base***

Equation (4.11) represents the diagram in Figure 4.3-4:

$$R_{eq} = R_{W1} + \left(\frac{1}{R_{SF}} + \frac{1}{R_{W2}} \right)^{-1} + R_{W2} \qquad (4.11)$$

Where:

R_{eq} = Equivalent resistance, [K/W or (°R hr)/BTU]

R_{W1} = Wood resistance on horizontal section, [K/W or (°R hr)/BTU]

R_{W2} = Wood resistance on vertical section, [K/W or (°R hr)/BTU]

R_{SF} = Extruded polystyrene resistance, [K/W or (°R hr)/BTU]

The resistance value can be calculated using the following equation:

$$R = \frac{L}{kA} \tag{4.12}$$

Where:

R = resistance, [K/W or (°R hr)/BTU]

L = Length, (m or ft)

k = Heat conduction coefficient, [W/(m K) or BTU/(ft °F)]

A = Cross-sectional area, (m^2 or ft^2)

The data for the different resistances is tabulated in Table 4.3-2:

	R_{W1}	R_{SF}	R_{W2}
Length (m)	0.0191	0.2477	0.2477
Area (m^2)	0.1277	0.1103	0.0174
Thermal conductivity, [W/(m K)]	0.17	0.03	0.17
Heat conduction resistance, (K/W)	0.8798	74.8565	83.7390

Table 4.3-2: ***Data for resistances in slab***

The equivalent value for the heat conduction coefficient is calculated by using equation 4.12:

$$k_{eq} = \frac{1}{R_{eq} L} \tag{4.13}$$

Where:

k_{eq} = Equivalent conduction coefficient, [W/(m K) or BTU/(hr ft °R)]

R_{eq} = Equivalent heat resistance coefficient, [K/W or (°R hr)/BTU]

L = Total conduction length, (m or ft)

A complete geometrical representation of the central section of the concrete slab can be found in Appendix C. The heat conduction coefficient for the ideal composite material is: 0.08 W/(m K).

4.3.2 Specific heat and density

An equivalent specific heat for the ideal material of the slab base can be found using the concept of volumetric specific heat. Thus, the sum of the volumetric specific heats of the different materials has to be equivalent to a volumetric specific heat of the idealized material. The equation used is shown below:

$$\rho_{eq} C_{eq} V_T = \rho_{W1} C_{pW1} V_{W1} + \rho_{SF} C_{pSF} V_{SF} + \rho_{W2} C_{pW2} V_{W2} \tag{4.14}$$

Where:

ρ = Density, (kg/m^3 or lb/ft^3)

C_p = Specific heat, [J/(kg K) or BTU/(lb °R)]

V = Volume, (m^3 or ft^3)

Sub index:

eq = Equivalent for section

W1 = Wooden section top and bottom

W2 = Wooden vertical section

SF = Extruded polystyrene section

T = Total volume.

The values used for this calculation are resumed in Table 4.3-3:

	Rw1	**RSF**	**Rw2**
Density, (kg/m^3)	415.00	43.20	415.00
Specific heat, [J/(kg K)]	2385.0	1220.0	2385.0
Volume, (m^3)	0.0049	0.0273	0.0043
Total value, (J/K)	4849.89	1438.82	4256.03

Table 4.3-3: ***Data used for volumetric specific heat equivalent***

The value found for the combined density and capacitance was: 288897 J/K. The value of density was found using the following relation:

$$\rho_{eq} = \frac{\rho_W V_W + \rho_{SF} V_{SF}}{V_T} \tag{4.15}$$

Where:

ρ = Density, (kg/m^3 or lb/ft^3)

V = Volume, (m^3 or ft^3)

Sub index:

eq = Equivalent for section

W = Wooden section top and bottom

SF = Extruded polystyrene section

T = Total volume.

The density found was: 136.9 kg/m^3. As a result, the specific heat was calculated to be: 2110 J/(kg K).

4.4 Initial conditions and physical properties as required input

In a transient calculation the initial values are required. An incorrect initialization of the system can lead to big mistakes in the computation. Each model has its own way of initializing of the system. In the case of the FD-RG model the initialization is done by assuming a fully steady state condition for the slab at the dry bulb temperature of the first time step. In the case of the BFG-FV model the initialization was performed manually with the initial temperature measured during the simulation time.

4.4.1 Experimental procedure

The dry experiment starts by cooling the concrete using the mechanical cooling system of the snow chamber. When the temperature difference between surface and bottom of slab temperatures was less than 1 °C (1.8 °F) it was assumed that the slab reached steady state. For the dry experiment, the top surface temperature reaches 4.5°C (40.1 °F) and the bottom temperature reached 5.5°C (41.9 °F).

For the snow-melting experiments, it is necessary to bring the slab surface temperature below freezing in order to accumulate snow without premature melting over the slab surface. Since the mechanical cooling can reach only 0.3°C (32.5 °F) without frosting the coil, extra cooling was required. The top surface concrete slab temperature was reduced to -8°C (17.6 °F) by spraying liquid nitrogen onto the slab.

4.4.2 Power input calculation

The power input to the slab was calculated by using equation (4.16), which calculates the heat transferred from the fluid into the slab:

$$W = \dot{m}_f C_{pf} \left(T_i - T_o \right) \tag{4.16}$$

Where:

W = Heat transferred into the concrete slab, (W or BTU/hr)

$\dot{m}$ = Mass flow rate of fluid into piping, (kg/s or lb/s)

C_{pf} = Specific heat of fluid into piping, [J/(kg K) or BTU/(lb °F)]

T_i = Temperature at inlet of piping, (C or °F)

T_o = Temperature at outlet of piping, (C or °F)

To evaluate the mass flow rate it is necessary to take into consideration the change in properties for the Ethylene Glycol with temperature. Therefore, the data available in the ASHRAE Handbook of Fundamentals (2001) for 50% concentrations was used to formulate correlations of the density and specific heat as a function of

temperature. Then, a polynomial regression was used to estimate these parameters at different temperatures. The correlation used for density is shown below:

$$\rho_f = C_1 T^4 + C_2 T^3 + C_3 T^2 + C_4 T + C_5 \tag{4.17}$$

Where:

ρ_f = Density of fluid, (kg/m^3 or lb/ft^3)

T = Temperature, (°C or °F)

C_1 = 6.0260×10-9 [kg/(m^3 °C^4)] or 3.584×10-11 [lb/(ft^3 °F^4)]

C_2 = -1.0871×10-6 [kg/(m^3 °C^3)] or -1.622×10-8 [lb/(ft^3 °F^3)]

C_3 = -2.3911×10-3 [kg/(m^3 °C^2)] or -4.473×10-5 [lb/(ft^3 °F^2)]

C_4 = -3.3812×10-1 [kg/(m^3 °C)] or -8.819×10-3 [lb/(ft^3 °F)]

C_5 =1.0823×103 (kg/m^3) or 6.789×101 (lb/ft^3)

The correlation used for specific heat was:

$$C_{Pf} = C_6 T^4 + C_7 T^3 + C_8 T^2 + C_9 T + C_{10} \tag{4.18}$$

Where:

C_{pf} = Specific heat of fluid into piping, [J/(kg C) or BTU/(lb °F)]

T = Temperature, (°C or °F)

C_6 = 6.0969E-08 [J/(kg C^5)] or -1.3872E-12 [BTU/(lb $°F^5$)]

C_7 = 6.0605E-06 [J/(kg C^4)] or 4.2577E-10 [BTU/(lb $°F^4$)]

C_8 = 1.6217E-04 [J/(kg C^3)] or - 2.0396E-08 [BTU/(lb $°F^3$)]

C_9 = 3.8531E+00 [J/(kg C^2)] or 5.1145E-04 [BTU/(lb $°F^2$)]

C_{10} = 3.2052E+03 [J/(kg C)] or 7.4920E-01 [BTU/(lb °F)]

Flow rate was calculated using equation (4.19):

$$\dot{m}_f = \rho_f F_f \tag{4.19}$$

Where:

$\dot{m}$ = Mass flow rate of fluid into piping, (kg/s or lb/s)

ρ_f = Density of fluid, (kg/m^3 or lb/ft^3)

F_f = Flow rate, (m^3/s or ft^3/hr)

Power uncertainty analysis

The error associated with the inlet and outlet temperature measurement is ±0.05°C. The resulting uncertainty can be calculated using the Taylor quadrature formula since these errors are assumed to be independent. The uncertainty associated with them is calculated with the following formula:

$$\Delta z = \sqrt{\Delta x^2 + \Delta y^2} \tag{4.20}$$

Where:

Δz = Resulting uncertainty

Δx = Uncertainty of 1st measurement.

Δy = Uncertainty of 2nd measurement

The thermal uncertainty is then ±0.07°C (±0.13 °F).

In the case of the flow rate, the uncertainty of the instrument is given by the manufacturer ±8% FS. This implies that for the 5 GPM (18.9 Lpm) rotameter, the expected error is: ±0.4 GPM (±1.5 Lpm). However, the instrument was calibrated for the range used flow rate of 1.5 GPM (5.7 Lpm). The error found was ±0.08 GPM (±0.3 Lpm).

The average temperature required evaluating the density property of the Ethylene Glycol. This property is calculated at the average of the inlet and outlet temperature. Using standard deviation error theory the uncertainty can be calculated as:

$$\Delta\rho = \sqrt{\left(\frac{4C_1\Delta T}{T}\right)^2 + \left(\frac{3C_2\Delta T}{T}\right)^2 + \left(\frac{2C_3\Delta T}{T}\right)^2 + \left(\frac{C_4\Delta T}{T}\right)^2 + \left(\frac{C_5\Delta T}{T}\right)^2} \qquad (4.21)$$

Where:

$\Delta\rho$ = Uncertainty in density calculation

ΔT = Uncertainty in temperature calculation

T = Temperature, (°C or °F)

From equation (4.21) it is possible to observe that the lower the temperature, the higher the expected error. The temperature of the fluid increases fairly quickly once the experiment starts and then rises slowly during the rest of the testing period. For purposes of calculating the density uncertainty, the temperature will be taken to be 43.3 °C (109 °F) as representative for much of the test. Under such condition the computation of the uncertainty of density calculation is: ± 4 kg/m^3 (±0.27 lb/ft^3).

In the case of the specific heat, using equation (4.22) the uncertainty was calculated to be: ±14 J/(kg K) [±3.3×10-3 BTU/(lb °F)].

$$\Delta Cp_{pf} = \sqrt{\left(\frac{4C_6\Delta T}{T}\right)^2 + \left(\frac{3C_7\Delta T}{T}\right)^2 + \left(\frac{2C_8\Delta T}{T}\right)^2 + \left(\frac{C_9\Delta T}{T}\right)^2 + \left(\frac{C_{10}\Delta T}{T}\right)^2} \qquad (4.22)$$

Where:

ΔC_{pf} = Specific heat uncertainty of fluid into piping calculated at evaluation temperature, [J/(kg K) or BTU/(lb °F)]

T = Evaluation temperature (°C or °F)

To evaluate the mass flow rate the error is calculated using standard uncertainty analysis to be:

$$\Delta\dot{m} = \dot{m}\sqrt{\left(\frac{\Delta FR}{FR}\right)^2 + \left(\frac{\Delta\rho}{\rho}\right)^2} \qquad (4.23)$$

Where:

$\Delta\dot{m}$ = Uncertainty associated with mass flow rate measurement, (kg/s or lb/h)

$\dot{m}$ = Mass flow rate calculated at the highest evaluation temperature (kg/s or lb/h)

ΔFR = Uncertainty associated with flow rate measurement, (m^3/s or ft^3/h)

FR = Flow rate measurement, (m^3/s or ft^3/h)

$\Delta\rho$ = Uncertainty associated with flow rate measurement, (kg/m^3 or lb/ft^3)

ρ = Density evaluated at the highest evaluation temperature, (kg/m^3 or lb/ft^3)

The uncertainty associated with mass flow rate is: 9.66×10-4 [kg/s]

Finally, for the uncertainty error on power is given by:

$$\Delta W = W\sqrt{\left(\frac{\Delta\dot{m}}{\dot{m}}\right)^2 + \left(\frac{\Delta C_{pf}}{C_{pf}}\right)^2 + \left(\frac{\Delta T}{T}\right)^2} \qquad (4.24)$$

Where:

ΔW = Uncertainty associated with power calculation, (W or BTU/h)

W = power calculation at evaluation temperature, (W or BTU/h)

$\Delta\dot{m}$ = Uncertainty associated with mass flow rate measurement, (kg/s or lb/h)

$\dot{m}$ = Mass flow rate calculated at the highest evaluation temperature (kg/s or lb/h)

ΔC_{pf} = Specific heat uncertainty of fluid into piping calculated at evaluation temperature, [J/(kg K) or BTU/(lb °F)]

C_{pf} = Specific heat of fluid into piping calculated at evaluation temperature, [J/(kg K) or BTU/(lb °F)]

ΔT = Uncertainty associated with temperature measurement, (°C or °F)

T = Differential Temperature, (°C or °F)

The uncertainty in power varies from test to test, depending primarily on the temperature difference and the power input. The resulting uncertainties for each of the tests are summarized in Table 4.4-4.

	Test Conditions		
	Dry	SM1	SM2
Power, W (BTU/h)	114.5 (390.8)	164.5 (561.4)	224.1 (764.6)
Uncertainty, W (BTU/h)	11.5 (39.3)	16.2 (55.2)	19.1 (65.2)
Uncertainty (%)	9.9	10.2	11.7

Table 4.4-4: ***Test uncertainties***

4.4.3 Initial conditions

The initial geometrical setup of both models was performed using the information shown in Table 4.4-5.

Data	Value
Length, m (ft)	0.9144 (3.00)
Width, m (ft)	0.8365 (2.74)
Height Layer 1, m (ft)	0.1524 (0.50)
Height Layer 2, m (ft)	0.4382 (1.44)
Pipe spacing, m (ft)	0.2921 (0.96)
Pipe depth, m (ft)	0.7620 (2.50)
Pipe diameter, m (ft)	0.0158 (0.05)
Pipe wall thickness, m (ft)	0.0024 (0.01)
Number of layers	2

Table 4.4-5: ***Data required for FD-RG and FV-BFG models***

The properties used to describe the layers of material in the slab are:

	Pipe	1st Layer	2nd Layer
Material	**PEX**	**Concrete**	**Equivalent Material**
Thermal conduction, W/(m K) [BTU/(h ft °F)]	0.25 [0.144]	1.19 [0.688]	0.08 [0.046]
Specific heat, [J/(kg K)] [BTU/(h ft °F)]	1840.0 [0.440]	871.4 [0.208]	2110.1 [0.504]
Density, (kg/m^3) [lb/ft^3]	944.0 [58.9]	2093.3 [130.6]	136.9 [8.5]

Table 4.4-6: ***Material properties specifications***

Additionally, the weather information is provided as a boundary file for each model. The variables included in the boundary file are: dry bulb temperature, dew point

temperature, sky temperature, rain precipitation, snow precipitation, and power input. However, for the FD-RG and for the FV-BFG there is a specific set of boundary conditions that are shown in Table 4.4-7.

	FD-RG	FV-BFG
Dry bulb temperature	☑	☑
Sky temperature	☑	☑
Humidity ratio	☑	
Dew point temperature		☑
Wind speed	☑	☑
Wind direction	☑	
Solar radiation	☑	
Solar angle of incidence	☑	
Sky condition		☑
Rain fall	☑	☑
Snow fall	☑	☑
Power	☑	☑

Table 4.4-7: ***Boundary file variables for investigated models***

Each of the required values was set as follows for each time step:

Dry bulb temperature: Estimated as the average of the air temperature measurements obtained with thermocouples positioned inside the snow chamber.

Sky temperature: Calculated as the Mean Radiant Temperature (MRT) of the inner surfaces of the snow chamber that views the upper surface of the concrete slab. The MRT is calculated as follows:

$$T_{MRT} = \frac{A_w e_w (T_1 + T_2 + T_3 + T_4) + A_r e_r T_r}{A_{MRT} e_{MRT}} \quad (4.25)$$

$$A_{MRT} = 4A_w + A_r \quad (4.26)$$

$$e_{MRT} = \frac{4A_w e_w + A_r e_r}{A_{MRT}} \quad (4.27)$$

Where:

T = Temperature, (°C or °F)

A = Area, (m^2 or ft^2)

e = Emissivity, (non-dimensional)[1]

Sub-indexes:

w = walls

r = roof

MRT = Mean radiant temperature total

$1 \cdot 4$ = Independent wall temperature

[1] The emissivity values used for walls (0.24) and roof (0.04) were obtained from Incropera and De Witt (1996).

Humidity ratio: Since the air introduced into the chamber passed thru the coil and the temperatures are surrounding freezing conditions the wet and dry bulb temperatures are similar. Therefore, it is assumed that the humidity ratio is that of the average temperature in the coil at the saturation point.

Dew point temperature: This parameter is used in the FV-BFG model only and it was considered to be a 0.5°C (1.8°F) lower value than the dry bulb temperature.

Wind speed: The concrete slab was shielded from any external air flow by the snow chamber and the air flow inside the chamber was highly reduced due to the expansion inside the chamber, therefore it was set to zero. The convection coefficient is obtained due to natural convection from the surface of the slab. The value was found to be 2.2 W/(m^2 °C) [0.39 BTU/(hr ft^2 °F)].

Wind direction: It was not necessary to set this value due to the neglected wind speed.

Solar radiation: The concrete slab was shielded from any direct radiation source by the snow chamber, therefore solar radiation was set to zero.

Solar angle of incidence: It was not necessary to set this value due to the neglected solar radiation.

Sky condition: This parameter is used to calculate the sky temperature in the FV-BFG model. For this reason it was overridden by the sky temperature value calculated as in equation (4.25).

Rain fall: Since there was no water precipitation over the concrete slab surface during the experimentation process the value considered for this parameter was zero.

Snow fall: The snow fall was assumed to be constant during the snow accumulation period and estimated as the average amount of snow accumulated each time step.

Power: The power was estimated for each time step as shown in section 4.4.2.

4.5 Experiments

Three experiments were performed..The first experiment, run under dry conditions, was primarily used to validate the conduction, convection and radiation sub-models. The second two experiments, run with snow-melting conditions, were used to validate the entire model.

4.5.1 Dry surface condition

In this case, the average surface temperature of the slab was calculated with the models and compared to the experimental result. However, due to the uncertainties associated with the power input measurement (discussed in section 4.4.2) there is some uncertainty in the model results. The upper and lower uncertainty bands were obtained by running the FD-RG simulation assuming the maximum and minimum error on power measurement respectively. The heat flux was calculated as: 148.57 W/m^2 [47.10 BTU/(h ft^2)].

From Figure 4.5-5 it can be seen that both models follow almost perfectly the average surface temperature during the transient period. During this period the model results are highly sensitive to the density and specific heat of the concrete. The fact that the slope of the experiment and the simulation are consistent confirms the calculated properties of the materials for this model[2]. While, it is not possible to assert which model is more accurate due to the uncertainty of the power measurement, both models appear to perform well.

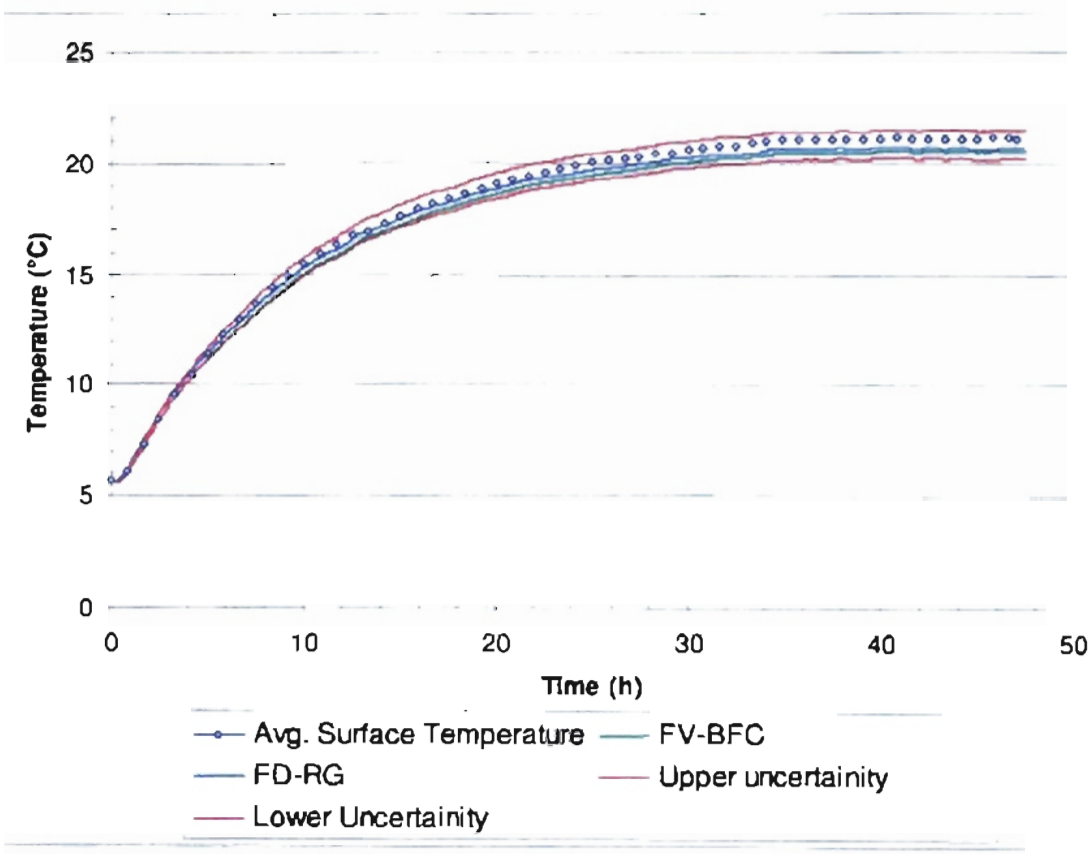

Figure 4.5-5: ***Average temperature comparison in dry case scenario***

[2] Indeed, early experience with models that showed a high sensitivity to the estimates of density and specific heat was the motivation for the careful determination of the properties described in section 4.2

For this simulation the runtime is approximately 3 minutes for the FD-RG model and 40 minutes for the FV-BFG model. The simulations ran on a Pentium III computer with 1.0 GHz processor speed and 256 MB of RAM memory.

4.5.2 Snow-melting experiments

The cases in which there is snow accumulation over the surface are somewhat more complicated than the dry surface case. The first complication is the difficulty of measuring the transient snow accumulation over the slab during snowfall. The production of snow inside the snow chamber is a manual process. It is very difficult to achieve a constant rate of snow production. Furthermore, it is difficult to produce a uniform snow distribution over the slab surface. All the snow accumulated over the central surface of the slab is introduced to the models as described in Section 4.4.3.

Two experiments were performed and are summarized in the following table:

TEST	**Snow accumulation,** mm [in]	**Heat Flux,** W/m^2 [BTU/(hr ft^2)]	**Snow melting Time,** hr
SM1	25.9 [1.02]	206.7 [65.5]	3.50
SM2	105.0 [4.10]	281.0 [89.1]	4.25

Table 4.5-8: ***Snow tests performed***

Test SM1 had a relatively low snow accumulation and heat flux. Test SM2 had relatively high snow accumulation and heat flux. The resulting snowmelt times were similar.

First snow-melting experiment

A first snow-melting experiment (SM1) was performed. The chronology of events is shown in Table 4.5-9:

Start (hrs)	End (hrs)	Event
0.00	0.75	Liquid Nitrogen introduction.
0.75	1.5	Snow accumulation period.
1.50		Heating system activated.
4.83	8.5	Snow melting period. At 8.5 hours, the surface is completely free of snow, except for the residual snow around the edge.
8.50	13.66	Observed drying period on surface of slab. At 13.66 hours, the surface of the slab appears dry.
29.60		Reach steady state.
41.25		Experiment ends.

Table 4.5-9: ***SM1 experiment chronology***

For the first test, the average surface temperatures calculated with the FD-RG and the FV-BFG models are shown in Figure 4.5-6.

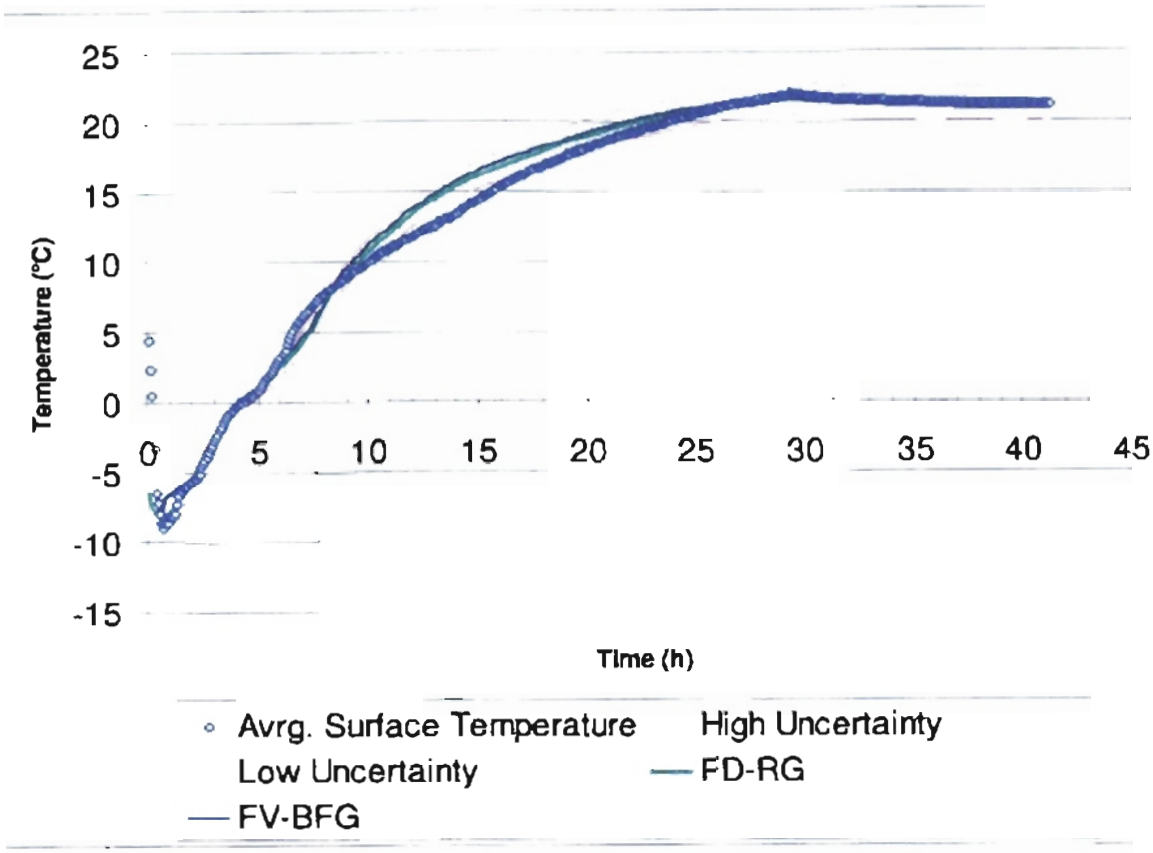

Figure 4.5-6: ***Average surface temperature for snow experiment***

The average surface temperature plot shows a pretty good comparison between the models and experiment during the initial transient behavior following the snowfall. However, after the surface temperature rises above the freezing point, the models over predict the slab surface temperature. The deviation cannot be explained by the uncertainty in the heat transfer rate. Finally, after about 20 hours, both models once again mach the experiment well.

One reason for the poor prediction during the 5 to 20 hours period may be the introduction of moisture into the slab by the melted snow. While the snow is melting, some of it is running off the surface to the sides. But, part is penetrating the concrete,

either through small cracks or diffusing through the pore structure. The change in moisture content (as stated previously in this chapter) has a significant effect on the thermal properties of concretes. According to Rhodes (1978), conductivity and specific heat tend to increase with the increase of moisture.

As a first attempt at accounting for the water penetration, the conductivity and specific heat of the slab were changed during the whole period. The equation (4.6) was used to estimate the specific heat of the concrete assuming different values of moisture content. In the case of the conductivity, a 40% increase over the oven-dry conditions was made based on the analysis made by Rhodes (1978) on saturated concrete. The results of the simulations made with the FD-RG model are shown in Figure 4.5-7.

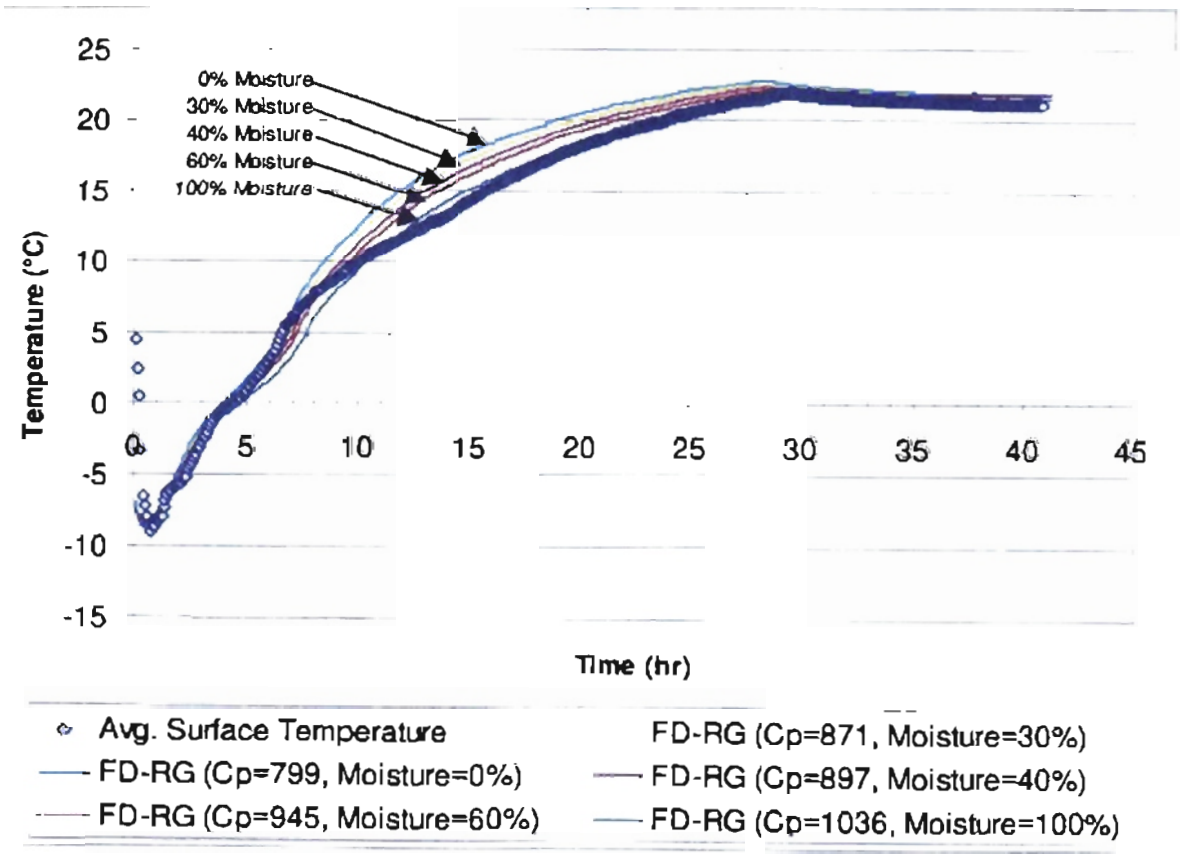

Figure 4.5-7: ***Average surface temperatures with different values of C_p for concrete***

In Figure 4.5-7 is possible to observe that the surface temperature for the 5 to 20 hour period gets closer to the experimental data with increased specific heat. The moisture content is also shown for each specific heat value used. However, in these plots the specific heat of the concrete has been changed during the whole period. A refinement of this model, which attempts to account for moisture penetration, is discussed in section 4.5.3.

Another area of interest is the prediction of the surface condition. A plot of surface temperature and Snow Free Area Ratio (SFAR) is shown in Figure 4.5-8. The experimental SFAR values were estimated visually from the pictures taken in 10-minute intervals. The surface was assumed to start the SFAR when it was observed first sight of the concrete slab. The surface was assumed to be free of snow, when the only snow present was located over edge of the concrete slab. Seven pictures are presented in Figure 4.5-9 through Figure 4.5-15. The first picture shows the condition of the surface when the SFAR predicted by the FD-RG model rises above zero. The second picture, Figure 4.5-10, shows the moment at which the experimental SFAR rises above zero. The sixth picture, Figure 4.5-14, shows the time step that the FD-RG model reported SFAR equal to 1. The seventh picture shows the moment in which the experimental SFAR was considered equal to 1.

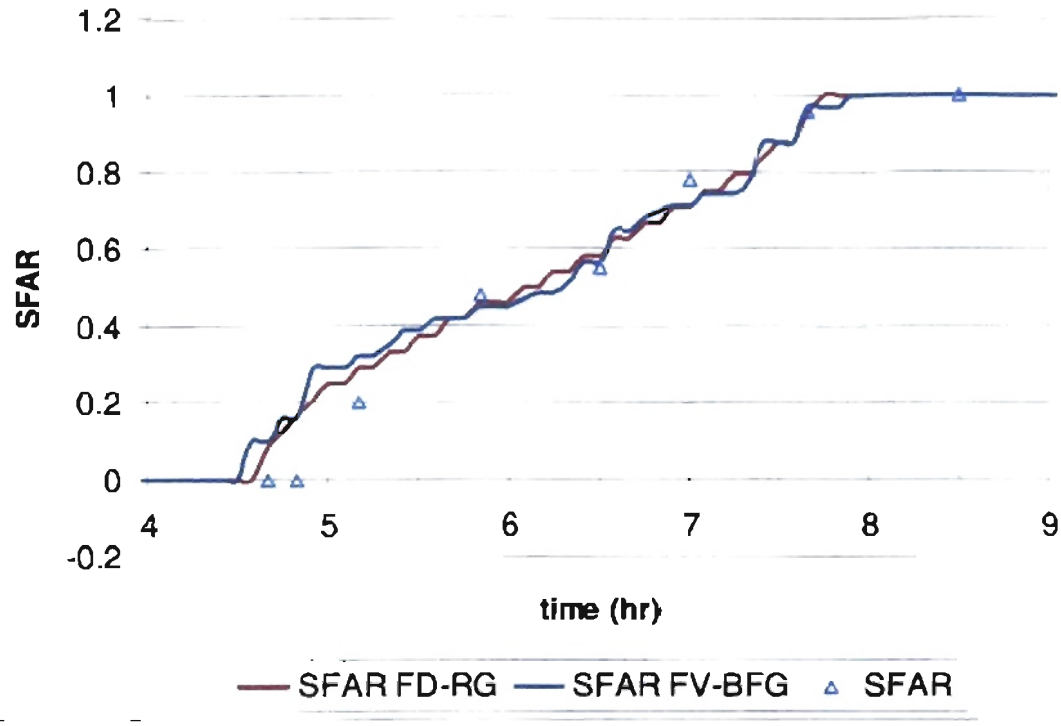

Figure 4.5-8: *Snow free area ratio vs. time for SM1 experiment*

The FD-RG model predicts that the SFAR should rise above zero by 4.66 hours. As shown in Figure 4.5-9, the SFAR at this time is still zero. However, ten minutes later, as shown in Figure 4.5-10, the SFAR has risen above zero. During the period between the 5.16-hour to the 7.75-hour there is a pretty good match with the experimental values. But, there is also a deviation in the SFAR prediction towards the end of the snow-melting period. At the end, the model under predicts the time required to reach the snow free conditions by 50 minutes (time between picture 6 and 7). As can be seen in Figure 4.5-14, this appears to be due to inhomogeneous accumulation of snow over the surface of the slab. As can be observed in Figure 4.5-9, the snow tended to accumulate around the edges of the slab. This increased amount of snow takes extra time to melt and distorts

the SFAR measurements. Table 4.5-10 shows the relationship between the actual time (shown in the photos) and elapsed time (reported as current experiment time).

Actual Time (hh:mm)	Elapsed time (hr)
16.28	4.66
16:38	4.83
16:58	5.15
17:38	6.25
18:18	7.08
19:28	7.75
19:58	8.50

Table 4.5-10: *Actual time and elapsed time during snow- melting period in SM1 experiment*

Figure 4.5-9: *FD-RG Predicted Snow Free Area Ratio 0.00, measured: 0.00*

Figure 4.5-10: ***FD-RG Predicted Snow Free Area Ratio 0.08, measured: 0.02***

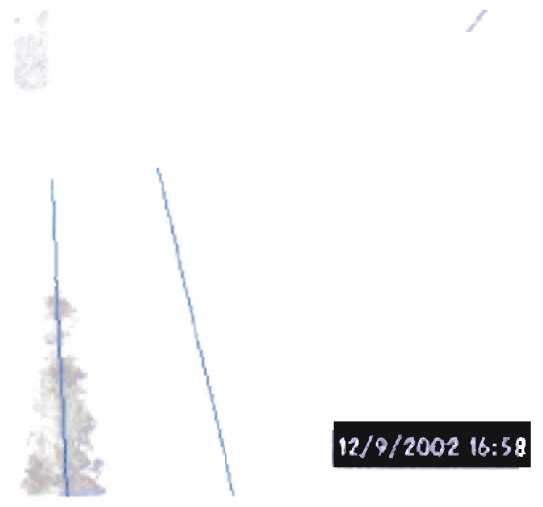

Figure 4.5-11: ***FD-RG Predicted Snow Free Area Ratio 0.25, measured: 0.20***

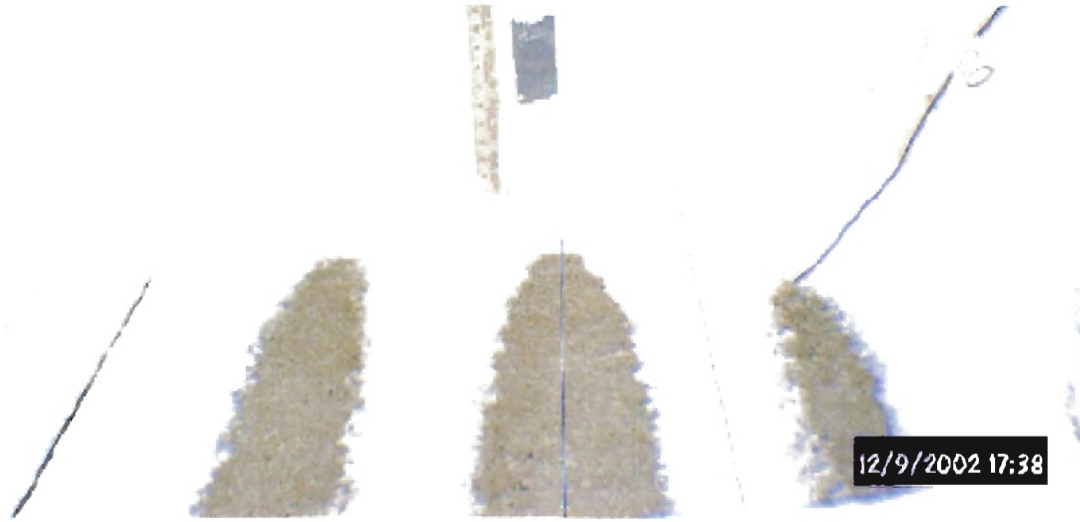

Figure 4.5-12: ***FD-RG Predicted Snow Free Area Ratio: 0.54, measured: 0.48***

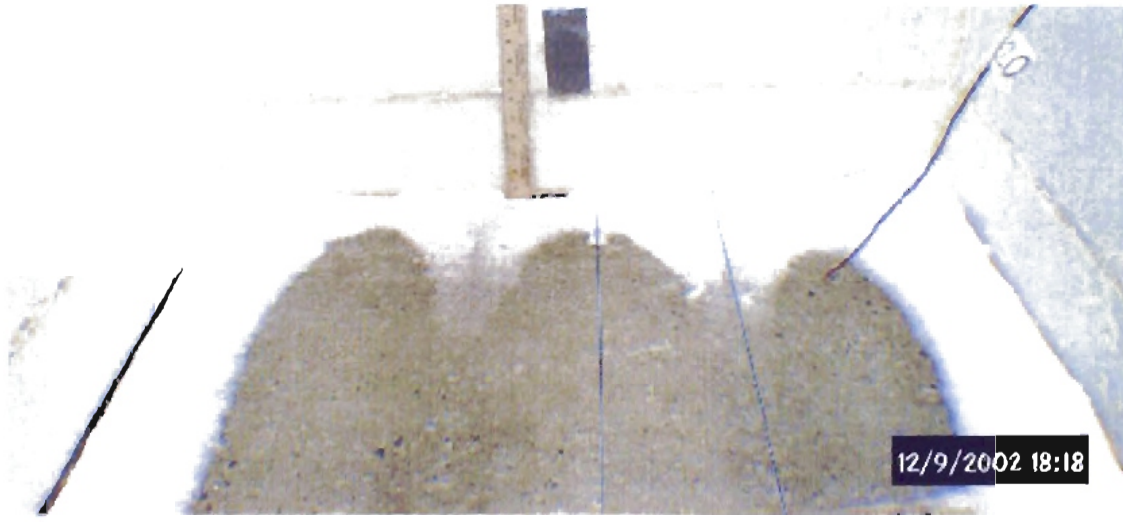

Figure 4.5-13: ***FD-RG Predicted Snow Surface Free Area Ratio: 0.71, measured: 0.65***

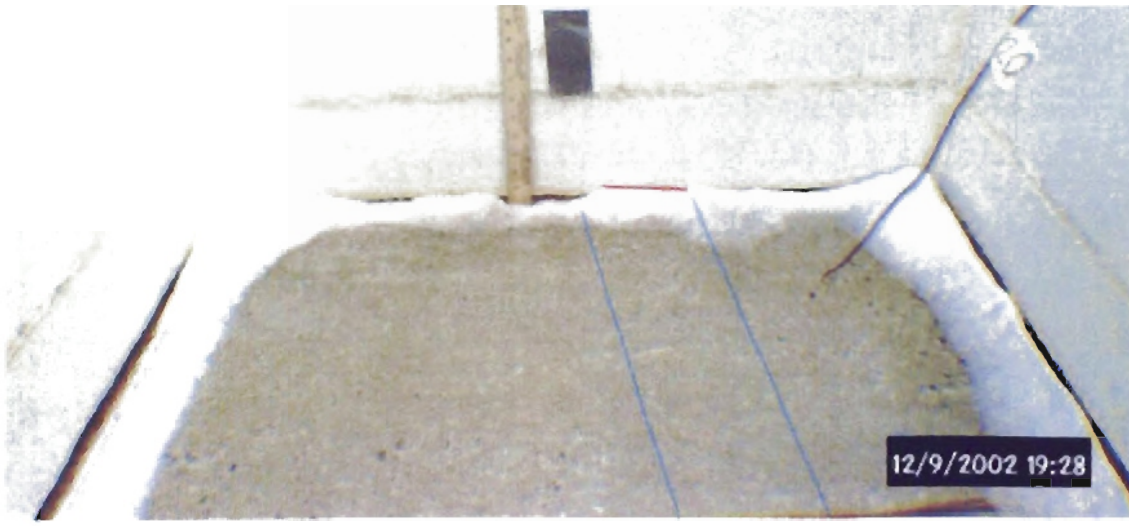

Figure 4.5-14: ***FD-RG Predicted Snow surface Free Area Ratio: 1.00, measured: 0.95***

Figure 4.5-15: ***FD-RG Predicted Snow surface Free Area Ratio: 1.00, measured: 1.00***

For this simulation the runtime is approximately 20 minutes for the FD-RG and 3.5 hours for the FV-BFG. The simulations ran on a Pentium III computer with 1.0 GHz processor speed and 256 MB of RAM memory.

Second snow-melting experiment

A second snow-melting experiment (SM2) was performed with a higher heating rate and a higher initial snow accumulation. The power output was set to be: 281.02 W/m^2 [89.08 $BTU/(hr\ ft^2)$]. The snow accumulation was 105 mm (4.1 in) measured close to the central section of the slab. Again, due to the method used to produce the snow, the snow accumulation was higher around the edges of the slab. The chronology of the events during this experiment is shown in the following table:

Start (hrs)	**End (hrs)**	**Action**
0	0.75	Liquid Nitrogen introduction.
0.75	3.00	Snow accumulation period.
3.00		Heating on slab activated.
4.17	11.08	Snow melting period. At 11.08 hours, the surface is completely free of snow, except for the residual snow around the edge.
11.08	23.75	Observed drying period on surface of slab. At 23.75 hours, the surface of the slab appears dry.
55.92		Reach steady state
80.00		Experiment ends

Table 4.5-11: ***SM2 experiment chronology***

The predicted surface temperatures calculated with the FD-RG and the FV-BFG models is shown in Figure 4.5-16.

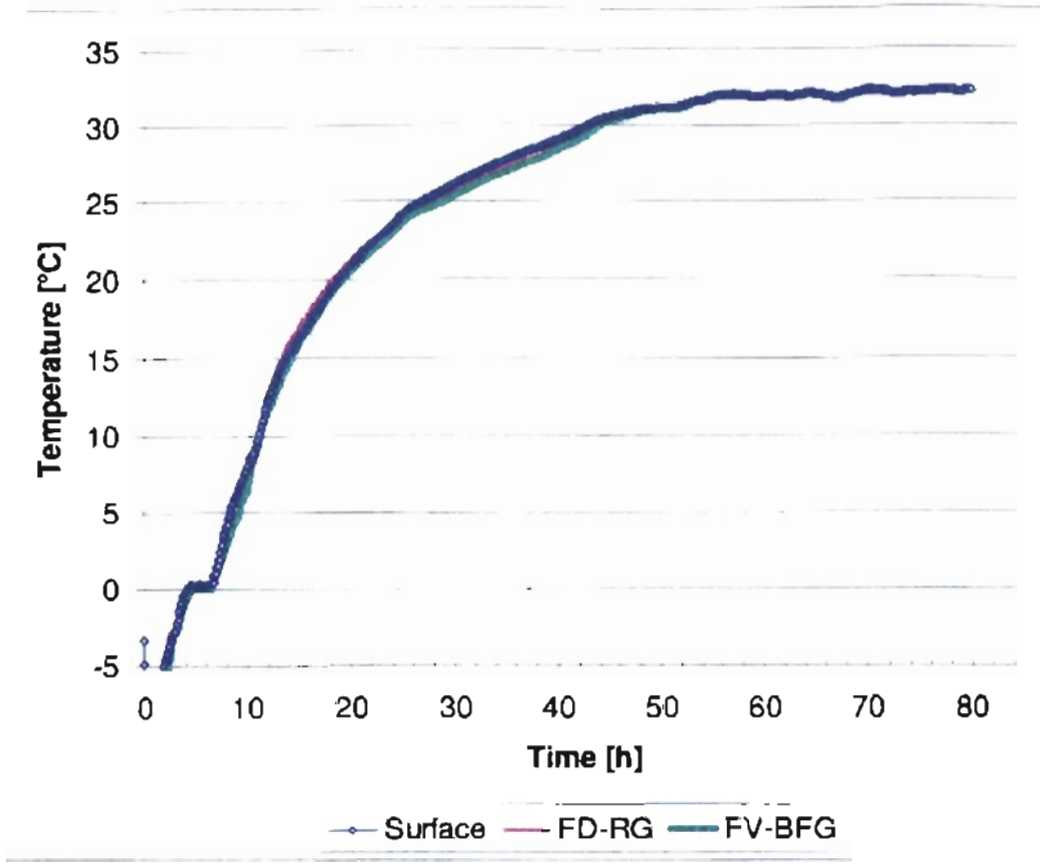

Figure 4.5-16: ***FD-RG model and FV-BFG model comparison***

Both models show a fairly good match with the surface temperature measurements even without modification of the model. However, there is a little difference of temperature in during the snow-melting period and the drying period. This divergence is attributed to the moisture penetration into the concrete slab. Therefore, the model was modified to try further improvement as described in section 4.5.3.

The experimental SFAR values were estimated visually from the pictures taken in 10-minute intervals. The same criteria for experimental SFAR determination where applied. Three pictures are presented in Figure 4.5-18 through Figure 4.5-20. The first picture shows the condition of the surface when the SFAR predicted by the FD-RG

model rises above zero. The picture shows that the surface of the central section of the slab starts to appear. But, the central section is still covered with slight amount of snow crystals and sludge mainly. In contrast, the left hand section shows already a SFAR of 0.15. Since the arrangement of the hydronic tubing inside the slab starts circulating the fluid thru the left hand piping as described in Figure 3.2-5. The second picture, Figure 4.5-10, shows the time step that the FD-RG model reported SFAR equal to 1. The tirth picture shows the moment in which the experimental SFAR was considered equal to 1. Figure 4.5-17 shows the comparison between the SFAR predicted by the FD-RG model and the FV-BFG model.

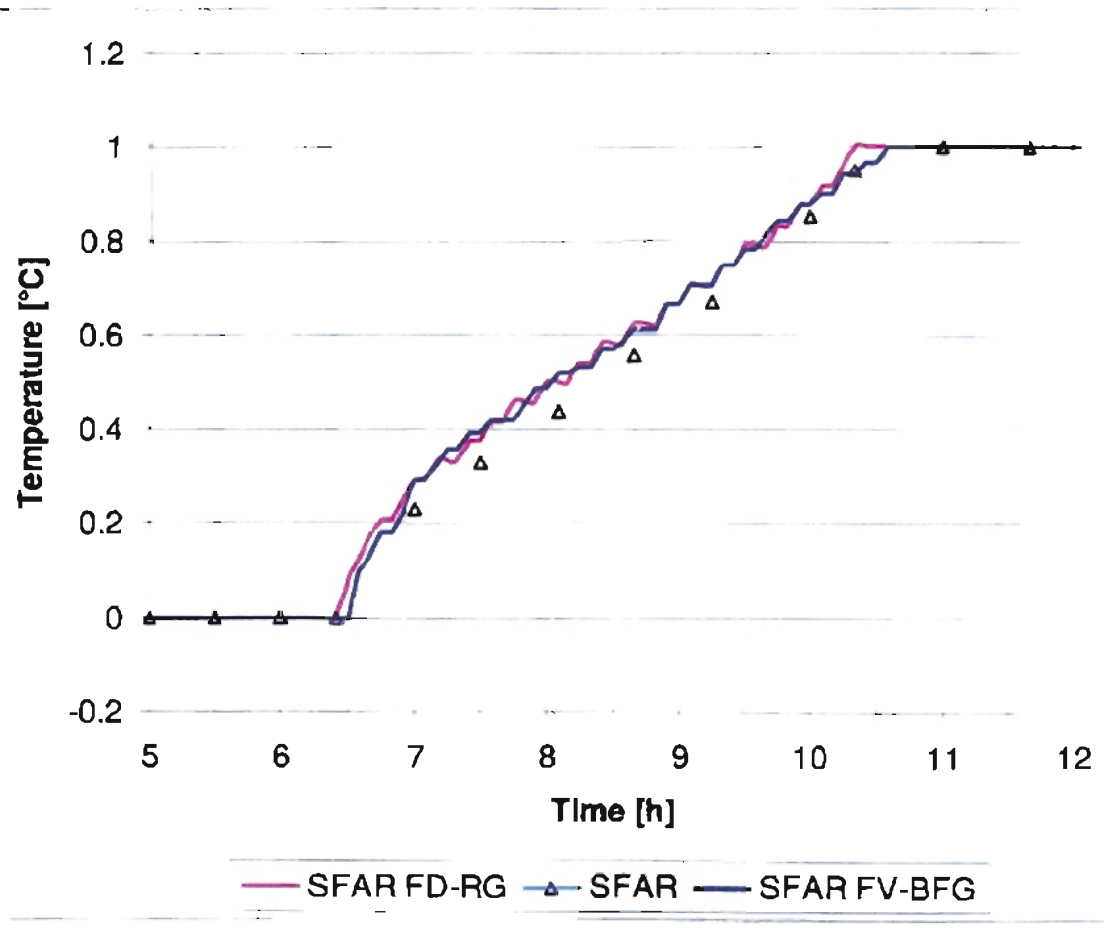

Figure 4.5-17: ***Snow free area ratio vs. time for SM2 experiment***

Table 4.5-12 shows the relationship between the actual time and the elapsed time for SM2 experiment:

Actual Time (hh:mm)	**Elapsed time** (hr)
18.15	6.42
22:13	10.33
22:52	11.08

Table 4.5-12: ***Actual time and elapsed time during snow- melting period in SM1 experiment***

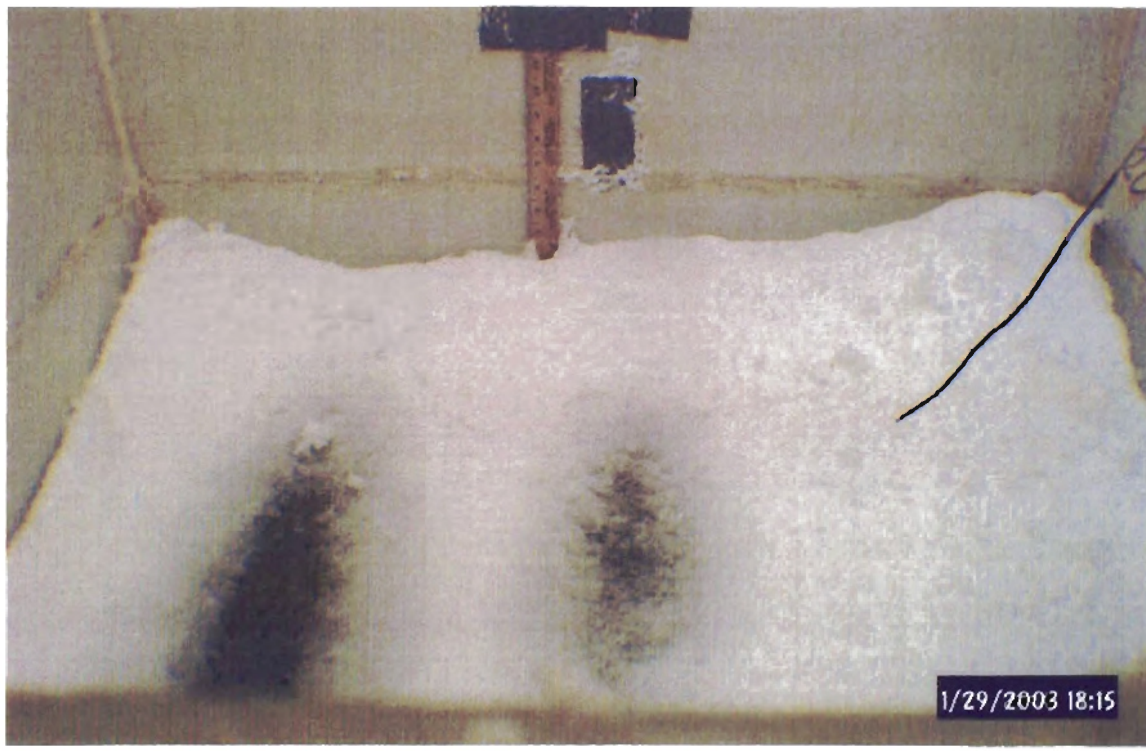

Figure 4.5-18: ***FD-RG Predicted Snow Free Area Ratio 0.00, measured: 0.00***

Figure 4.5-19: *FD-RG Predicted Snow Free Area Ratio 1.00, measured: 0.95*

Figure 4.5-20: *FD-RG Predicted Snow Free Area Ratio 1.00, measured: 1.00*

The SFAR values predicted by the FD-RG model matche consistently with the experimental values and again the snow melting is under predicted by 40 minutes. In the case of the SFAR predicted by FV-BFG model the snow melting time is under predicted by 25 minutes. These discrepancies can be attributed to inhomogeneous accumulation of snow over the surface of the slab as shown in Figure 4.5-18.

For this simulation the runtime is approximately 30 minutes for the FD-RG and 5.30 hours for the FV-BFG. The simulations ran on a Pentium III computer with 1.0 GHz processor speed and 256 MB of RAM memory.

4.5.3 Revised model with moisture penetration

After further consideration, it was decided to attempt to roughly model the moisture penetration into the slab and the moisture migration out of the slab after the water starts to evaporate from the surface. For this reason it was necessary to perform an experiment to estimate the water content absorbed by the slab's concrete during the snow-melting period. This experiment is described in section 4.2.4.

In order to investigate the moisture penetration effect, the FD-RG model was modified. The concrete properties such as specific heat and heat conduction were changed on a cell-by-cell basis on each time step. The penetration of such changes was estimated using equation (4-10)[3]. The thermal properties were changed and maintained under saturation conditions during the whole snow-melting period and until the surface of

---

[3] The energy transported by the water was neglected; only the thermal properties were modified.

the slab appears to be dry. The estimated moisture penetration profile is shown in Figure 4.5-21 for SM1 experiment and in Figure 4.5-22 for SM2 experiment

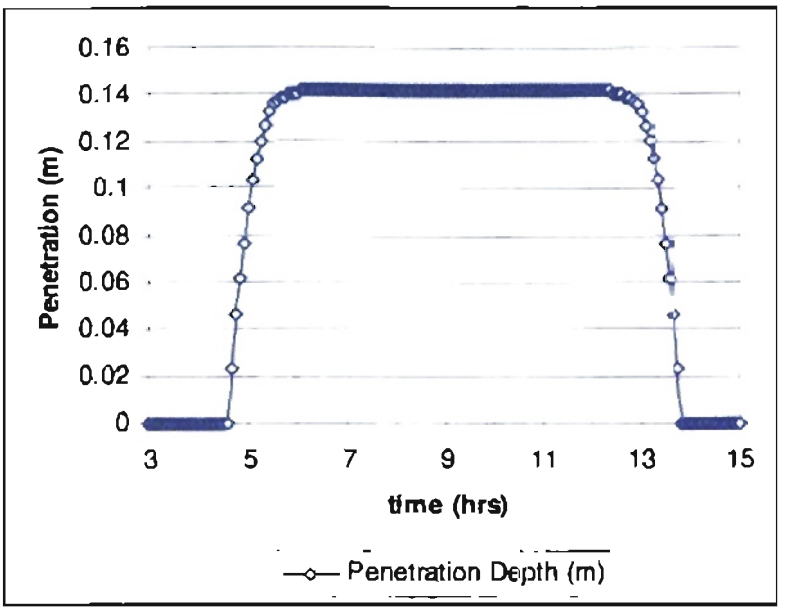

Figure 4.5-21: ***Estimated moisture penetration depth in SM1 experiment***

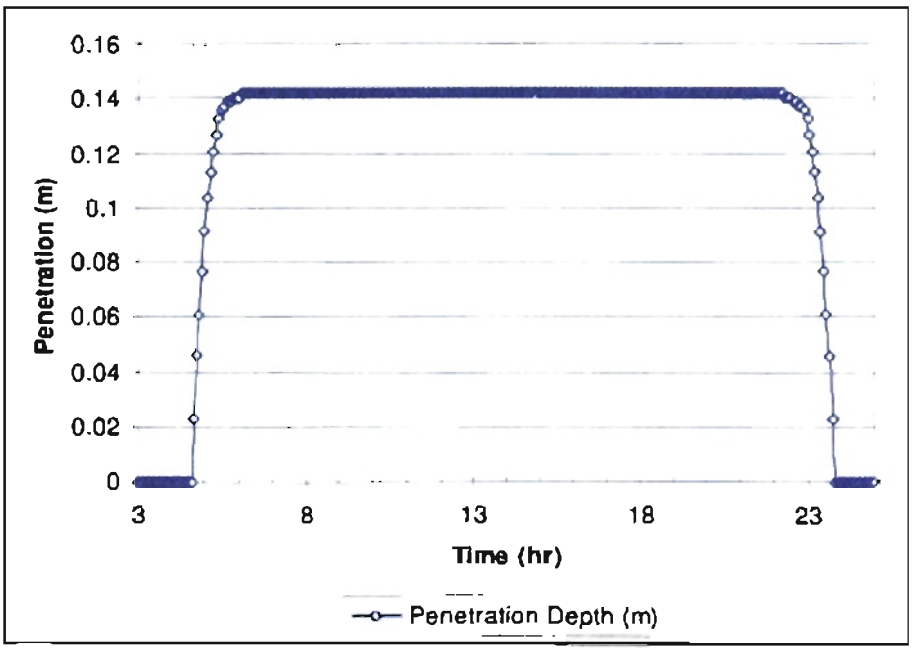

Figure 4.5-22: ***Estimated moisture penetration depth in SM2 experiment***

The surface temperature profile for the original FD-RG model and the revised model for SM1 are shown in Figure 4.5-23:

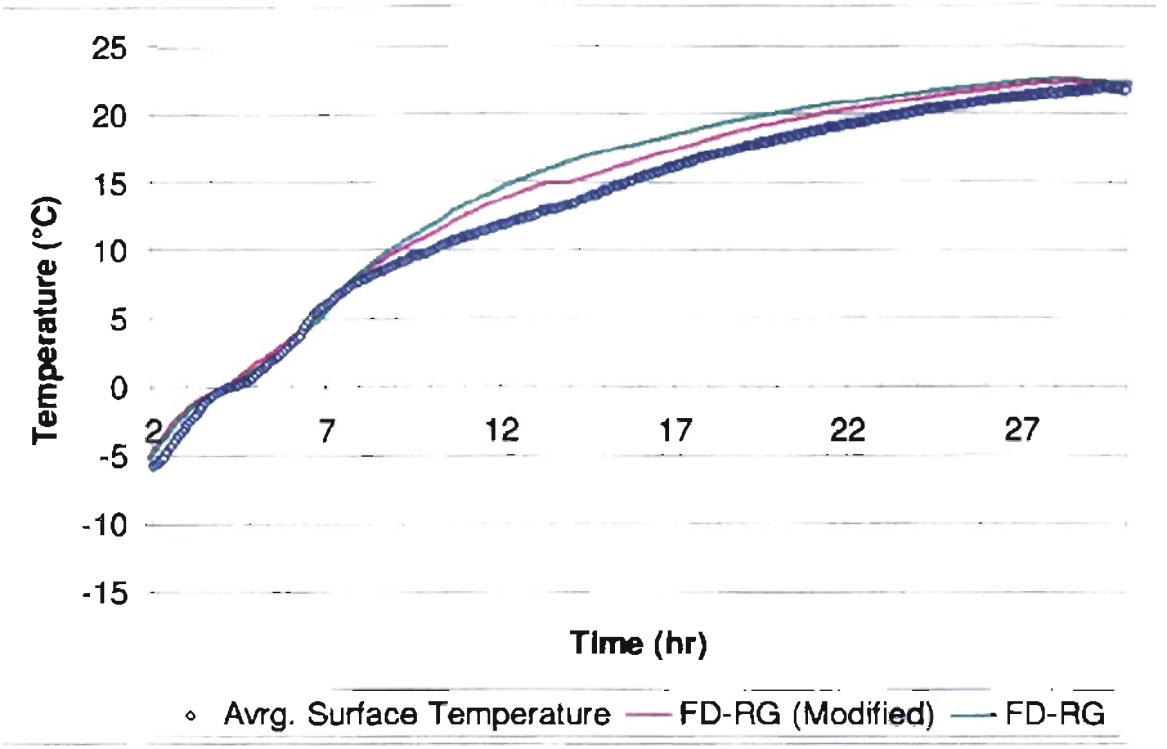

Figure 4.5-23: ***Surface temperature comparison between modified and original FD-RG model in experiment SM1.***

Figure 4.5-23 shows a slight improvement in the surface temperature prediction during the melting and drying periods compared with the experiment. For this simulation the runtime is approximately 23 minutes for the FD-RG model, using the same computer as described before. It is not clear that the minor improvement gained justifies the 15% increase in computational time. Furthermore, in a real application the system should be turned off once the snow has melted. However, a more refined model of moisture transport might give improved results.

The surface temperature profile for SM2 is shown in Figure 4.5-24. The modified FD-RG model shows some improvement in the temperature prediction. But again, a slight improvement was achieved with a 20% computational time increase.

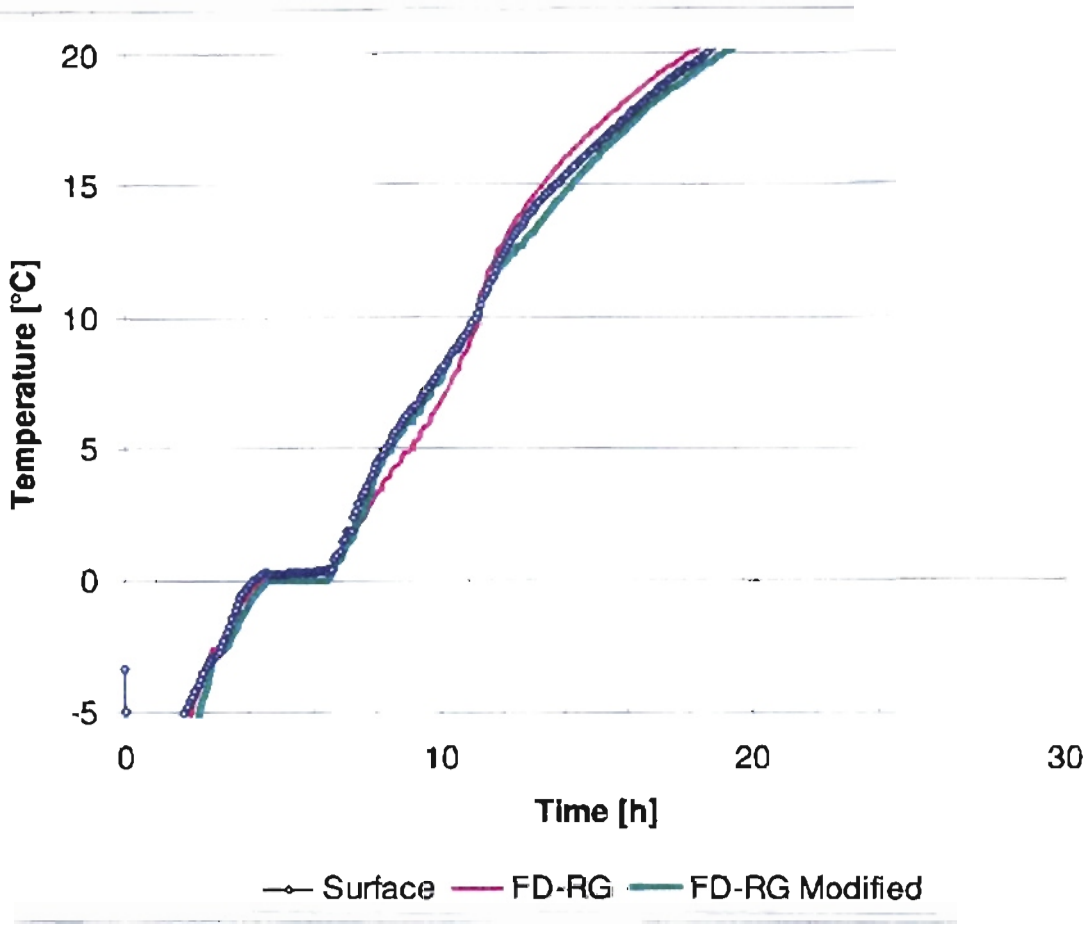

Figure 4.5-24: ***Surface temperature comparison between modified and original FD-RG model in experiment SM2.***

4.6 Summary

The results of the experiments and model comparisons may be summarized as follows:

- The thermal properties of the concrete slab materials need to be precisely established in order to obtain a reliable model of the system.

- It was found that both models give adequate predictions of the surface temperature and SFAR of the slab under environmentally controlled conditions.

- The modifications of thermal properties in order to account for moisture penetration increase the required computational time by about 15%, while giving only slight improvement in accuracy. This may be due to the very rough nature of the model; additional research is recommended to determine whether or not a more accurate water penetration model gives significantly improved temperature predictions.

- The FD-BFG model gives approximately the same results as the FD-RG model, but requires much greater computational effort, as shown in Table 4.6-13. Therefore, it is recommended that the FD-RG model be used for snow-melting simulations.

Experiment	FR-RG time (hrs)	FV-BFG (hrs)
Dry surface	0:03	0:20
SM1	0:25	3:30
SM2	0:35	5:20

Table 4.6-13: ***Run-time used by snow-melting models***

CHAPTER 5

CONCLUSIONS AND RECOMENDATIONS

5.1 Conclusions

As result of the work the following conclusions have been reached:

- The environmentally controllable snow chamber has proven to be useful for simulating a range of weather conditions, including low temperatures and snow fall.
- The two models investigated, the finite difference, rectangular grid (FD-RG) and finite volume, boundary-fitted coordinates (FV-BFG) gave adequately accurate predictions of time-varying surface temperatures and snow-free area ratios (SFAR) when accurate thermal properties are specified.
- The water penetration into the slab during the snow-melting process changes the thermal properties of the concrete. This, in turn, has a moderate effect on the predicted surface temperatures. A rough model of the water penetration improved the surface temperature prediction, although room for further improvement remains.
- The computational time required by the FV-BFG model is substantially higher than that required by the FD-RG model. However, there is no corresponding

improvement in accuracy. Therefore, it was recommended that the FD-RG model be used in the future for simulation of snow melting conditions on hydronically-heated slabs.

5.2 Recommendations

The following recommendations for future research may be made:

- The modification of the FD-RG model to account for water penetration gives slight improvement in accuracy. However, it did not carefully model either the water penetration or drying of the concrete slab. It may be true that a higher fidelity model of the moisture movement might result in significant improvements in the model accuracy. Therefore, development and testing of a more accurate water penetration model is recommended.
- In order to reduce the uncertainty related to the measurement of flow rate, a different measurement device, with higher accuracy and the capability to be read at every time step, is recommended.
- The mechanical cooling system was limited by frosting of the coils, so that the temperature of the chamber could not be controlled 0.3 °C (32.5 °F). Currently, liquid nitrogen must be manually introduced to further reduce the temperature. Therefore, improvements to the mechanical cooling system are recommended.
- Inhomogeneous distribution of the snow causes some difficulties in interpretation of the results. Investigation into improved snow production methods is recommended.

- Thermal properties under dry and saturation conditions have only been investigated for a single type of concrete. The moisture content of a slab could change depending on the porosity and permeability of the materia. In the case of concretes, depending on the basic composition (i.e. Siliceous, Dolomitic, etc) the specific heat can range very widely with moisture. Therefore, measurements of other concrete types that might be used in bridge decks are recommended.
- The experiments described in this thesis covered only a few conditions. Additional investigation under other controlled conditions and different values of heat flux is recommended.
- Finally, the experiments described in this thesis have limitations with respect to application to real-world conditions, since the sky temperature, wind speed, etc. are artificial. Therefore, it is necessary to perform similar experiments under outdoor snowfall conditions.

BIBLIOGRAFY

Aoki, K., Hattori, M. and Ujiie, T. (1987). "Snow Melting by Heating from the Bottom." 1987 International Symposium on Cold Regions Heat Transfer. University of Alberta, Edmonton, Alberta, Canada, American Society of Mechanical Engineers (ASME): 189-194.

ASHRAE (2001). ASHRAE Handbook-Fundamentals. Atlanta: American Society of Heating, Refrigerating and Air-Conditioning Engineers, Inc.

ASHRAE (1999). ASHRAE Handbool-HVAC Applications. Atlanta: American Society of Heating, Refrigeration and Air-Conditioning Engineers, Inc.

ASTM (2002). Standard Test Method for Steady-State Heat Flux Measurements and Thermal Transmission Properties by Means of the Guarded-Hot-Plate Apparatus. C 177-93. Annual Book of ASTM Standards. 04(06): 21-42.

Chapman, W.P. (1952). "Design of Snow Melting Systems." National Trade Journals. 49(4): 96-102.

Chapman, W.P. and Katunich, S. (1956). "Heat requirements of snow smelting systems." ASHRAE Transactions. 62: 149-153.

Chiasson, A.D., Spitler, J.D., Rees, S.J. Smith, M.D. (1999). "A model for Simulating the performance of a Pavement Heating System as a Supplemental Heat Rejecter with

Closed-Loop Ground-Source Heat Pump Systems". ASME journal of Solar Energy.

Goodwin, S.E., Litvin, A. and Whiting, D. (1978). "Specific Heat of Selected Concretes." Journal of the American Concrete Insitute. 75 (32): 299-305.

Hockersmith, S.L. "Experimental and Computational Investigation of Snow Melting and on Heated Horizontal Surfaces". M.S. Thesis: Oklahoma State University. Stillwater, Oklahoma.

Incropera, F.P. and DeWitt, D.P. (1996). Introduction to Heat Transfer. Third edition. New York: John Wiley & Sons.

Kilkis, I.B. (1994b). "Design of Embedded Snow-Melting Systems: Part 2, Heat Transfer in the Slab – A Simplified Model." ASHRAE Transactions. 100(1): 423- 433.

Kilkis, I.B. (1994a). "Design of embedded snow-melting systems: Part 1: Heat Requirements – An overall assessment and recommendations ." ASHRAE Transactions. 100(1): 423- 433.

Leal, M.R. and Miller, P.L. (1972). "An Analysis of the Transient Temperature Distribution in Pavement Heating Installations." ASHRAE Transactions. 78 (2): 61-66.

Liu, X. Rees, S.J. Spitler, J.D., (2002). "Simulation of a Geothermal Bridge Deck Anti-icing System and Expirimental Validation." Proceedings of the Transportation Research Board 82nd Annual Meeting. Washington, D.C. January 12-16, 2003.

Löfgren, S. (2001). "The chemical effects of deicing salt on soil and stream water of five catchments in southeast Sweden." Water, Air and Soil Pollution. 130: 863-868.

McQuiston, F.C., Parker, J.D. and Spitler, J.D. (2000). Heating, Ventilation, and Air Conditioning: Analysis and Design 5th Edition. New York: John Wiley and Sons.

Nixon, W.A. (1993). "Improved cutting edges for ice removal". Iowa institute of hydraulic research. University of Iowa, Iowa city.

Ramsey, J., M. J. Hewett, T.H. Kuehn, and S. D. Petersen (1999). "Updated Design Guidelines for Snow Melting Systems". ASHRAE Transactions. 105(1): 1055-1065.

Rees, S.J. (2000). "An Introduction to the Finite Volume Method: Tutorial Series." OSU Mechanical & Aerospace Engineering. Class notes.

Rees, S.J. (2000). "Using the General Elliptical Multi-block Solver.GEMS 2D." OSU Mechanical & Aerospace Engineering. Class notes.

Rees, S.J., Spitler, J.D., Xiao, X. (2002). "Transient Analysis of Snow-Melting System Performance." ASHRAE Transactions. 108(2):406-423.

Rhodes, J.A. (1978). "Thermal Properties." Significance of Tests and Properties of Concrete and Concrete-Making Materials. American Society for Testing and Materials. 17: 242-261.

Schnurr, N.M. and Rogers, D.B. (1970). "Heat Transfer Design for Optimization of Snow Melting Systems. ASHRAE Transactions. 76 (2): 257-263.

Spitler, J., S. Rees, X. Xia, and M. Chulliparambil (2001). "Development of a Two-Dimensional Transient Model of Snow-Melting System and Use of the Model for Analysis of Design Alternatives". ASHRAE 1090-RP Final Report, Oklahoma State University School of Mechanical and Aerospace Engineering.

Smith M.D. (2003). Personal conversation in the IGSHPA Laboratories. Oklahoma State University.

APPENDIX A

INSTRUMENT CALIBRATION

A.1 Introduction

All measurement devices have an error associated with it. It is possible to minimize this error by calibration. Some of the instruments used were factory-calibrated. In other cases, experimental procedures were required and comparison against certified instrument produced a calibration equation.

A.2 Variables & Calibration

During the experimentation four variables required measurement. These variables were: weight, volume, flow rate, and temperature.

The determination of weight and volume was required during the experimentation procedure to calculate the specific heat of the concrete used. Both variables were measured using factory-calibrated instruments. Weight was measured using a digital balance with ±0.1g. Water volume used into the calorimeter was measured using a graduated cylinder. The graduation shows divisions of 0.01 liters. Therefore, it is possible to estimate the uncertainty in ±0.005 liters (half of the graduation division).

In the case of flow rate, this variable was used to calculate the power input to the slab. This variable was measured using an in-flow rotameter. Again the instrument is factory-calibrated with an uncertainty of ±8% FS.

Finally, Temperature was used during the whole experimentation process. However, most of the thermocouples used in the slab were installed prior a calibration procedure during the original construction process. These conditions made impossible to recalibrate the thermocouples. Still, those thermocouples were access was possible were calibrated.

The thermocouples were immersed in a constant temperature bath. Then, an ASTM certified thermometer with a 0.1°C graduation was used to record the temperature. For thermocouples used to measure the inlet and outlet the range between 0 to 80°C was used. In the case of thermocouples used for specific heat, the calibration range was –3 to 30°C. Then the collected thermocouple reading was plotted against the certified thermometer readings. Finally, a linear regression of the data was completed. The equation obtained from the regression was used to correct the readings. The uncertainty associated with this calibration is ±0.05°C (half of the ASTM thermometer graduation).

The plots and equation obtained for each thermocouple are shown bellow:

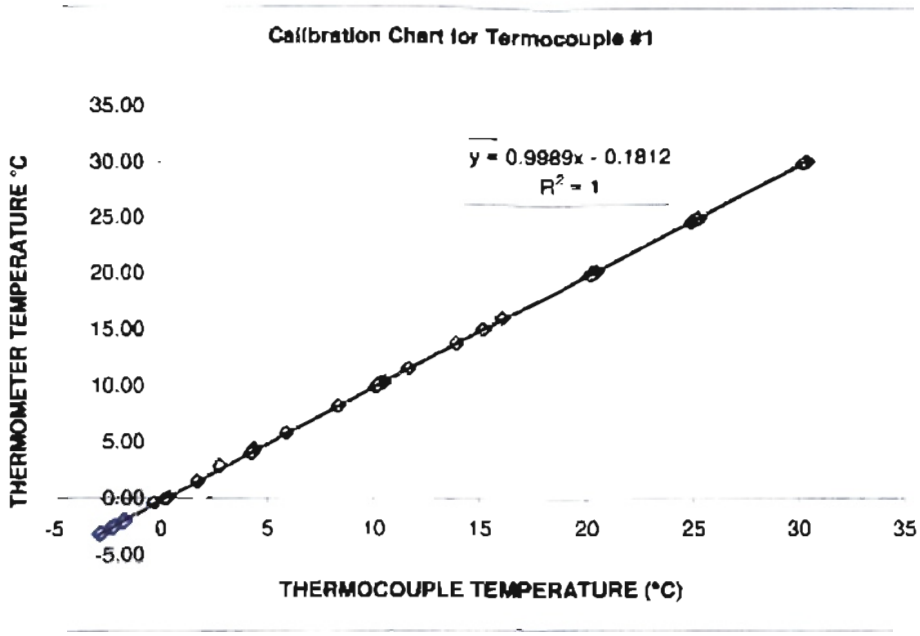

Figure A-1: ***Calibration chart for thermocouple inside sample for Cp determination***

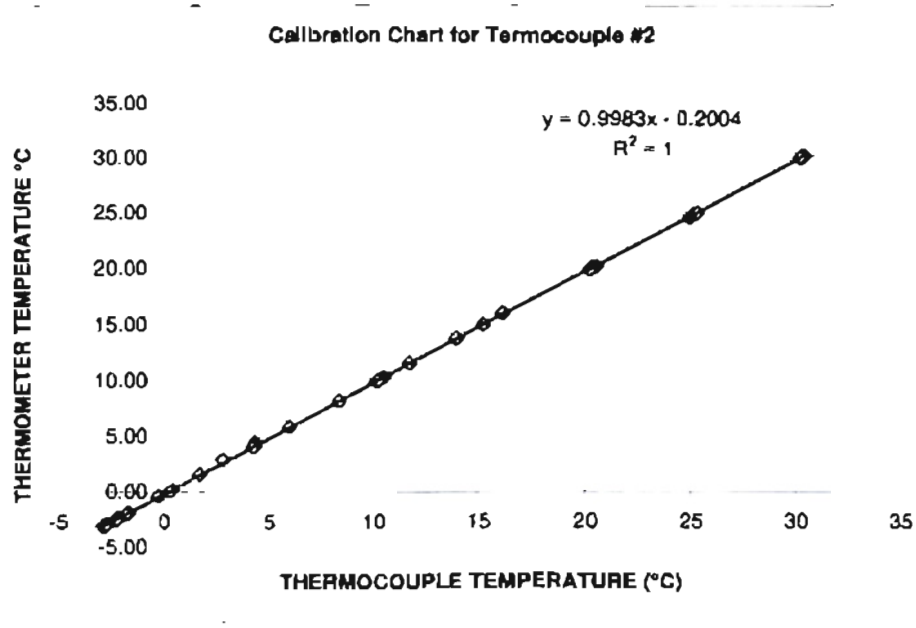

Figure A-2: ***Calibration chart for thermocouple outside of sample for C_p determination***

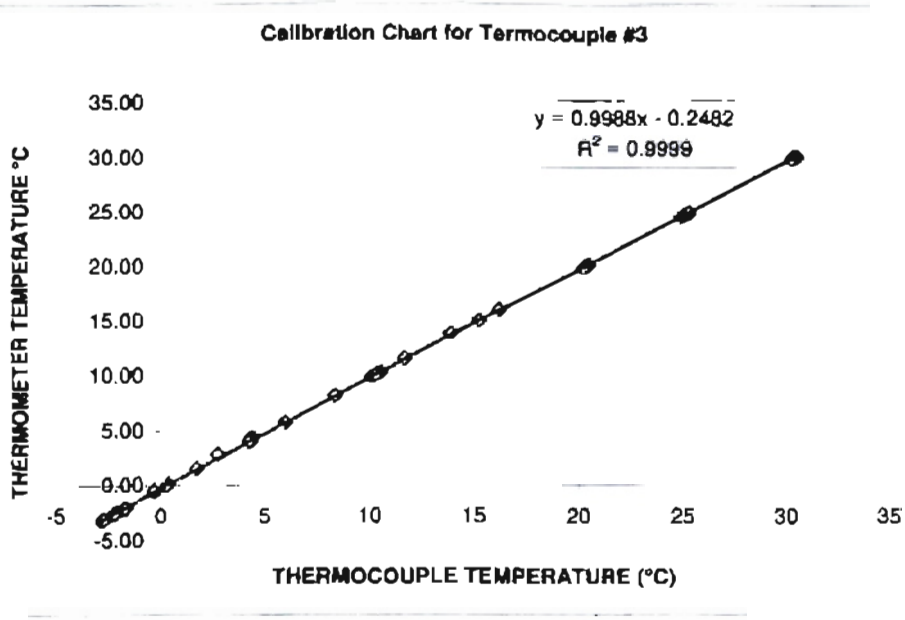

Figure A-3: ***Calibration chart for thermocouple in water bath for C_p determination***

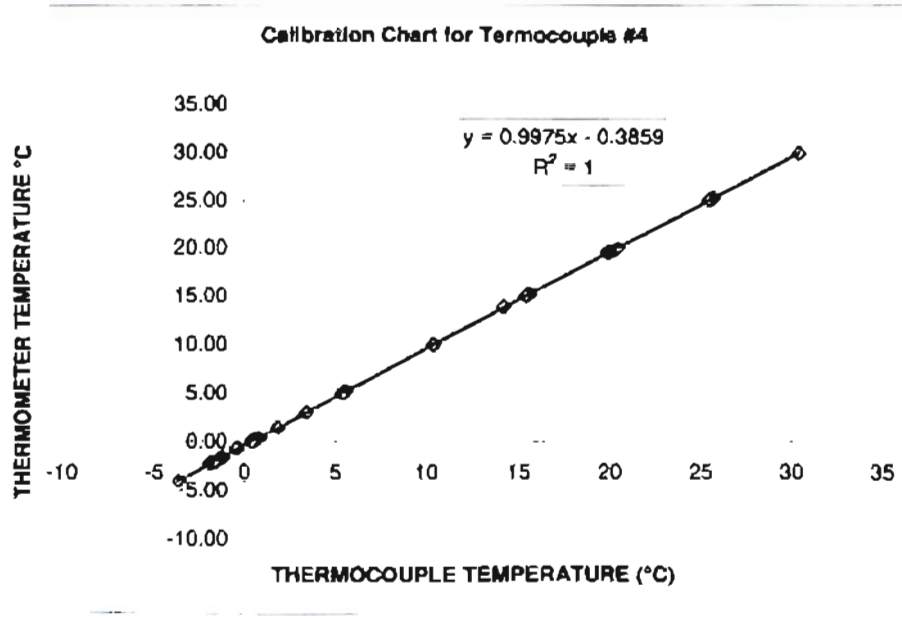

Figure A-4: ***Calibration chart for thermocouple into calorimeter for C_p determination***

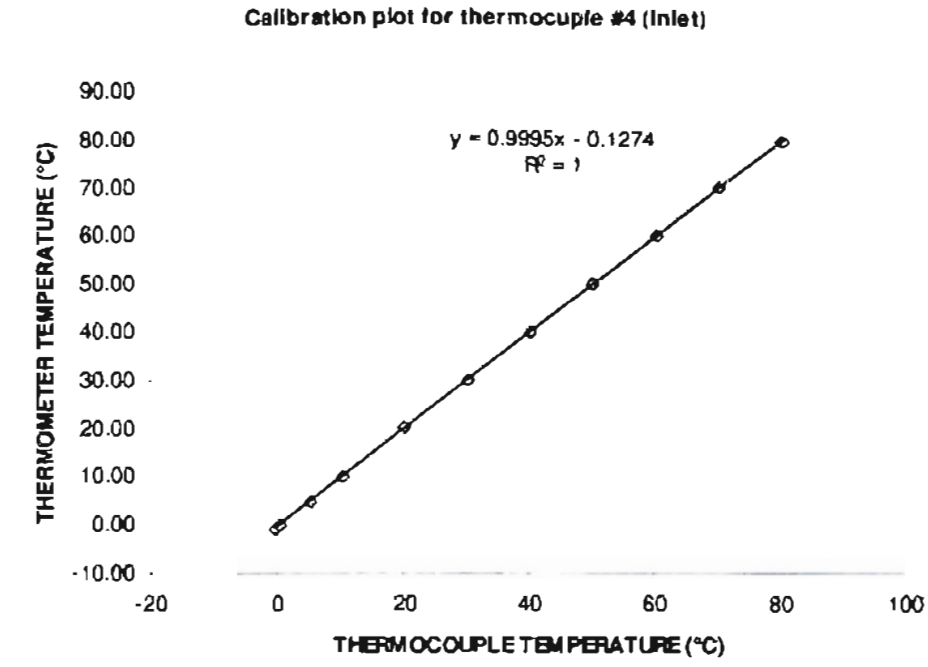

Figure A-5: *Calibration chart for thermocouple at inlet of hydronic piping*

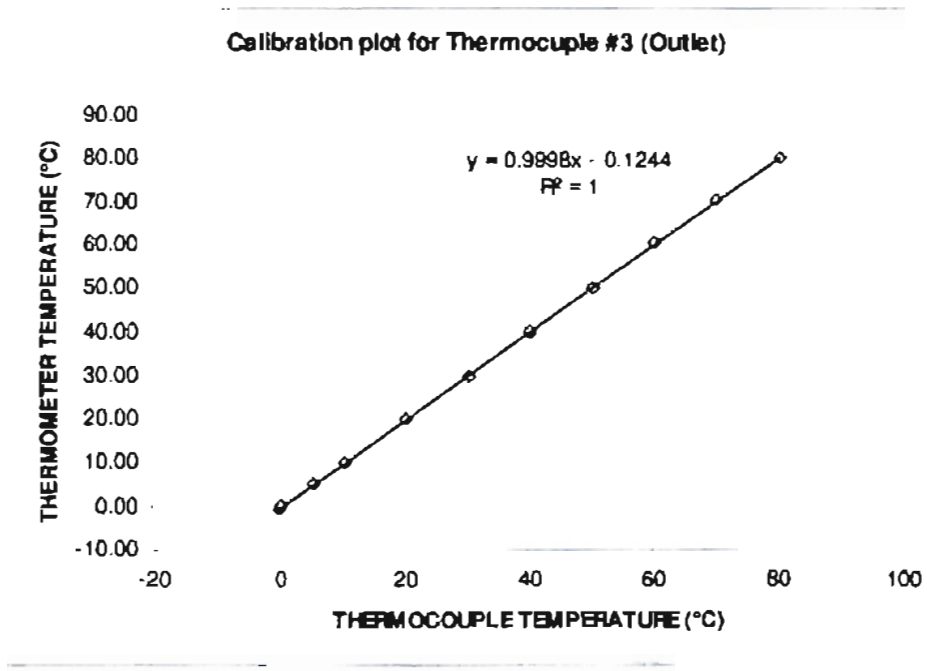

Figure A-6: *Calibration chart for thermocouple at outlet of hydronic piping*

APPENDIX B

DATA LOGGER CONTROLLER

B.1 Introduction

The data acquisition for the snow melting experiment requires synchronization between the data logging, picture taking, and the light required to acquire the picture. There were two reasons to design the control system. The first is that reduction of undesired radiation from the light source. The second is to ease the correlation of calculated data with acquired data.

B.2 Description of the system

The system uses a Basic Stamp II micro controller to coordinate the required actions. Parallax Inc manufactures the micro controller. This device is capable to perform up to 4000 instructions/second. However, the resonator is accurate in 1%. Under these circumstances, the clock will be off around 15 seconds at the end of one day of operation if the timing instructions are used. The device has remarkable capacity to control short periods of time (e.g. milliseconds). But it has problems handling longer periods. So, it was necessary to provide an accurate time base for the controller to work on the desired time step for this application.

The time base circuit is provides a pulse with a frequency of 1Hz. Principle of operation is the use of a 32768 Hz crystal working on a RC circuit. This arrangement provides a base of 2 Hz that is used in combination with a binary counter (4060) that divides the count in a 1 Hz pulse. The output of this circuit is introduced to one of the 16-input/output pins of the Basic Stamp. The timing circuit is shown in Figure B-7.

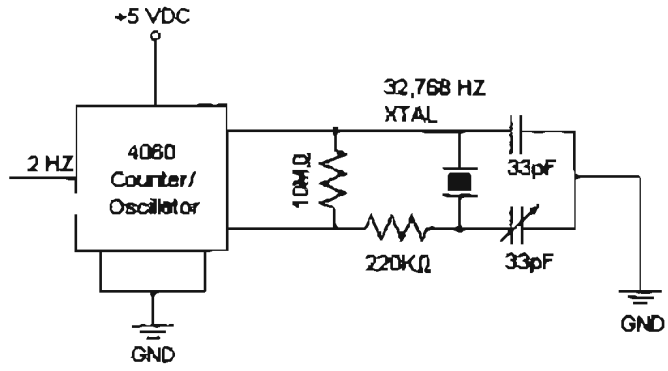

Figure B-7: ***Time base diagram***

Part of the code is used to compare the state of the input pin with the input value. Every ¼ of second, the value will change. The time available to perform any command is then one quarter of second. This is enough time to produce any operation (e.g. Data login, light control).

The computation required is the addition of seconds to a counter. When the counter reach the desired time, the signal to activate the data loggers or the signal to turn the light on is given. The timed activities are repeated in a 10-minute (0-599 s) period. The activities are shown in Table B-1.

Time (s)	Activity
0	Pulse to activate data logging
3	Turn light off
299	Pulse to activate data logging
597	Turn light on

Table B-1: ***Microprocessor activity list***

A 5V and10-millisecond pulse is given when the instruction to produce the data logging is specified. The FLUKE Hydra II series data logger is equipped with an external logging command input. The action triggers the scan button and acquires a set of data from the system. Both data loggers used are connected in parallel to this signal. Therefore, the acquisition occurs at the same time.

A PNP transistor is used to turn the light on and off. A signal of 5V and 5mA is given to the gate pin. This closes the circuit and allows power to the solid-state relay (SSR) used. The power required by the SSR is higher than the one available from the micro controller. Therefore, the source for the SSR needs to be independent from the microprocessor circuit. The SSR close the circuit when the control signal is given and the light is turned on. The control signal is kept during the period time of that the camera requires. Once the control signal is off, the SSR opens the circuit again and the light turns off. A detail of this circuit is shown below:

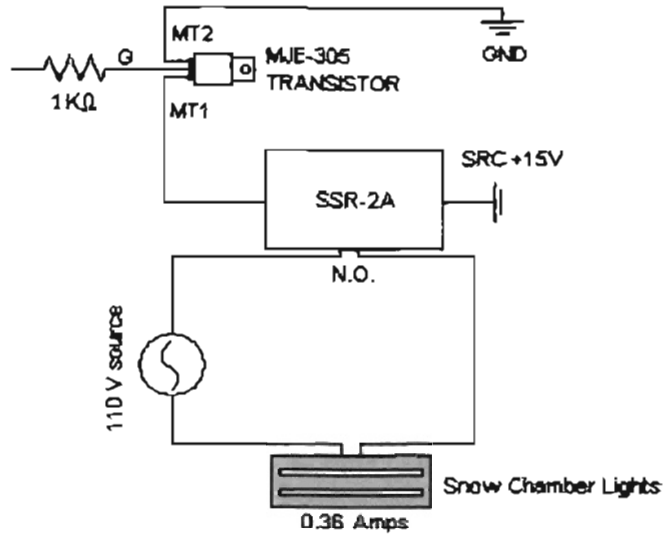

Figure B-8: ***Light control circuit***

One pulse button is directly wired to the reset pin of the Stamp. On activation the pin passes a 5V signal to the stamp and the micro controller is reset.

The language used to program the Stamp micro controller is the Parallax BASIC (PBASIC). The complete list of the code used is shown bellow in Figure B-9:

```
'{$STAMP BS2}
'Variables

sec   var   Word

Main:
if pin2 = bit0 then tick
if sec= 0 then P_B4
if sec=5 then Light_off
if sec=299 then P_B4
if sec=594 then Lights
if sec=599 then P_B4
goto Main

tick:
b0 = b0 + 1        ' Increment b0 counter.
if b0 < 4 then Main      ' If b0 hasn't reached 4, back
'to Main.
b0 = 0                   ' Else clear b0,
sec = sec + 1            ' increment the seconds count,
goto Main                     ' Do it again.

P_B4:
pulsout 7,3 'Command scanning to Hydra II
goto Point_A


Lights:
toggle 8    'Change state of pin8 to ON
goto Point_A


Light_off:
low 8       'Change state of pin8 to OFF
goto Point_A
```

Figure B-9: ***List of source code for Basic Stamp II***

The complete diagram of the system is shown in Figure B-10:

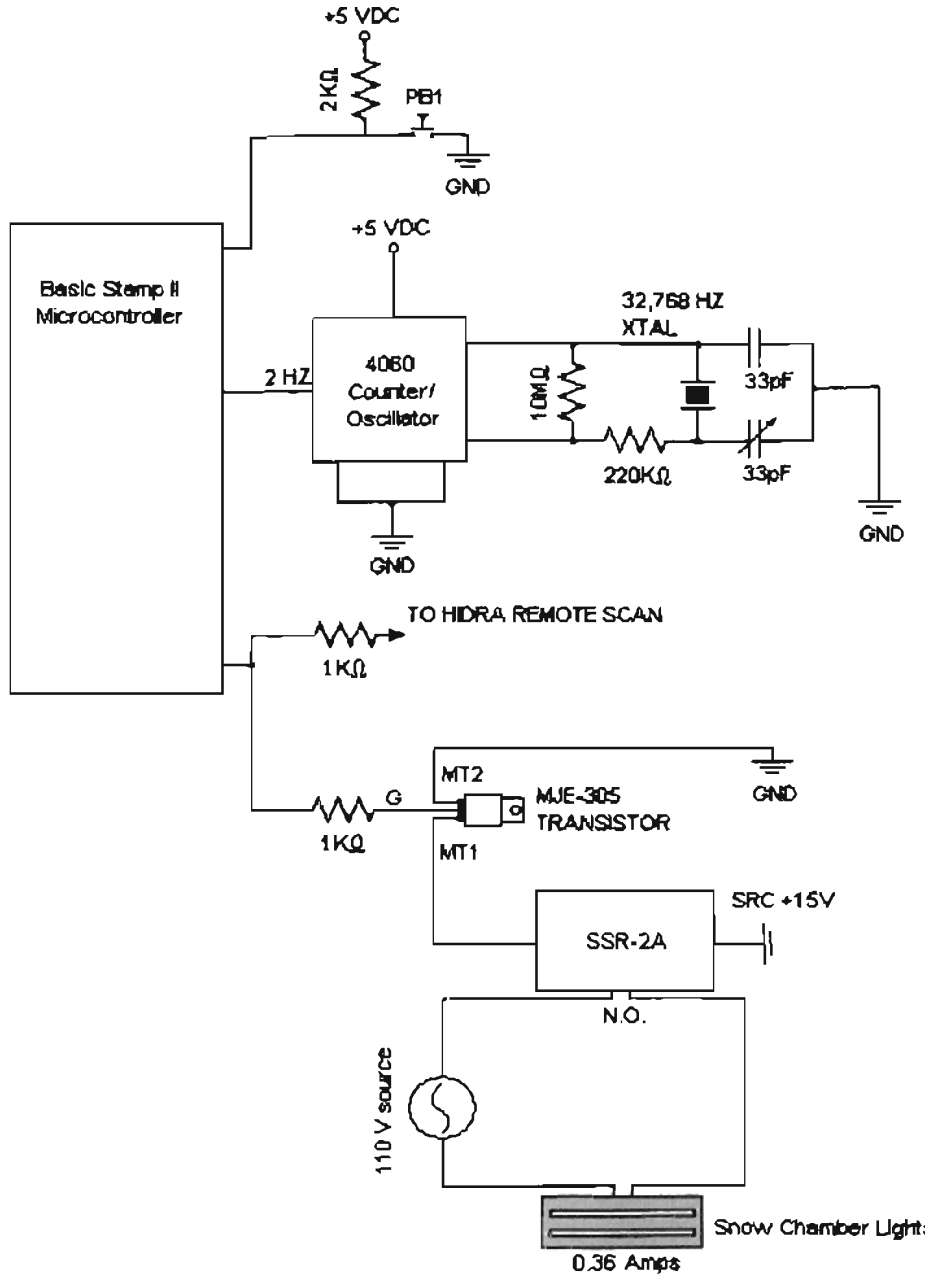

Figure B-10: ***Complete diagram of data acquisition controller system***

APPENDIX C

GEOMETRIC INFORMATION OF CONCRETE SLAB

C.1 Concrete slab

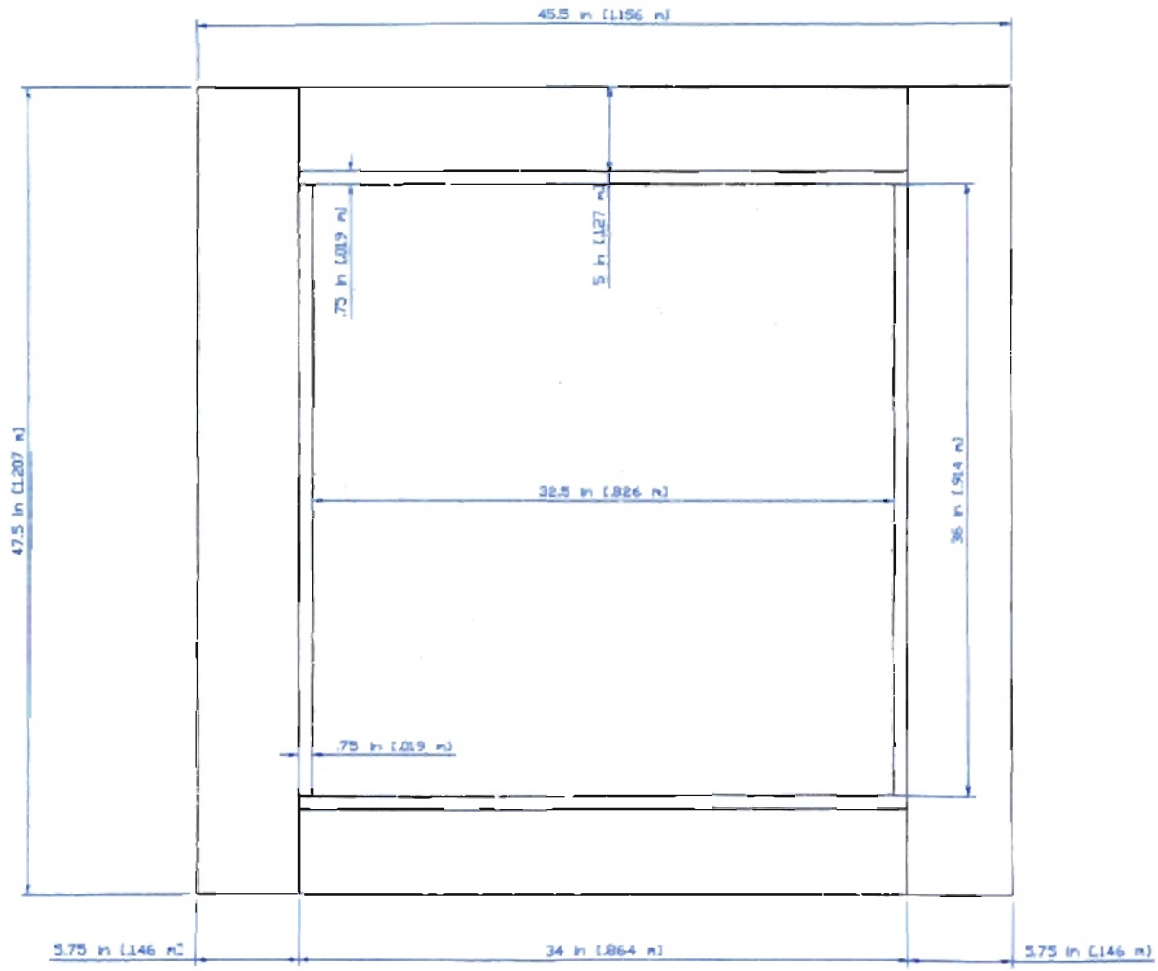

Figure C-1: ***Upper slab surface***

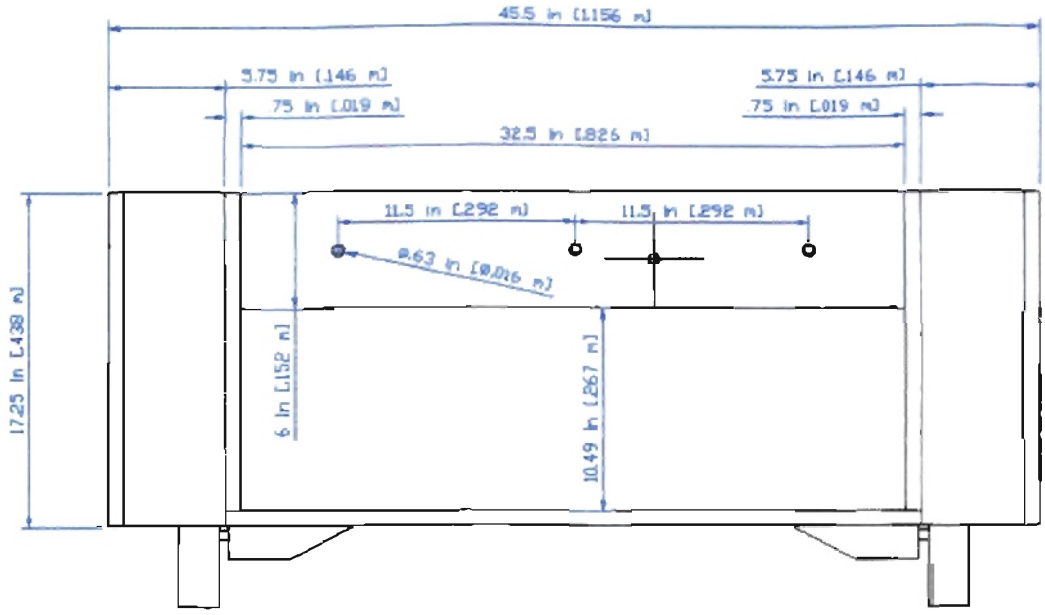

Figure C-2: ***Slab frontal diagram***

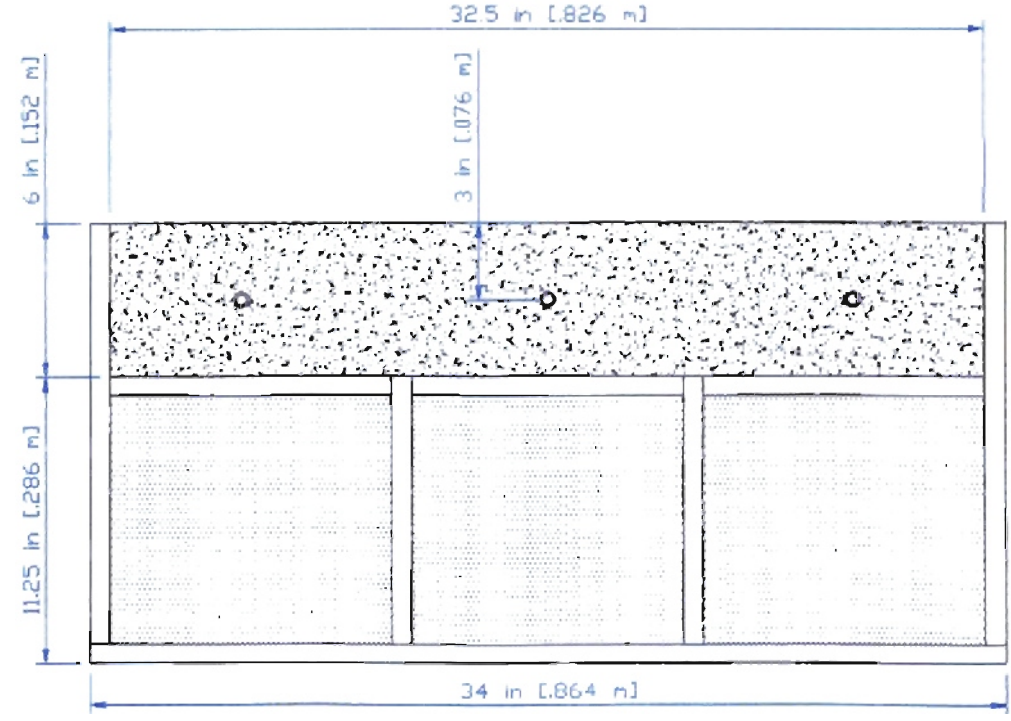

Figure C-3: ***Central section of slab***

C.2 Main thermocouple placement dimensions

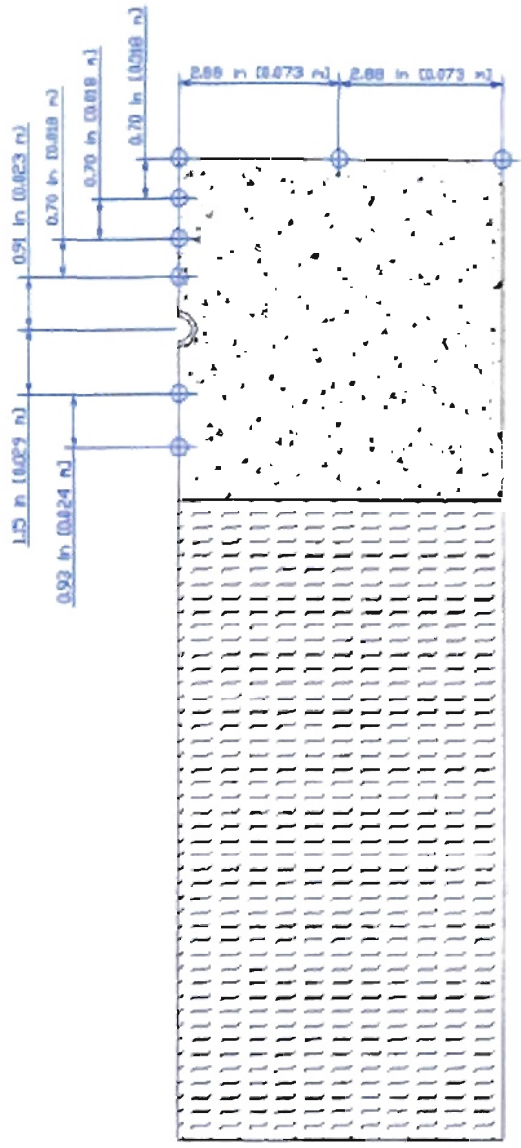

Figure C-4: ***Main thermocouple placement***

C.3 Central section

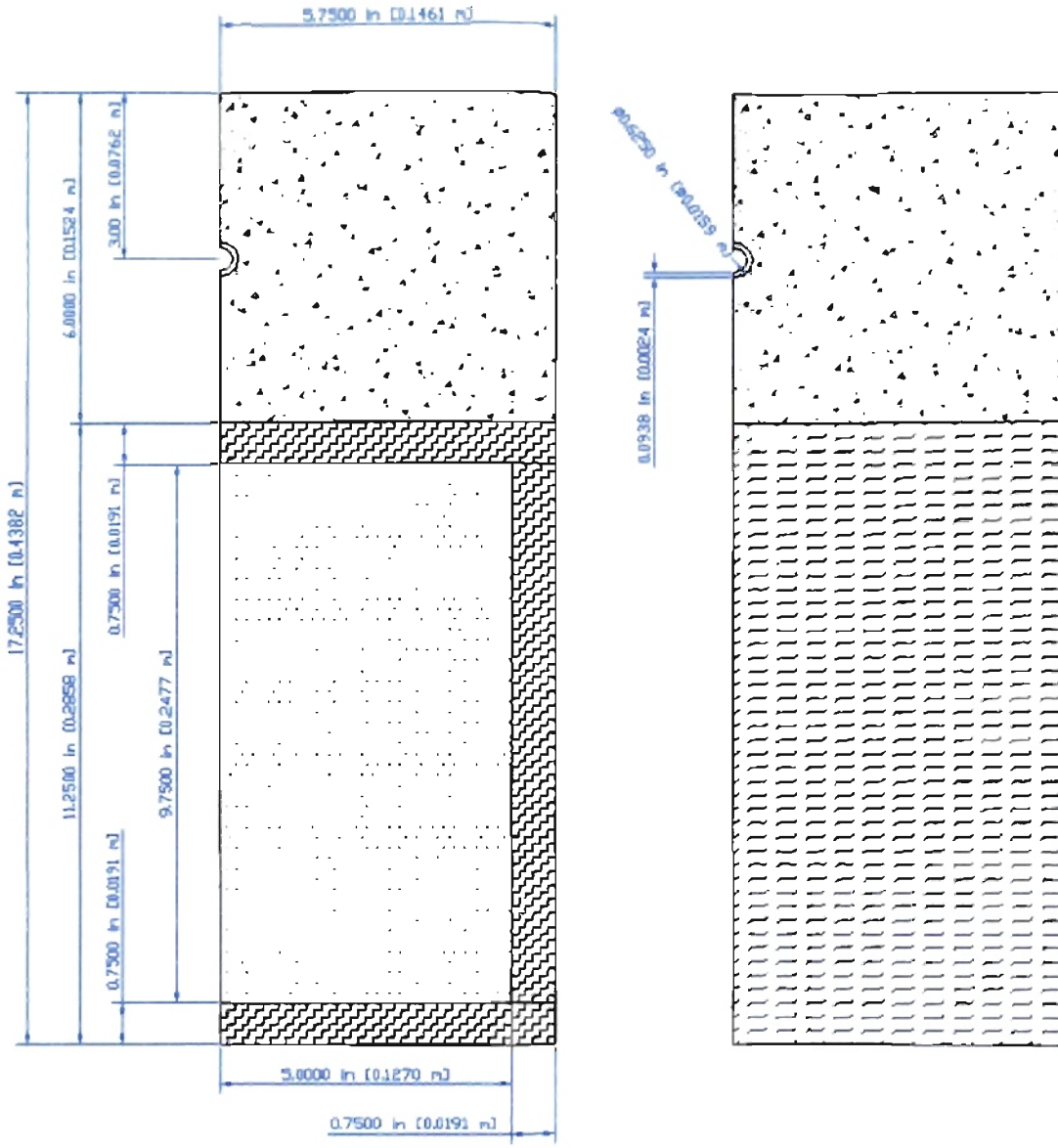

Figure C-5: ***Central "real" and "modeled" section dimensioning***

APPENDIX D

CHARTS AND DATA USED FOR CONCRETE CONDUCTIVITY CALCULATION

D.1 Sample 1:

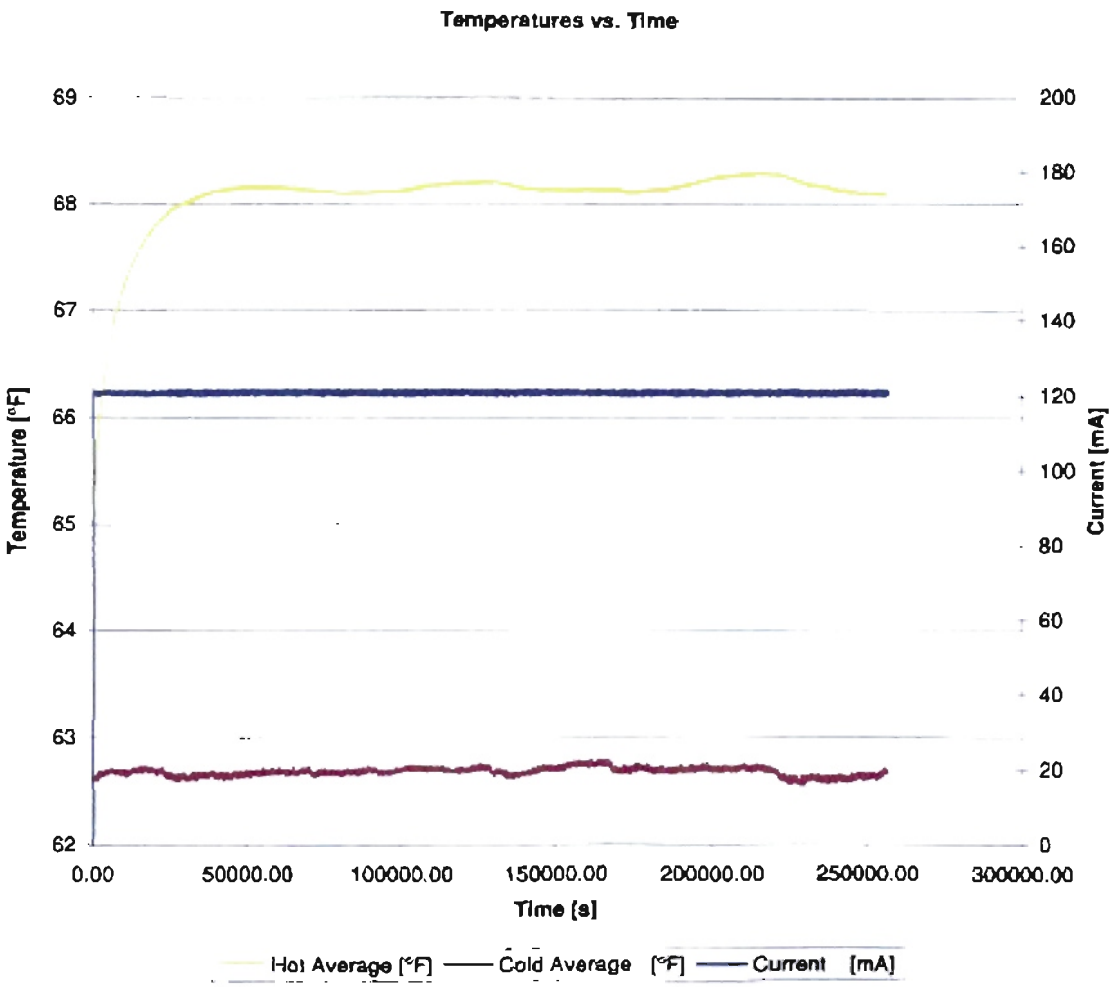

Figure D-1: ***Temperature chart in sample 1***

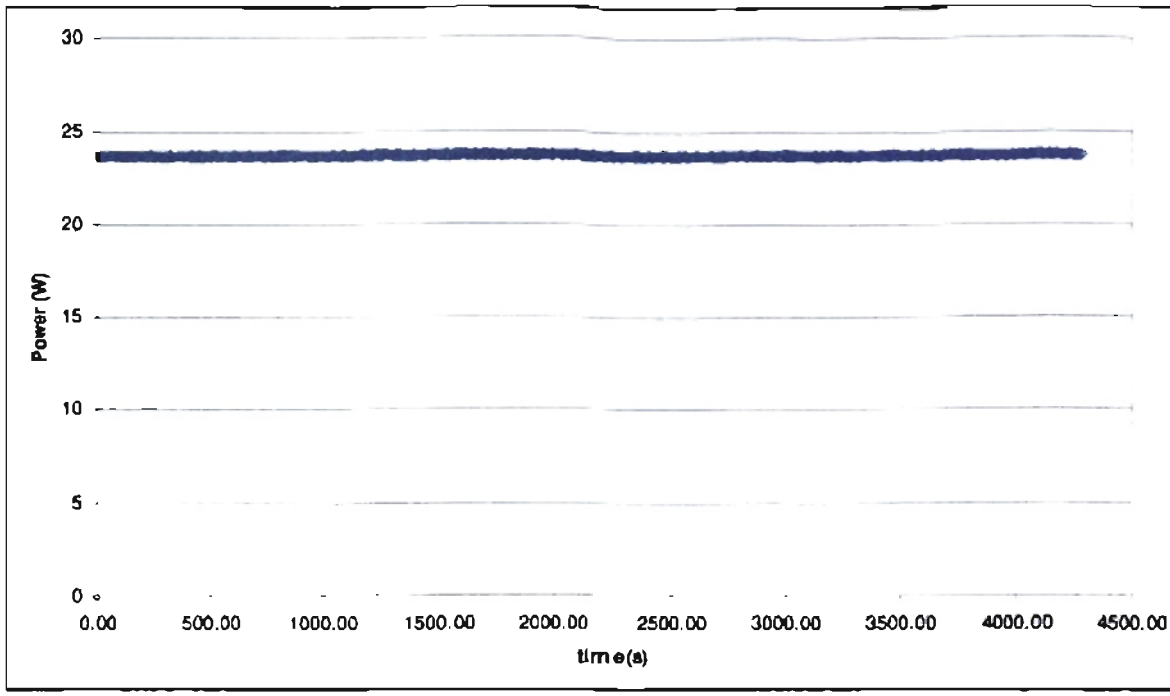

Figure D-2: ***Power measurement on thermal conduction calculation for sample 1***

D.2 Data obtained for sample number 2:

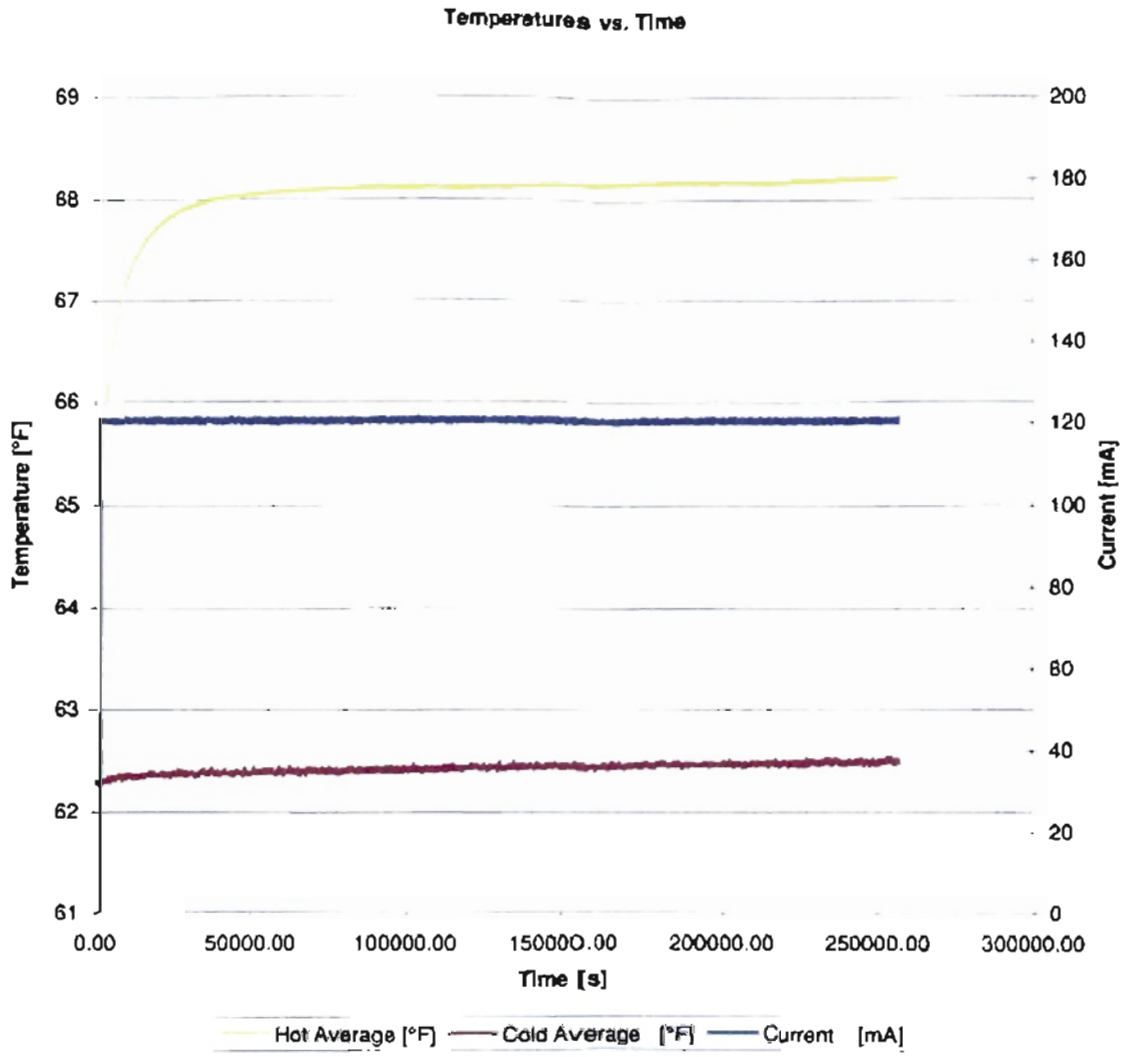

Figure D-3: ***Temperature chart in sample***

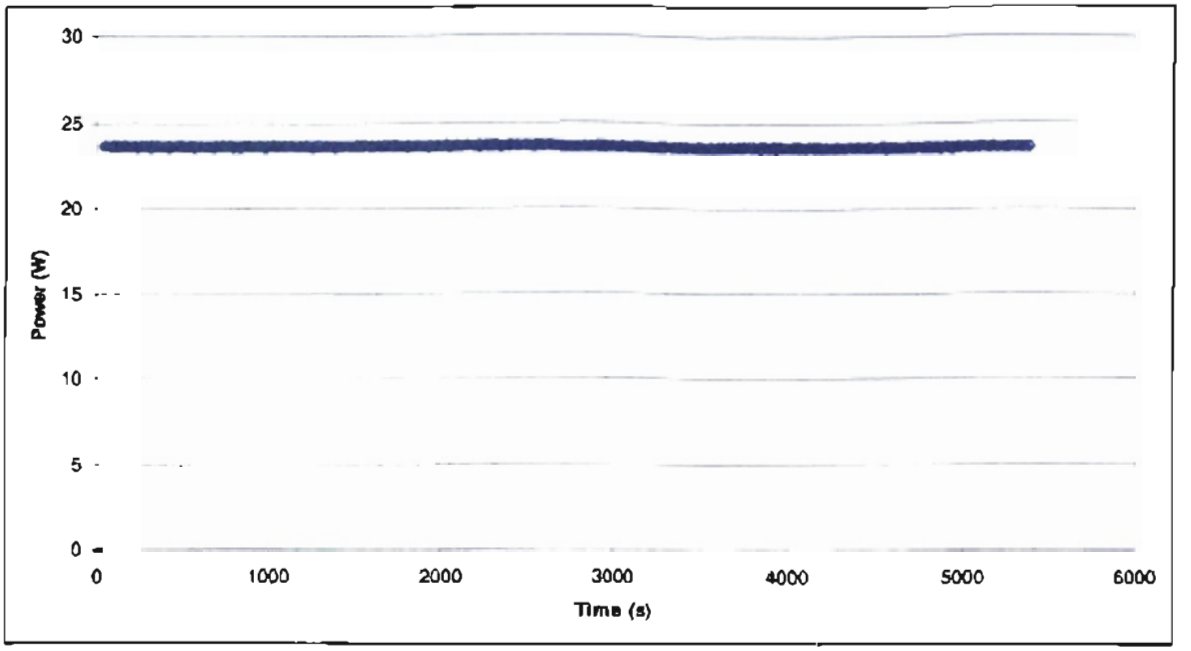

Figure D-4: *Power measurement for thermal conduction calculation for sample 2*

VITA

Candidate for the degree of
Masters of Science

Thesis: EXPERIMENTAL AND COMPUTATIONAL INVESTIGATION OF SNOW MELTING ON A HYDRONICALLY HEATED CONCRETE SLAB.

Major Field: Mechanical & Aerospace Engineering

Biographical:

Education: Graduated from "San Gabriel" High School, in September 1991. Received a Bachelor of Science degree in Mechanical Engineering from Escuela Politécnica del Ejercito, in September 1998. Completed the requirements for the Masters of Science degree with a major in Mechanical and Aerospace Engineering at Oklahoma State Universiy in December, 2003.

Experience:

Repsol – YPF Ecuador Inc. Quito – Ecuador. (March 1998 – To date)

Maintenance Coordinator (August 2003 – To date). Responsibilities include developing and implementation of maintenance planning. Implementation of RBM/RCM philosophy for five maintenance departments (mechanical, electrical & generation, instrumentation & control, civil works and camps logistics).

Chief Commissioner Engineer (March 2003 – August 2003). Team leader for the commissioning of 75K BOPD facilities upgrade. Five teams were involved: mechanical, electrical, instrumentation, production & process, and QA/QC. In charge of the development of commissioning procedures and standards for the company. Follow up of all the contractors executing works for the facility upgrade.

Production Supervisor (March 2000-December 2001). Responsible for the production of the Northern Production Facility (25000 BOPD) and four well pads (36 wells).

Projects Engineer (January 1998 – August 1998). Promoted to Project Supervisor (December 2000). Designed basic and conceptual crude oil processing facilities, well pads and pipelines. Implemented pipelines optimization by simulation. Projected constructions, managed its implementations, and audit them.

International of Equipment, Petroleum and Communications S.A. Quito – Ecuador. (Aug. 1997 – March 1998)

Assistant Engineer. Planned project related to heat transfer. In charge of assisting in proposals development and calculations related to heat transfer for projects in the area.

Oklahoma State University, as graduate student: Research Assistant and Teaching Assistant. Mechanical Engineering Department. January 2001 to December 2002.

Profesional Memberships: ASHRAE. American Society of Heating Ventilation and Air Conditioning.